2009

Evaluation of extraction chromatography resins for rapid actinide analysis

Julie Marisa Gostic
University of Nevada Las Vegas

EVALUATION OF EXTRACTION CHROMATOGRAPHY RESINS FOR RAPID ACTINIDE ANALYSIS

By

Julie Marisa Gostic

Bachelor of Arts
College of Charleston
2000

Masters of Science
University of Massachusetts, Lowell
2004

A dissertation submitted in partial fulfillment of
the requirements for the

Doctor of Philosophy Degree in Radiochemistry
Department of Chemistry
College of Science

Graduate College
University of Nevada, Las Vegas
December 2009

UNLV
UNIVERSITY OF NEVADA LAS VEGAS

THE GRADUATE COLLEGE

We recommend that the dissertation prepared under our supervision by

Julie Marisa Gostic

entitled

Evaluation of Extraction Chromatography Resins for Rapid Actinide Analysis

be accepted in partial fulfillment of the requirements for the degree of

Doctor of Philosophy
Radiochemistry

Kenneth Czerwinski, Committee Chair

Kenton Moody, Committee Member

Gary Cerefice, Committee Member

Ralf Sudowe, Graduate Faculty Representative

Ronald Smith, Ph. D., Vice President for Research and Graduate Studies
and Dean of the Graduate College

December 2009

ABSTRACT

Evaluation of Extraction Chromatography Resins for Rapid Actinide Analysis

by

Julie M. Gostic

Dr. Kenneth R. Czerwinski, Examination Committee Chair
Professor of Chemistry
Chair of the Department of Radiochemistry
University of Nevada, Las Vegas

In this work, physical and chemical parameters associated with extraction chromatography separation procedures were investigated for rapid actinide analysis. A vacuum box system was designed in-house and was characterized in terms of flow rate reproducibility, matrix effects on flow rate for sequential elution, and actinide separation efficiency using different types of resin (TEVA, DGA and TRU). Results indicated that the columnar kinetics of the resins were sufficiently rapid to run high purity samples through the unit over a wide range of flow rates for all resin types. Single matrix interferences at a metal ion ratio of $1:10^6$ relative to the actinide of interest affected separation efficiency with some resins and a flow rate dependency was observed. After parameter optimization, the system was used to isolate Pu for isotopic analysis from dissolved particles from a nuclear warhead that was destroyed in a fire 50 years ago. Isotopic analysis was obtained by a combination of radiometric and mass-based methods using cerium fluoride (CeF_3) micro-precipitation for sample preparation. The results of these experiments were compared to historical record surrounding the source of the particles.

ACKNOWLEDGEMENTS

I would like to take this opportunity to express my sincerest gratitude to those individuals that helped me reach this milestone in my educational career. First, I would like to thank my thesis advisor, Ken Czerwinski for having the foresight and tenacity to build a multi-disciplinary radiochemistry program at UNLV. I have benefited from his hard work and dedication to the program and would like to thank him in particular for his efforts. I would also like to thank the members of my thesis committee for their patience and support throughout my research and writing. In particular, I would like to thank Ken Moody for his thoughtful commentary and hours of time spent reviewing this body of work. Gary Cerefice and Ralf Sudowe have also been very influential in my professional growth and development and I thank them for their guidance and support throughout my graduate career at UNLV.

I could not have accomplished this without the love and support of friends and family. To my husband, I am eternally grateful for your unwavering support and willingness to complete our PhDs together. I would like to dedicate this work to those on whose shoulders I stand, Linda Jones, Mike Ryan, Nancy Carder, Sy Baron, David Borsook, Jeanette Cohan, Lino Becerra, Clay French, Mark Tries, Jim Eagan, and Dave Medich.

TABLE OF CONTENTS

LIST OF TABLES

LIST OF FIGURES

CHAPTER 1

INTRODUCTION

1.1 Background

The nation's recurrent focus on emergency response and preparedness in the event of a nuclear or radiological incident has given impetus to develop rapid forensic analysis methods for radionuclide identification and quantification. The methods need to be both reliable and accurate in that the information obtained about the material may be used to prevent future illicit activities or help determine source origination (1). Analytical response following a nuclear incident will vary significantly from routine surveillance monitoring procedures and will pose specific challenges including, large scale sampling and handling of non-standard environmental and anthropogenic matrices with a wide range of activity from background to hot particle levels (2-5). As an example, samples collected from a nuclear incident may consist of various forms of urban rubble, i.e. building materials, asphalt, concrete, glass, etc., and from a chemistry perspective, are very complex. Traces of the material of interest are essentially embedded in a sea of other elements and must be physically or chemically isolated for accurate analyses. In developing effective rapid response analytical protocols, each of these challenges must be addressed. This leads to an inherent paradigm shift in the assessment criteria that are used to determine the suitability of a method.

Nuclear forensic analysis must be approached from a "360° view", meaning that the sample must be scrutinized from every angle to determine what information is available and how it relates back to the source term (5). This

requires the use of both non-destructive and chemical dissolution techniques. Non-destructive analyses include high resolution imaging and bulk elemental distribution using various microscopy and spectroscopy techniques (6-8). The information obtained can help identify some of the primary constituents without complete destruction of the original sample material. The utility of non-destructive characterization is limited in that complete isotopic analysis is not achievable. The isotopic signature can provide information regarding the fabrication process and the date of origin of the material (5,9) but usually requires complete dissolution of the sample, followed by chemical isolation of the radionuclides of interest.

Classical radioanalytical techniques used for forensic analyses are often very robust and accurate (1), but require a considerable amount of time from sample dissolution to final report. For materials obtained prior to an event, the number of samples collected is limited to the quantity of material intercepted and, in most cases, the material is intact and true to its origin (5,9). In situations where a nuclear or radiological incident has occurred, the number of samples acquired may be in the thousands and the ability to provide accurate data for such a volume of potentially diverse samples in a short time period is diminished.

Recent research efforts have been directed towards developing actinide separation methods that optimize chemical yields (10-14) and decrease total processing time but few of these methods have been evaluated for bulk sampling processing.

1.2 Bulk Sample Processing Through Automation

Bulk sample processing can be accomplished more effectively with automation and, in recent years, modularized platforms have been developed for bench scale chemistry applications including sample dissolution, chemical separations, and sample preparation. However, current forensic radioanalytical methods have not been adapted for these types of platform automated systems. Translating manual into automated methods requires a greater understanding of the physical and chemical parameters that are important from an engineering standpoint. Each step must be evaluated first on a basic level to determine which portions of the process are critical for achieving acceptable results. Once the fundamental chemical reactions are understood, each step can then be approached from an engineering perspective to optimize the procedure for automation.

1.3 Method Selection

The primary focus of this work was to evaluate mixed actinide separations procedures for potential automation. Many techniques have been developed for radionuclide separations from aqueous solutions including precipitation, solvent extraction, ion exchange chromatography (IC) and extraction chromatography (EC). The chemistry used for analyte concentration and separation depends on the activity concentration in the sample, the degree of separation that is required due to matrix interferences, and operational time constraints. Most radioanalytical

procedures make use of multiple methods to optimize efficiency and minimize potential interferences.

EC combines the selectivity and versatility of solvent extraction with the simplicity and columnar fractionation capabilities of IC (15). This is accomplished by incorporating the organic extractant into the stationary phase which is supported on an inert polymer or silicate resin. EC methods are well-suited for automated chemical separations as demonstrated in various continuous flow-through separation units (16-23). The EC resins have high analyte selectivity, simplistic elution schemes, rapid kinetics, and they can be stored dry prior to immediate use (24). The manufacturer, Eichrom Technologies, Inc. packages the resin into cartridges, which reduces preparation time and minimizes variations associated with in-house packing. The cartridges are stackable, providing an efficient way of separating multiple radionuclides based on analyte affinity for different extractant compounds.

Recent publications (10-12, 25-28) have demonstrated the utility of vacuum-assisted separations for a wide range of sample matrices. A vacuum box system was used to accelerate chemical separations and to process multiple samples simultaneously. This discrete approach to batch sample analysis reduces the risk of cross-contamination between samples and decreases experimental variability within a given batch.

In this work, a vacuum box system was designed in-house and was modeled after a commercially available solid phase synthesis unit. The vacuum box system was characterized in terms of flow rate reproducibility, matrix effects on

flow rate for sequential elution, and actinide separation efficiency using three different types of resin, TRU, DGA and TEVA. The results of the characterization studies are presented in Chapters 3 and 4.

1.4 Source Preparation and Analysis

After chemical separation and purification is achieved, samples must be analyzed to determine the total concentration of each radionuclide. In nuclear forensic analysis, Pu and U are of particular interest in that they are the primary components in nuclear materials and their relative isotopic abundance can be linked to the intended use of the material and the fabrication process (1,5). Isotopic analysis is accomplished using radiometric techniques, i.e. high resolution gamma and alpha spectrometry (GS and AS), or high resolution mass analysis, i.e. mass spectrometry (MS). When used in combination, these techniques provide a more comprehensive analysis.

In most cases, sample preparation for radiometric and mass analysis is separate, which further increases processing time. It would be useful to determine if a single sample preparation technique could be used for both radiometric and mass based isotopic analyses. In Chapters 5 and 6, cerium fluoride (CeF_3) micro-precipitation used for AS sample preparation was selected for evaluation as a single source preparation method. Samples were prepared from stock solutions where the Pu isotopic content was known and from dissolved particle solutions known to contain WGPu. This method was chosen based on short preparation time (12 samples/hr), good energy resolution for

alpha analysis (~32 keV), and high actinide recovery as scavenged by the precipitate (29). Additionally, the filters could be used for mass analysis to confirm the relative isotopic ratios determined from gamma and alpha analysis (Chapter 6).

1.5 Thesis Organization

In this thesis, preliminary studies (Chapter 3) focused on the characterization of the EC separation unit using TRU and DGA resins and Am to establish some of the chemical and engineering boundary conditions associated with the separation method. Engineering controls, such as flow rate reproducibility, pressure regulation, and cartridge failure were tested using various acid matrices. Once the unit was physically characterized, method efficiency was evaluated in terms of the effects of flow rate on extraction efficiency of Am present in solution at various concentrations. Americium was selected for preliminary study based on its tendency to exist in a single trivalent oxidation state in acid solution and well-characterized extraction behavior on both DGA and TRU resins under the given matrix conditions (30,31). The effects of matrix ion contaminants on Am extraction efficiency were also characterized. Matrix ions contaminants selected for characterization were chosen based on their abundance in environmental and nuclear material matrices, or due to their use in sample enrichment steps conducted prior to chemical separations.

Once the Am characterization studies were completed, the EC separation unit was characterized with TEVA resin for Pu method efficiency (Chapter 4).

Plutonium extraction efficiency is more complex in that multiple Pu oxidation states can be present in solution, and redox agents must be used to force Pu into the most extractable species. Various parameters affecting Pu separation efficiency were characterized including, the age of the reagents used, the sample rest time (i.e. the time from redox agent addition to column loading) along with those previously mentioned for the Am studies.

Once the EC unit was characterized for Am and Pu, aqueous samples were prepared from solutions containing dissolved WGPu hot particles (Chapter 5). The particles were manually isolated from soil cores that were sampled from a site where a fire involving a missile tipped with a nuclear warhead occurred over four decades ago. The particles were dissolved in a HNO_3/HF/H_2O_2 solution and chemistry was performed on the EC unit with TEVA and DGA resins. Plutonium was selectively removed from other matrix constituents on TEVA and Am and U were isolated on DGA. The relative Pu isotopic ratios were determined using CeF_3 sample preparation and alpha and gamma spectrometry.

The Pu isotopic analysis of the various hot particle solutions required the development of a series of CeF_3 precipitated Pu standards (Chapter 6). Samples were prepared with activity concentrations between 0 and 2400 Bq and instrument response for alpha and gamma spectrometry was characterized. Additionally, preliminary mass analysis was performed with inductively couple mass spectrometry (ICP-MS) using a laser ablation sample introduction unit.

Each data chapter is presented in manuscript format with a detailed introduction and materials and methods section. Chapter 2 provides a general overview of the instrumentation and methods used in this work.

CHAPTER 2

INSTRUMENTATION AND METHODS

2.1 Introduction

A short description of the instrumentation and general methods used for experimentation is presented in this chapter. More detailed descriptions of methods are provided in Chapters 3 through 6 as related to the specific experiments in which they were employed.

2.2 Chemical Separations

The focus of this work was to characterize chemical separations of the actinides using extraction chromatography resins for the development of an automated radioanalytical platform. Extraction chromatography (EC) combines the selectivity and versatility of solvent extraction with the simplicity and columnar fractionation capabilities of ion exchange chromatography (IC) (32). The active component of the resin is an organic extractant that is affixed to an inert polymer or silicate resin. The resins are packed into columns, which form the stationary phase for dynamic, flow-induced chemical exchange. The aqueous sample is loaded on the column and the metal ions of interest interact with the stationary phase. The extent of chemical interaction between the metal ion and the stationary phase is based on the conversion of the hydrated metal ion to the extractable organophilic species. A more detailed description of EC is provided in references (15,24,33).

Eichrom Technologies, Inc. (Darien, IL, USA) has incorporated EC resins into pre-packed, stackable 2 mL cartridges. These cartridges can be stacked for more rapid separations that are simpler in design, produce less waste and have higher recovery rates versus traditional analytical methods (24). The resins used for experiments in this work are provided in Table 1.

Table 1. Extraction chromatography resins used for actinide separations

Resin*	Active Component	Research Applications
TEVA Resin (10)	Trialkyl methylammonium nitrate (or chloride)	Tc, Th, Np, Pu, Am/lanthanides
TRU Resin (7)	Octylphenyl-N,N-di-isobutyl carbamoylphosphine oxide (CMPO) dissolved in tri-n-butyl phosphate (TBP).	Fe, Th, Pa, U, Np, Pu, Am, Cm
DGA Resin (8)	N,N,N',N'-tetraoctyl-3-oxapentanediamide	Actinides, Lanthanides, Y, Ra

*Relevant reference in parentheses after resin name

The EC resin cartridges were placed in a vacuum extraction unit that was developed in-house to control the sample loading and elution flow rates. The box (Figure 1, A) held 15 resin cartridges (3 x 5 configuration) and was modeled after a commercially available, fully automated solid phase synthesis unit manufactured by J-Kem Scientific, Inc (Figure 1, D). The internal pressure of the box was controlled by a vacuum pump coupled to a digital vacuum regulator

(Figure 1, B and C, J-Kem Scientific, Inc. and Edwards). A more detailed description of the in-house system is provided in Chapter 3.

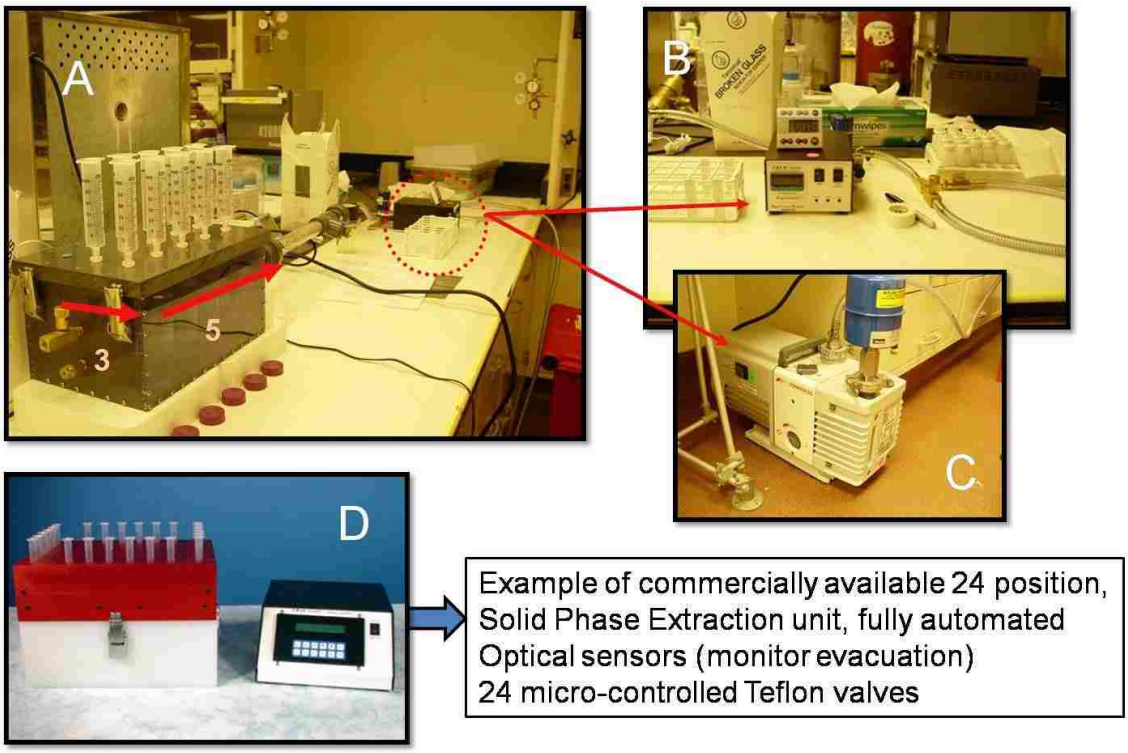

Figure 1. Vacuum extraction unit developed in-house and the commercially available automated solid phase extraction unit manufactured by J-Kem Scientific, Inc.

Three types of EC resins were used in this work, TEVA, TRU and DGA. The active component of each resin and references to the initial characterization studies are presented in Table 1. TEVA resin was selected for Pu isolation and TRU/DGA resins were selected for Am isolation. Selection was based on the resin selectivity parameter, K', for each of the actinides of interest. This parameter is defined as the number of free column volumes to elution peak

maximum (24) and is a measure of the affinity to the extractant of the metal species in a given matrix solution. A review of the experimental determination of the K' factor is provided elsewhere (31). As an example, the K' for Pu on TEVA resin is 10^4 in 3 M HNO_3, but only 0.1 and 10 for Am and U, respectively (34). Under the same loading conditions, Am and U are retained to a greater extent on either TRU ($K'_{Am} = 10^2$, $K'_U = 2 \times 10^3$) or DGA ($K'_{Am} > 10^4$, $K'_U = 10^2$) resins (30, 31). These resins can be used in combination to selectively purify each actinide of interest by manipulating the loading and elution matrices. The chemical separations procedures used for each experiment are described in detail in subsequent chapters.

2.3 Radionuclide Standards

2.3.1 Americium

Americium stock solutions were prepared from a traceable standard solution (1198-21-4, 01-Jul-06, Isotope Products, Valencia, CA, USA). The ^{241}Am stock solutions were prepared in various HNO_3 matrices with activity concentrations from 5 to 50 Bq/mL of stock solution. Stock solution activity was verified by liquid scintillation counting (LSC).

2.3.2 Plutonium

Plutonium stock solutions were prepared from traceable standard solutions (1198-16-1, August-06, Isotope Products, Valencia, CA, USA). The Pu isotopic content for the original standard solution is provided (Table 2). The presence of the relatively short-lived ^{241}Pu isotope ($t_{1/2}$=14.4 years) in the Pu solution,

required that the in-growth of the ^{241}Am decay product be determined for accurate evaluation of the chemical separation efficiency of the TEVA extraction chromatography method (Chapters 4-6). Information on the amount of ^{241}Am present in the standard solution was not provided by the manufacturer; however, an estimate of the Am was determined from the Pu isotopic information provided with the standard.

The following formula was used to determine the ^{241}Am activity concentration in the Pu solution:

$$Activity\%(Am) = A_{o,241} \times \frac{\lambda_2}{\lambda_2 - \lambda_1} \times (e^{-\lambda_1 t} - e^{-\lambda_2 t}) \qquad \text{Equation 1}$$

where $A_{o,241}$ is the initial activity percent of ^{241}Pu present in the Pu standard on the isotope verification date of March-2005, λ_1 is the decay constant of ^{241}Pu and λ_2 is the decay constant of ^{241}Am and t is the time elapsed from isotope verification to the date of solution preparation for experimental purposes, February- 2008 (35). The estimated ^{241}Am concentration in the Pu solution using the above equation was 0.038% of the total activity.

The presence of ^{241}Am in the standard solution was verified by alpha spectrometry using a standard cerium fluoride (CeF_3) precipitation method (29,36,37). A small aliquot of the Pu aqueous standard was added to a 3 M HNO_3 solution with a total activity concentration equivalent to 2200 Bq/g of solution verified by LSC counting.

Table 2. Plutonium isotopic content of aqueous standard (Isotope Products, 1198-16-1)

Nuclide	[1]Atom %	[1]Activity %	[2,3]Decay Corrected Atom%	[2,3]Decay Corrected Activity %
^{238}Pu	1.4×10^{-3}	0.325	1.4×10^{-3}	0.32
^{239}Pu	97.937	84.355	97.929	84.36
^{240}Pu	2.0542	6.501	2.05	6.50
^{241}Pu	6.1×10^{-3}	8.82	5.3×10^{-3}	7.65
^{242}Pu	1.0×10^{-3}	5.5×10^{-5}	1.0×10^{-3}	5.5×10^{-5}
^{241}Am	Not provided	Not provided	7.9×10^{-4}	0.063 (calc) 0.053±0.003 (obs)

Certificate Date for ^{239}Pu Activity: 01-August-06

Isotopic Verification Date: 22-Mar-2005

[1] The relative uncertainty associated with each value is 15% (±1σ) for the minor isotopes per discussions with the manufacturer.

[2] The ^{241}Am was separated from the batch standard solution on 23-July-2003; however, no separation efficiency or activity percent from ^{241}Am in-growth from ^{241}Pu decay was provided with certificate information. Therefore the ^{241}Am values were calculated based on the decay of ^{241}Pu from the isotopic verification date to the experiment date. Additionally, a small aliquot of the aqueous standard was precipitated and counted by alpha spectrometry to verify ^{241}Am activity.

[3] Decay correction date range: Feb/April-2008

The CeF_3 filters (n=5) were prepared from gravimetric aliquots (Section 2.4), with a total activity concentration of 2000 Bq/filter. Dried filters were counted by alpha spectrometry (Canberra Industries, Inc., Meriden, CT USA) for 10 minutes. The alpha energies of ^{241}Am and ^{238}Pu are between 5.4 and 5.5 MeV and are difficult to resolve by alpha spectrometry because of extensive peak overlap (Figure 2). The relative ratio of ^{241}Am to total alpha activity was determined using the following relationship:

$$\frac{{}^{241}_{\alpha}Am + {}^{238}_{\alpha}Pu}{Total\ Spectrum\ Counts}(obs) - \frac{{}^{238}_{\alpha}Pu\ Activity\ \%}{Total\ Alpha\ Activity\ \%}(calc) = \frac{{}^{241}_{\alpha}Am}{Total\ Alpha\ Activity\ \%} \qquad \text{Equation 2}$$

The observed ratio was determined by peak area integration of the combined ^{238}Pu and ^{241}Am region (channels 573-610, 5.31 to 5.57 MeV) relative to the total counts across the full spectrum (channels 1 to 1024). The ^{241}Am alpha activity percent was 0.053 ±0.003 (1σ). This value was ~40% greater than the expected value of 0.038. Peak area integration of the $^{239+240}$Pu region (channels 522 to 558, 4.96 to 5.21 MeV) relative to the total spectrum counts was also determined. The deviation from the expected activity percent of $^{239+240}$Pu (provided by the manufacturer) was less than 2%. The large discrepancy in the ^{241}Am activity percent was not expected; however, the certificate also stated that the last separation date of ^{241}Am from the ^{239}Pu standard stock solution was in July of 2003. No Am separation efficiency data was provided; if one assumed that the separation efficiency was greater than 99% in July of 2003, then the increased

presence of ^{241}Am in solution was from decay of ^{241}Pu from the separation date to the isotopic verification date.

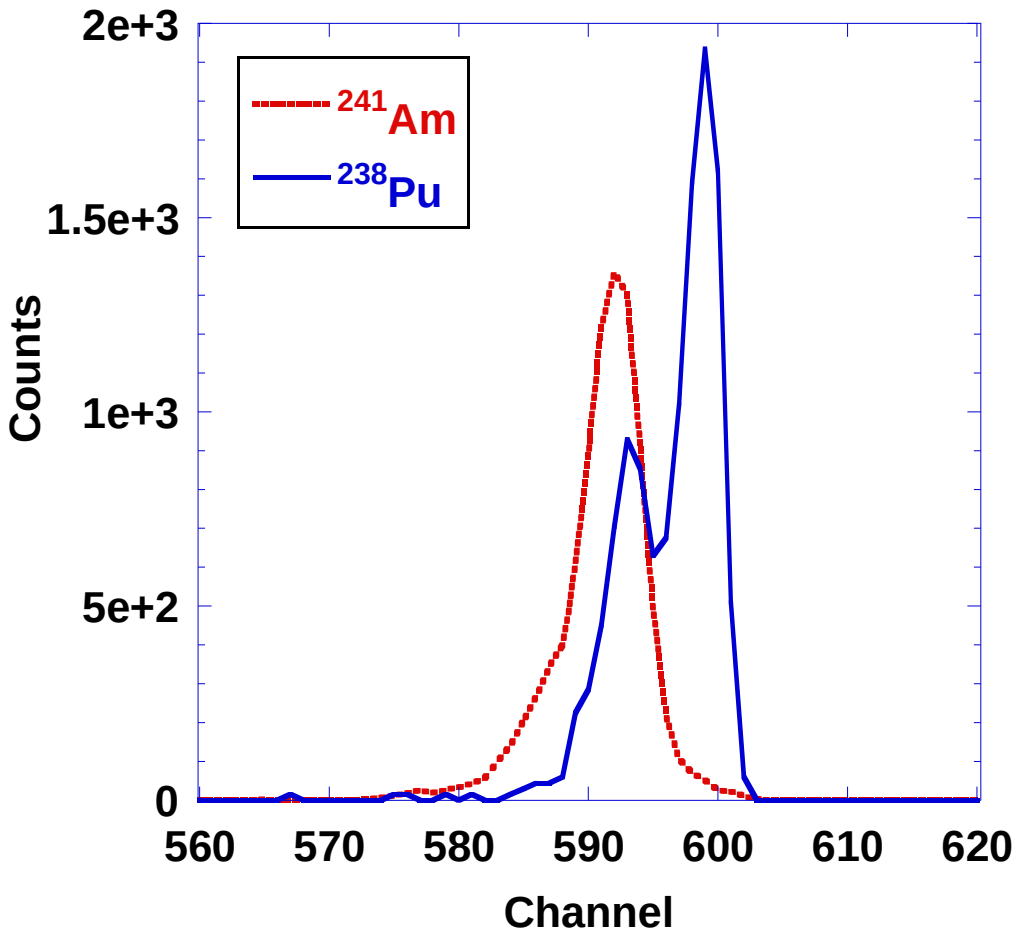

Figure 2. Alpha spectra for ^{238}Pu and ^{241}Am. The spectrum for each radionuclide was acquired separately with an Alpha Analyst system.

The ^{241}Pu activity percent in solution at the date of separation can be determined based on the rate of decay law (35):

$$A_{o,241} = A_{t,241} \times e^{-\lambda t} \qquad \text{Equation 3}$$

where $A_{t,241}$ and $A_{o,241}$ are the activity percent of ^{241}Pu present at the time of isotopic verification and at the time of initial Am separation, respectively. The *t* in Equation 3 is the time elapsed from the date of Am separation to the isotopic verification date, 608 days and λ is the decay constant for ^{241}Pu. The ^{241}Am percent activity concentration in solution, calculated from the date of the last chemical separation, was 0.063%. The relative uncertainty associated with each isotopic mass and activity percent value was ±15%, therefore the value obtained by alpha spectrometry with the CeF_3 precipitated standard was in good agreement with expectations and was used for all activity corrections for the Pu separation studies.

2.4 Cerium Fluoride Precipitation Sample Preparation

High resolution alpha spectrometry samples of Am and Pu were prepared by CeF_3 precipitation for isotopic analysis and actinide separation efficiency determination. This method was chosen based on fast preparation time, high actinide recovery, good energy resolution, and sample reproducibility (29,36,37).

A cerium nitrate carrier ($Ce(NO_3)_3 \cdot 6H_2O$) was added to the sample solution containing the actinides of interest along with an excess of concentrated HF. The sample was set aside for approximately 30 minutes to optimize the formation of the CeF_3 precipitate, Ksp= 8×10^{-16} (38). The relative similarities in size and charge of Ce (and other lanthanides) to the actinides in the tri- and tetravalent oxidation states causes the actinides to co-precipitate with the carrier. The solution containing the precipitate was filtered through a 0.1 µm, 25 mm diameter

polypropylene Resolve filter (Eichrom, Darien, IL USA) and rinsed with DI water. Excess water was driven off with ethanol and the filters were dried prior to alpha analysis. The method described above is a standard method (29) available from the filter manufacturer, Eichrom Technologies, Inc. The filters were also counted by gamma spectrometry and were subjected to mass analysis by inductively couple plasma mass spectrometry using a laser ablation solid sampling technique.

2.5 Alpha Spectrometry

Alpha spectrometry is a useful tool to distinguish between various alpha emitting radionuclides and evaluate isotopic composition. The spectrometer is made up of a series of vacuum chambers that house solid-state semiconductor detectors. Under vacuum, the alpha particles emitted from a sample placed in front of the detector travel the short distance from the filter and deposit their energy within the active region of the detector. The energy deposited by each alpha particle is converted to a charge which is collected, amplified, and binned by a multi-channel analyzer (MCA) which converts the electronic signal to a digital signal. The resulting spectra can be processed to determine the number of counts associated with narrow energy ranges across an entire energy spectrum. A more detailed description of alpha spectrometry can be found in (39).

A 12 chamber alpha spectrometer system (Canberra Industries, Inc., Meriden, CT, USA) was used for all alpha analysis experiments. The passivated implanted planar silicon (PIPS) detectors had an active area of 450 mm^2 and the

sample position with respect to the detector face was fixed using the manufacturer provided sample trays and chamber tray steps. The sample tray was placed in the fourth tray step, which was approximately 16 mm from the detector face. The CeF_3 filters were placed in small polystyrene Petri dishes (30 mm x 10 mm) and covered with an o-ring to prevent filter curling during chamber evacuation.

2.5.1 Detector Calibration

Background spectra were collected over a 24 hour time period for each vacuum chamber prior to and after sample analysis to determine the residual alpha activity in the chamber. The background activity ranged from 0 to $6x10^{-3}$ cps across all vacuum chambers. Higher activity samples, i.e. greater than 50 Bq/ sample, were counted in the high background chambers. Filters with expected activity levels less than 50 Bq were counted in the low background chambers. Each alpha detector was efficiency calibrated using electroplated ^{241}Am and ^{210}Po calibration sources (Table 3). Counting efficiency was determined using the following formula:

$$\frac{Observed\ Counts}{Reference\ Area} x100\% = Detector\ Efficiency \qquad \text{Equation 4}$$

where observed counts were the counts collected in a user specified region of interest (ROI) and reference area was the expected number of counts based on decay corrected activity calculations. Each standard was counted 3 times in a given chamber for 1000 seconds. Alpha detection efficiency was approximately 16% across all detectors for both calibration standards. The spectrometer was also efficiency calibrated with CeF_3 precipitated standards that were developed

in-house. It was important to determine the counting efficiency for a source with the same geometry and that was prepared in similar fashion to experimental samples.

Table 3. Efficiency calibration source information

Calibration Standard	**^{210}Po**	**^{241}Am**
Source ID	HRC-73	HRC-121
Source Type	Electroplated	Electroplated
Active Area	0.5 inches	0.5 inches
Certification Date	1-Aug-2006	1-Dec-1991
[1]Original Activity	2250 Bq	3193 Bq
Half-life	138.38 (days)	432.7 years
[2]Estimated activity (decay corrected)	18 Bq	3106 Bq
Alpha Energy	5.304 MeV	5.484 MeV

[1] Standard uncertainty of ± 5%

[2] Activity as of 18-Mar-09 and 26-Feb-09, for Po and Am, respectively.

A series of CeF_3 filters were prepared with the ^{239}Pu aqueous standard solution using the manufacturer recommended method (29). Total filter activity ranged from 10 Bq to 2300 Bq. The standards were counted for 10 minutes to 2 hours depending on the total activity to achieve a standard counting error of ≤ 2% of the total counts in the 5.15 MeV alpha peak region. The average detection

efficiency for the CeF_3 standard filters, across all activities was 11 ± 1%, which assumes no losses in source fabrication.

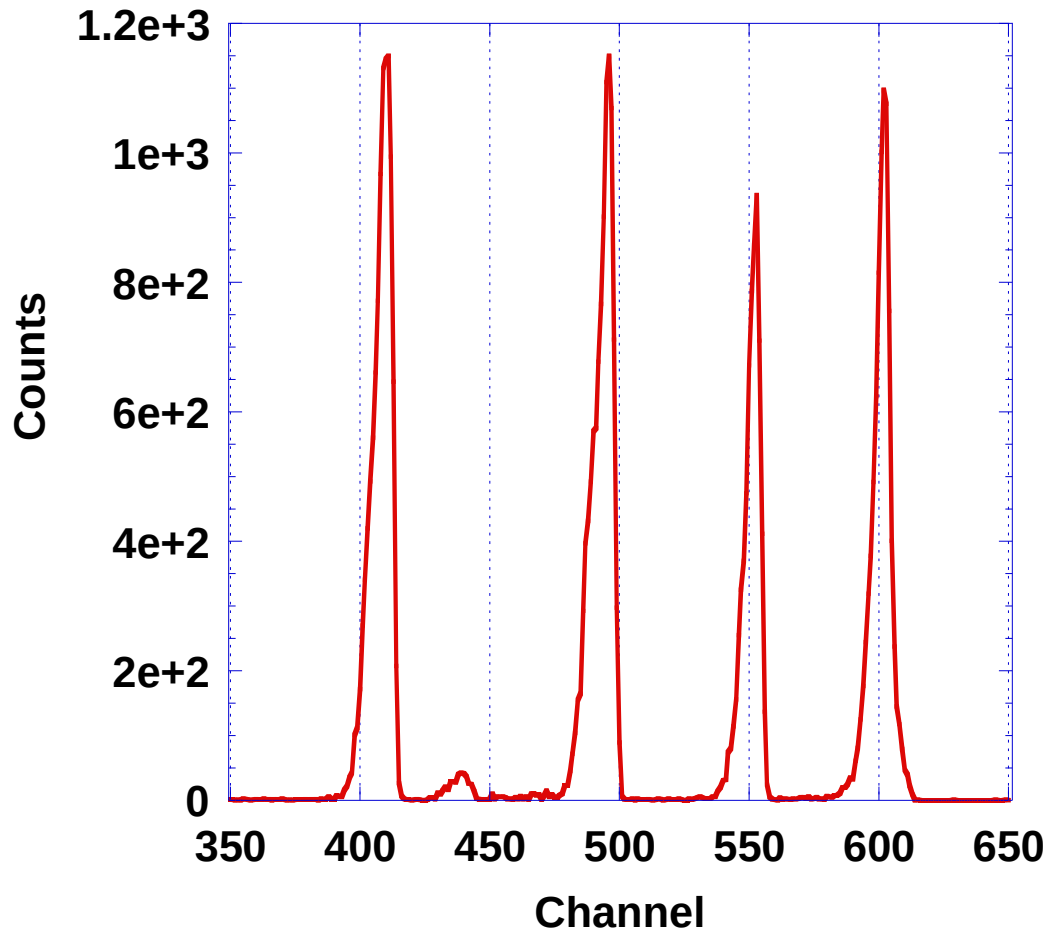

Figure 3. Mixed alpha spectrum for the electroplated source used for detector energy calibration. Source contained a mixture of ^{234}U, ^{235}U, ^{238}U, ^{239}Pu, and ^{241}Am.

Energy calibration was performed with an in-house electroplated mixed actinide source of ^{239}Pu, ^{241}Am and $^{234+235+238}U$. The source pedigree was unknown (i.e., there was no documentation available); however, the energy

resolution was sufficient for calibration purposes. The channel containing the maximum counts associated with the dominant alpha peak was assigned the appropriate alpha energy for each of the previously mentioned radionuclides and a calibration curve was generated based on peak assignment. The mixed alpha spectrum and energy calibration curve are provided in Figure 3 and Figure 4.

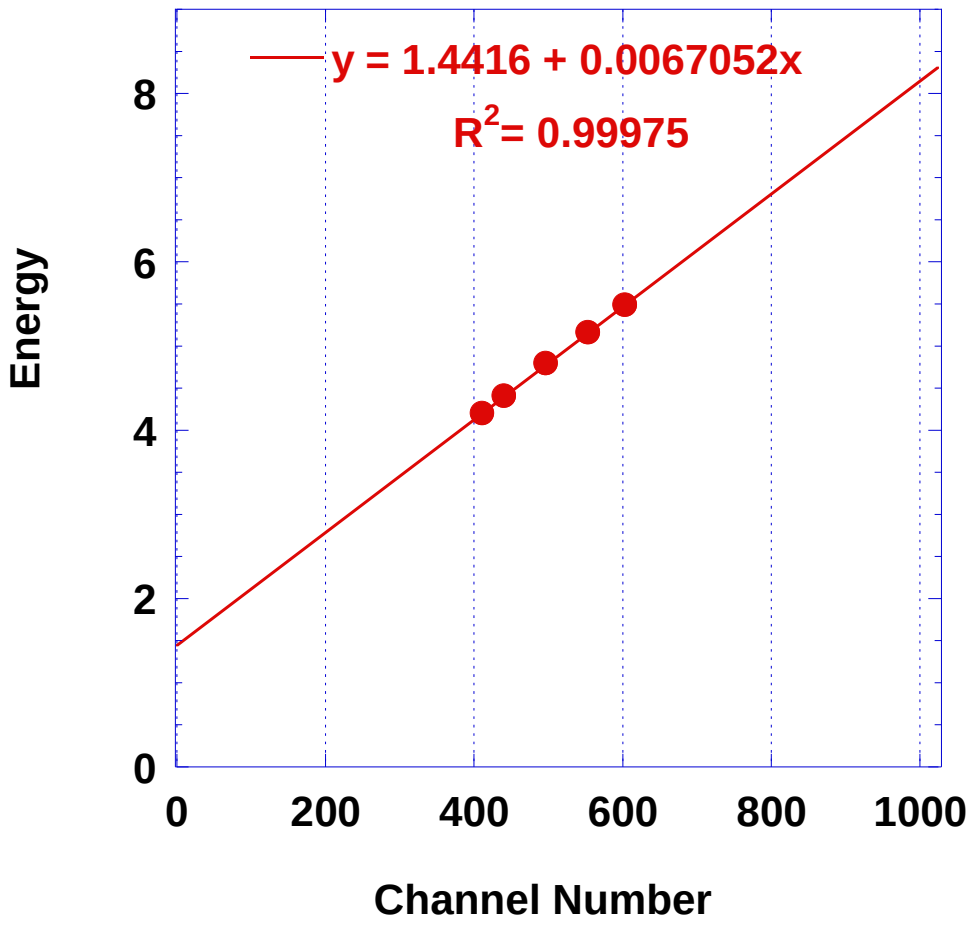

Figure 4. Energy calibration curve for the mixed alpha electroplated source. The equation represents the linear calibration function for energy in terms of the channel number where Energy=1.44 MeV + 0.0067*Channel Number.

2.5.2 Data Analysis

Spectra were obtained in both CNF and IEC file format. The CNF file type is a telnet configuration file which stores the session data for the alpha analyst system. It was used for spectrum viewing and data analysis with the manufacturer software, Genie 2000 (Canberra Industries, Inc.). The IEC file format was opened and re-configured in Microsoft Excel for manual peak integration analysis. Peak area was determined by integrating the number of counts in a ROI. The channel boundary limits of the ROI were based on the alpha energies of the radionuclides of interest and the energy calibration. The energy ranges used for Pu and Am analysis are provided in Table 4. The percent intensity (Column 3) represents the percent of the total alphas emitted from the decay of the radionuclide that are within the specified energy range for a nominal source produced according to the procedure described in Section 2.4.

Table 4. Alpha energy ROIs used for data analysis

Radionuclide	Energy Range (MeV)	% Intensity
$^{239+240}$**Pu**	4.96 to 5.21	>99.9%
^{241}**Am and** ^{238}**Pu**	5.31 to 5.57	>99.9%

2.6 Gamma Spectrometry

Gamma spectrometry is a technique that is commonly used for radionuclide identification and activity determination. The photon emitted from the decaying

nucleus interacts within the active volume of the detector. The energy deposited by the photon produces charge carriers within the active volume that migrate through an applied electric field and are collected at electrical contacts. The current generated by charge carrier collection is processed in terms of pulse height and charge collection time using a preamplifier and an amplifier. For each photon, the amplifier output was fed into a multichannel analyzer where events with energies between 0 and 515 keV were stored in 4096 channels. For quantitative analysis, the spectrometer must be calibrated in terms of photon energy and photon intensity (or flux density). Sample geometry and placement with respect to the detector face also affect detection efficiency. A more detailed review of gamma spectrometry can be found in the literature (39).

2.6.1 Detector Calibration

Separation efficiency and Pu isotopic information were characterized by gamma spectrometry. A broad energy germanium (BEGe) detector (Canberra Industries, Inc., Meriden, CT, USA) coupled with GENIE 2000 Gamma Acquisition and Analysis software (v3.1a) was used for all experiments. Detector specifications include an active area of 38 cm^2, a crystal thickness of 30 mm and a nominal efficiency (relative to a 2” cube of NaI) of 34% with the composite carbon window. The detector was energy calibrated using a standard CeF_3 filter containing 2000 Bq of ^{239}Pu (Source ID: 1198-16-1) developed in-house. The standard was counted for 48 hours and peak analysis was conducted with Interactive Peak Fit (v1.2), which is an add-on component of the GENIE 2000 software. The peaks selected for Pu isotopic identification and Am separation

efficiency from dissolved weapons grade Pu (WGPu) particle solutions are provided in Table 5.

Table 5. Photon energy and radiative yield information used for determining Pu isotopic ratios and Am separation efficiency by gamma spectrometry.

Radionuclide	Photon Energy (keV)	Radiative Yield (%)	BEGE Detector Efficiency
^{241}**Am**	59.54	35.9	0.243
^{239}**Pu**	38.7	0.0105	0.235
	51.6	0.0271	0.243
	129	6.31×10^{-3}	0.179
^{240}**Pu**	45.1	0.045	0.231

Photon energy and percent yield based on information provided by the National Nuclear Data Center, Brookhaven National Laboratory

The efficiency calibration was determined using the Interactive Peak Fit software linear curve fitting function, which estimated a 5th order polynomial as the best fit function:

$$-1.522 \times 10^4(E) - 1.615 + \frac{1.744 \times 10^2}{E} - 1.143 \times 10^4(E^2) + \frac{3.284 \times 10^5}{E^3} - \frac{3.456 \times 10^6}{E^4} = \log(\varepsilon)$$

Equation 5

where *E* is the energy in units of keV and ε is the calculated detection efficiency for a given photon energy. Efficiency values for some of the Pu photons of interest are listed in Table 5.

2.6.2 Data Analysis

The CeF_3 precipitated samples were counted by gamma spectrometry for 24 hours. The total activity of each sample was limited to 2000 Bq to minimize dead time affects across samples and to achieve good counting statistics for Pu isotopic ratio determination. Each CeF_3 deposit contained roughly the same amount of material so that attenuation effects on the intensities of the low energy photons were subsumed into the efficiency function. Three photon energies were used for determining ^{239}Pu content. These photons were chosen based on the relative proximity to the single photon energy useful for ^{240}Pu evaluation. The relative ratio of ^{239}Pu to ^{240}Pu was determined based on the following relationship:

$$\frac{\frac{C_{\gamma,239}}{\varepsilon_{\gamma,239} \times Yield}}{\frac{C_{\gamma,240}}{\varepsilon_{\gamma,240} \times Yield}} = R_{239/240} \qquad \text{Equation 6}$$

where *C* was the net counts in the photopeak, ε_γ was the BEGe detection efficiency, and *Yield* was the radiative yield associated with a given photon emission line. A more detailed description of the gamma spectrometry is provided in subsequent chapters.

2.7 Liquid Scintillation Counting

LSC is a counting technique that is commonly used for determining gross alpha and beta activity in an aqueous solution. An aliquot of the sample solution is dissolved in a scintillation cocktail consisting of an organic solvent, scintillator and emulsifier. Charged particles emitted from the decay of radioactive nuclei transfer kinetic energy to the cocktail. The energy transfer ultimately results in the release of photons by the process of photoluminescence that exit the sample vial and impinge on the photocathode surface of the photomultiplier tube (PMT). The sample vial is situated between two PMTs to increase counting geometry, and the energy deposited is converted to an electrical current. A more complete review of liquid scintillation counting and liquid organic scintillators can be found in the literature (39,40).

2.7.1 LSC Sample Preparation

The LSC cocktail chosen for all experiments was Ultima Gold AB (Perkin Elmer, Waltham, MA USA) because of its stability in the presence of strong mineral acids, high sample capacity and quench resistance. The cocktail consists of a diisopropylnaphthalene (DIPN) solvent with a 2,5-Diphenyloxazole (PPO) fluor. Aliquots for LSC were taken from each sample prior to chemical separation by EC and from each collected fraction resulting from EC. The type of mineral acid and concentration varied depending on the separation procedure used and the type of resin studied, but included HNO_3, HCl and/or HF acids. Aliquot volumes ranged from 0.100 mL to 1 mL depending on the total activity

concentration of the sample. This volume range was well below the sample capacity of the cocktail, i.e. 2.5 mL of 3M HNO_3 per 10 mL of cocktail.

Sample aliquots were placed in plastic, 20 mL LSC vials to which 10 mL of LSC cocktail was added. The sample/cocktail mixture was immediately agitated with a vortex mixer and counted on a Tri-carb 3100 LSC machine (Perkin Elmer, Boston, MA, USA). Samples were prepared in batches with sample blanks and method blanks. The sample blank contained no acid or sample component in the LSC cocktail. Method blanks were prepared for each sample matrix solution type, i.e. 3 M HNO_3, 5 M HNO_3, 4 M HCl, 0.1 M HCl/0.05 M HF/ 0.03 M $TiCl_3$, etc. for each sample volume used.

2.7.2 LSC Counting Method

The counting protocol was optimized for alpha-energy detection in the normal counting mode using QuantaSmart, the LSC operating software. The LSC machine contains a multi-parameter multichannel analyzer (MCA) that has an operational energy range of 0 to 2000 keV. While most alpha decay energies are between 4-7 MeV, most of the energy deposited is dissipated in the solvent, leaving only approximately 1/10 the original alpha energy to interact with the scintillator molecules (41). The proportional decrease in alpha-energy deposition does not hinder detector counting efficiency (~100% for alpha detection) but it does shift the energy spectral output into the beta energy spectrum. The signals for alpha and beta can be partitioned based on signal response time (39,41), however, for the experiments performed only total activity concentration per sample was desired. The peak integration parameters for all actinide studies

were between 50 keV and 1000 keV, denoted as the CPMB region. The low-energy beta particles arising in ^{241}Pu decay fell into the 0 - 50 keV energy region, which was denoted CPMA. All other counting protocol parameters were set to the manufacturer recommended settings with one exception. The samples were set to count for the full count time of one hour or until the counting error reached 2S% (2% of the 2σ standard deviation of the total counts) in the CPMB energy window (50-1000 keV). The 2S% is a standard protocol option that serves as a normalization parameter for the comparison of multiple sample measurements, i.e. the error reported for each measurement represents 2% of twice the standard deviation of the counts collected in the CPMB region of the spectrum. The average background count rate in the CPMB window was 8.83 ± 0.77 (1σ) cpm for sample blanks.

2.7.3 LSC Efficiency Calibration: Mineral Acid Affects

Prior to separation experiments, a series of aqueous Am standards with activity concentrations ranging from 0.5 to 50 Bq ^{241}Am were prepared in 10 mL of LSC cocktail to characterize acid matrix effects on counting efficiency and energy spectrum shifts. It was determined that higher acid concentrations resulted in a 25 to 50 keV energy peak shift. An example of the peak shift due to mineral acid concentration is shown in Figure 5 for 0.5 and 4 M HCl. Although the higher mineral acid concentration affected the peak shape and location, there was no effect on counting efficiency.

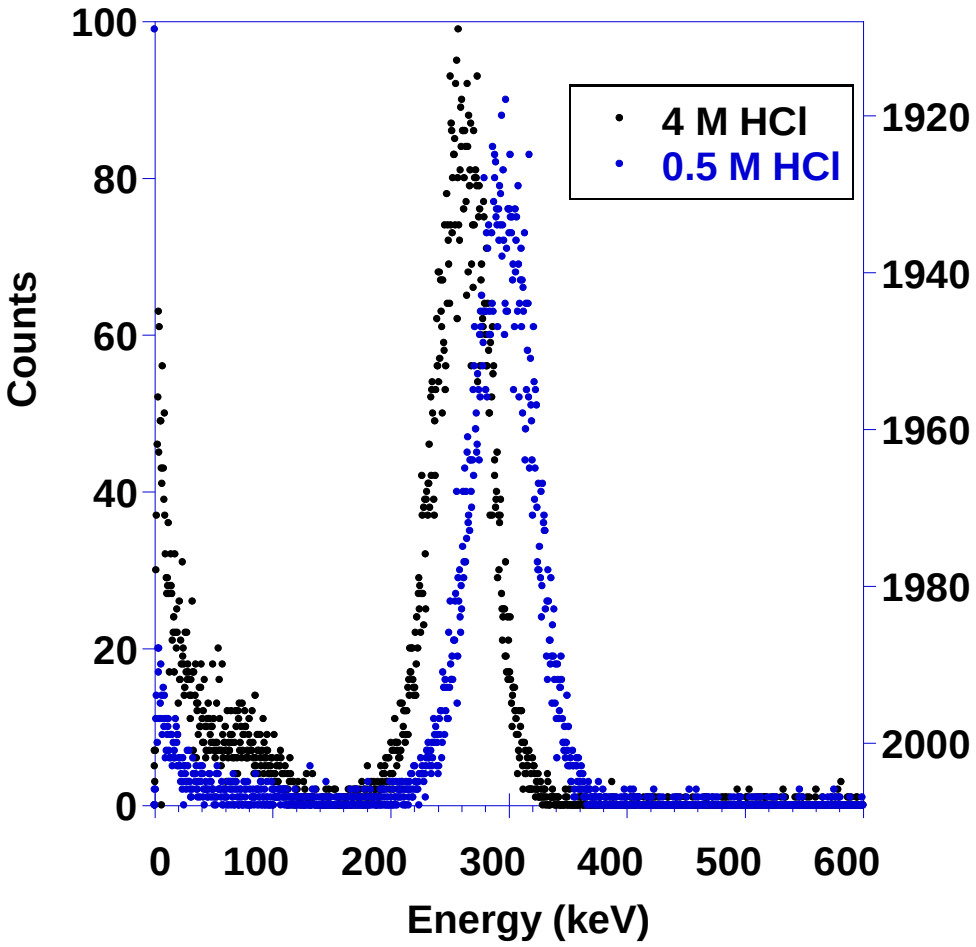

Figure 5. Energy spectral shift due to higher mineral acid concentration of dissolved sample. The ^{241}Am activity concentration was 10 Bq/mL with a total sample volume of 1 mL in 10 mL of Ultima Gold AB LSC cocktail. Peak integral counts are equivalent; therefore the spectral shift (ΔE centroid = 25 keV) did not result in decreased counting efficiency (100±3%).

Samples were also compared across mineral acid matrices, i.e. HNO_3 vs. HCl to mimic the experimental conditions. Figure 6 and Figure 7 compare the sample loading and primary elution (E1) acid matrices for TRU and DGA resins (Chapter 3). The sample loading solution for TRU (and TEVA) separation experiments was 3 M HNO_3 and 5 M HNO_3 for DGA. The Am elution matrices were 0.5 M and 4 M

HCl for TRU and DGA, respectively. The peak shape and centroid energy are significantly different between the loading and elution matrices (Figure 6 and Figure 7); however, there were no significant counting efficiency losses (ε = 100 ± 4%).

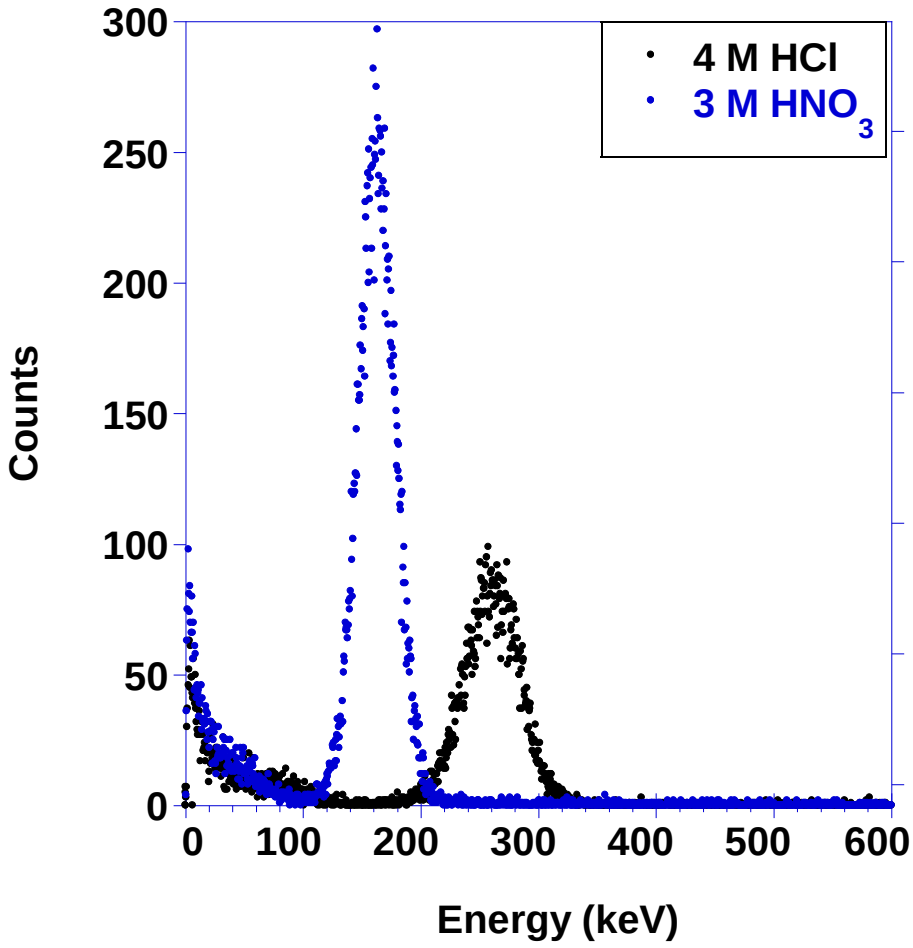

Figure 6. Energy spectral shift from the sample loading acid matrix (3 M HNO_3) to the primary elution matrix for Am (4 M HCl). The ^{241}Am activity concentration was 10 Bq/mL with a total sample volume of 1 mL in 10 mL of Ultima Gold AB LSC cocktail. Peak integral counts are equivalent; therefore the spectral shift (ΔE centroid = 100 keV) did not result in decreased counting efficiency (100±4%).

Significant color quenching occurred in the high HNO_3 solutions within 24 hours of sample preparation. The cocktail changed from clear and colorless to bright yellow, which was attributed to the NO_2 by-product of HNO_3 dissolution and it was determined that samples should be prepared in small batches to minimize chemical and color quench effects (40,42).

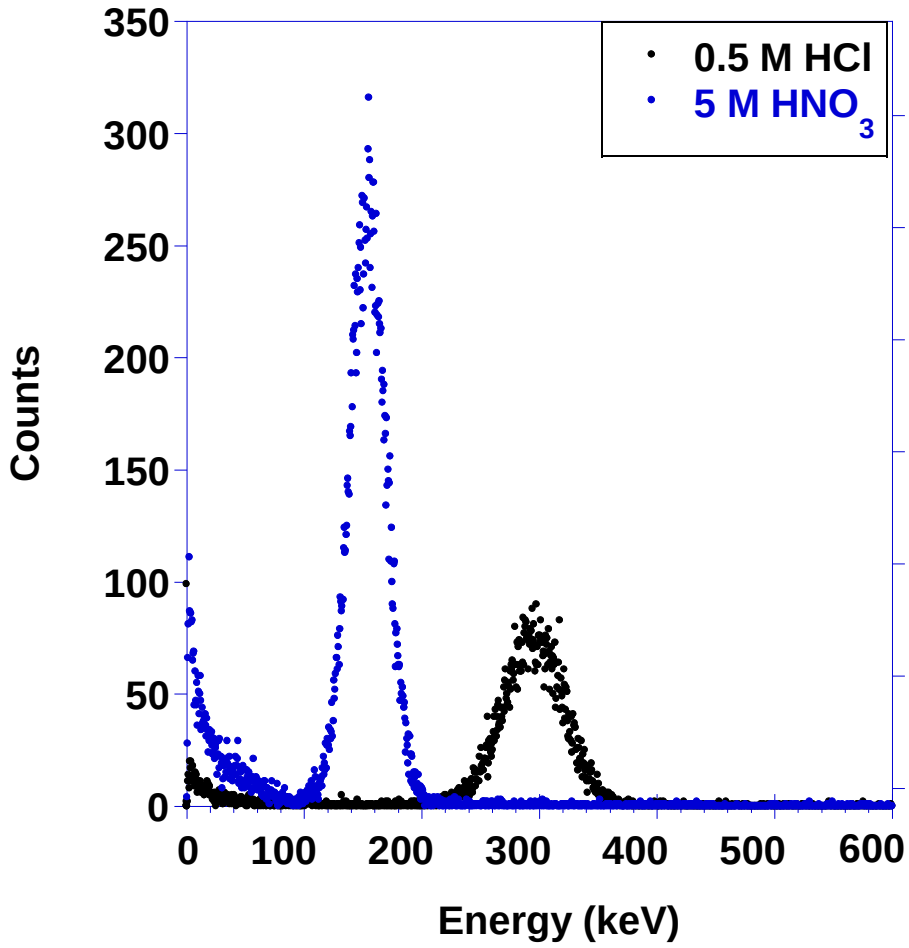

Figure 7. Energy spectral shift from the DGA sample loading acid matrix (5 M HNO_3) to the primary elution matrix for Am (0.5 M HCl). ^{241}Am activity concentration was 10 Bq/mL with a total sample volume of 1 mL in 10 mL of Ultima Gold AB LSC cocktail. Peak integral counts are equivalent; therefore the spectral shift (ΔE centroid = 150 keV) did not result in decreased counting efficiency (100±4%).

2.7.4 LSC Analysis

A batch report was provided by the operating software that contained the sample number, count rate and standard deviation over the user-established energy window range, and a quench indication parameter called the transformed spectral index of the external standard (tSIE). The tSIE value is an estimate of the degree of sample quenching (chemical or color-related) and is used as an indicator of sample integrity. The results of LSC counts with tSIE values below 200 were discarded. Most of the LSC samples collected for the experiments had tSIE values between 300 and 900. The tSIE parameter was used only for qualitative purposes; no corrections were made to the sample count rate value determined by the operating software based on the tSIE parameter. The counting data for each post-separation sample was compared to the pre-separation counting data to determine chemical recovery and method efficiency.

2.8 Inductively Coupled Plasma-Atomic Emission Spectrometry

Inductively coupled plasma atomic emission spectrometry (ICP-AES) is an atomic spectrometry technique that makes use of the energy emitted when an excited electron transitions to the ground state. The electronic properties of each element produce a unique photon emission spectrum. Under most circumstances, ICP-AES is conducted on aqueous samples at or near room temperature. The sample is pumped through a nebulization chamber where it is converted to an aerosol with compressed argon gas. Droplets are carried by the argon into a torch assembly chamber and are atomized and the electrons are

promoted to an excited state by the intense heat (6000-10,000 K) of the argon plasma. Photons are emitted as the excited atom returns to its ground state and are detected by an array of solid state silicon detectors called charge-injection devices (CID). Photons of a given wavelength are absorbed by a particular pixel within the CID, and the signal is converted to a charge that is proportional to the original intensity of photons at that wavelength. For elemental analysis, specific wavelengths are chosen based on the composition of the original sample and the relative intensity of the photons at that wavelength. A more detailed explanation of ICP-AES instrumentation can be found in the literature (43,44).

For elemental analysis experiments (Chapters 3-5), an iCAP 6500 series (Thermo Scientific, Inc., Cambridge, UK) ICP-AES was used. It is an Echelle-based spectrometer, meaning that the wavelengths of the photons emitted by the excited atom are arrayed across an Echelle grating from low to high wavelength. The CID detector is manufactured to a certain size and shape to match the Echelle spectrum (i.e. captures light intensity across the entire wavelength spectrum from 166 to 847 nm). Each bright spot on the CID corresponds to the intensity of photons at a given wavelength, emitted by a specific element, with a brighter spot indicating higher concentration of the element in the sample solution. Additional information about the iCAP 6500 ICP-AES is available from the manufacturer.

2.8.1 Sample Preparation

Immediately prior to sample analysis, a series of single element calibration standards was prepared to determine the detector response over a wide range of

analyte concentrations. Each element was either a Cl^- or NO_3^- salt that was initially dissolved in 10 mL of 3 M HNO_3 with concentrations ranging from 0.1 to 1.0 M. An aliquot of each analyte solution was taken and diluted with 3 M HNO_3 so that the analyte concentrations were between 0.1 and 10 mM. ICP-AES standards were prepared from these solutions using a 1:10 dilution with de-ionized (DI) water. The dilution scheme for each calibration point is provided in (Table 6).

For hot particle elemental analysis experiments (Chapter 5), ICP standards (BDH Aristar, UK) were used for detector calibration. Calibration standard concentrations ranged from 0.1 to 1 mM and were prepared in 1% (wt/wt%) HNO_3. All sample solutions were prepared gravimetrically for ICP-AES analysis. Samples were collected both prior to and after chemical separation of the Am and Pu studies. Hot particles were dissolved and filtered through a polypropylene filter prior to ICP-AES sample preparation.

2.8.2 Instrument Settings

The instrument settings optimized by the manufacturer upon installation were used for all experiments. The plasma parameter settings were as follows: radio-frequency (RF) power at 1150 W, the pump rate at 50 rotations per minute (rpm), the auxiliary argon gas flow at 0.5 L/min, the nebulizer gas flow at 0.51 L/min and the coolant argon gas flow at 12 L/min. The nitrogen purge gas flow was fixed in normal mode.

Table 6. ICP-AES calibration standard preparation

[1]Original Solution Concentration (M)	Aliquot Volume (mL)	3M HNO_3 Added (mL)	Adjusted Solution Concentration		1:10 Dilution for AES in DI Water	
			$[HNO_3]$ M	$[M^+]$ mM	$[HNO_3]$ M	[M] mM
1	0.1	10	3	10	0.3	1
0.75	0.1	10	3	7.5	0.3	0.75
0.5	0.1	10	3	5	0.3	0.5
0.25	0.1	10	3	2.5	0.3	0.25
0.1	0.1	10	3	1	0.3	0.1
Second Dilution for Lower Concentrations						
1	1*	10	3	1	0.3	0.1
0.75	1*	10	3	0.75	0.3	0.075
0.5	1*	10	3	0.5	0.3	0.05
0.25	1*	10	3	0.25	0.3	0.025
0.1	1*	10	3	0.1	0.3	0.01

* Aliquot volumes were taken from the adjusted solution standards.

[1] Original solutions and second dilutions were prepared gravimetrically.

2.8.3 Analyte Analysis

The wavelengths used to determine analyte concentration are summarized in Table 7. The wavelengths were chosen based on relative intensity and potential analyte interferences as suggested by the ICP-AES software provided by the manufacturer. Three replicate measurements were taken for each sample with a sample flush time of 30 seconds and an analysis pump rate of 50 rpm in precision mode. Signal integration time was set at 15 seconds for low wavelength ranges (<234 nm) and 5 seconds for high wavelength ranges (>234nm). Samples run for both pre- and post- separation studies were compared to the element calibration curve for concentration determination and to one another for sorption characterization. The amount sorbed to the extraction chromatography resin was determined using the following relationship:

$$F = 1 - \left[\frac{CPS_{post}}{CPS_{pre}} \times \frac{V_{pre\ ,aliquot}}{V_{post\ ,aliquot}} \times \frac{V_{total\ ,post}}{V_{total\ ,pre}}\right] \qquad \text{Equation 7}$$

where F is the fraction of the analyte remaining on the resin, CPS_{post} and CPS_{pre} are the signal intensity at the analyte wavelength before and after chemical separation, $V_{pre,aliquot}$ is the aliquot volume taken prior to chemsitry, $V_{post,aliquot}$ is the aliquot taken after chemistry, and $V_{total,pre}$ and $V_{total,post}$ are the total volumes of the pre-separation load solution and the post-separation eluent used in the analysis. Elemental analysis of the dissolved hot particles was determined from the raw signal intensity of the element, in units of counts per second (cps) in terms of the functional form fit to the calibration data, derived from signal intensity and a known range of analyte concentrations.

Table 7. Matrix ion photon wavelengths used to determine signal intensity on the ICP-AES.

Counter Ion	Photon Wavelength (nm)	Relative Intensity
Nitrogen	174.2	1.8×10^4
Calcium	393.3	7.0×10^7
Manganese	257.6	1.0×10^7
Magnesium	279.5	5.0×10^7
Zirconium	339.1	3.5×10^6
Silicon	251.6	6.0×10^5
Phosphorous	177.4	1.5×10^5
Iron	259.9	2.0×10^6
Aluminum	167.0	1.83×10^6
Rubidium	424.4	2.5×10^4
Cadmium	228.8	2.0×10^6
Lead	220.3	1.2×10^5
Gallium	294.3	4.0×10^5
Platinum	214.4	1.5×10^5
Titanium	334.9	5.0×10^6
Uranium	367.0	5.0×10^4

The relative intensity value is based on the detector sensitivity for the element over other elements with similar photon wavelengths.

2.9 Inductively Coupled Mass Spectrometry

Inductively coupled plasma mass spectrometry (ICP-MS) is a technique that is commonly used for elemental isotopic abundance analysis. This instrument detects the subtle differences in the mass-to-charge (m/z) ratio of each isotope of an element based on the principle that all the isotopes of a given element will have the same nuclear charge (number of protons) and, consequently, the same probability of having a given ionic charge (electron deficit), but a different atomic mass due to the differences in neutron number. ICP-MS sample introduction for aqueous solutions is similar to ICP-AES, in that the sample is converted to an aerosol with a compressed gas and carried into the plasma torch chamber where it is atomized and ionized by the intense heat of the plasma and induction in the torch region. The ions are forced into an interface region where adjustments in atmospheric pressure and temperature are made (transition into the high vacuum mass collector). Prior to entering the mass collector, a charged metallic lens is used to focus the ion beam into the mass filter. Mass filtration and collection is accomplished by varying the radiofrequency and voltage inside the multipole collector. Small changes in the current and RF parameters allow certain ions to pass through to the detection chamber, while others remain in the quadrupole collector. Ions reaching the detector collide with the dynode, which releases a cascade of electrons and generates a measurable current. A more detailed explanation of ICP-MS can be found in (43,44).

In Chapter 6, Pu mass analysis was performed with an ELAN DRC II ICP-MS system (Perkin Elmer, Inc., Shelton, CT, USA). This system uses a dynamic

reaction cell (DRC) that is situated between the ion focusing lens and the mass collector. The purpose of the DRC is to remove chemical interferences such as polyatomic species (e.g. ^{238}U-H at mass 239), prior to mass analysis (45).

2.9.1 Sample Preparation

A series of ^{239}Pu mass calibration standards was prepared to determine the detector response and limit of detection (LOD) for two different sets of samples. The first set was prepared in 1% (wt/wt%) HNO_3 and mass concentrations ranged from 0 to 100 ng ^{239}Pu/g solution. The second set was prepared for solid analysis using the CeF_3 co-precipitation method previously outlined with the same mass concentrations 0-1000 ng ^{239}Pu/filter. All sample solutions were prepared gravimetrically for mass analysis, including the solutions prepared for filtration. Solution volume was normalized to 10 mL.

2.9.2 Instrument Settings

Instrument settings are discussed in Chapter 6. The operation parameters were optimized by the manufacturer upon installation. The radio-frequency (RF) power was set at 1100 Watts, the nebulizer gas flow at 0.90 L/min, the argon auxiliary gas flow was 1.20 L/min, the plasma gas flow was 15.00 L/min and the vacuum pressure at < $7x10^{-6}$ torr. Prior to analysis, a daily performance system check was conducted with a multi-elemental tuning solution and standard instrument optimization procedures provided by the manufacturer were followed. The system check ensured that instrument sensitivity, analyte precision, oxide and doubly charged ratios were at acceptable levels prior to sample analysis. Aqueous samples were measured consecutively using an autosampler (CETAC

Technologies, Omaha, NE, USA) and atomized in a quartz nebulizer. The solid filter sample measurements were taken manually and the sample was atomized by laser ablation (LSX 500, CETAC Technologies). More details about the laser ablation system are provided in Chapter 6.

2.9.3 Analyte Parameters

The analyte was ionized by introducing the sample as an aerosol into the plasma chamber. The ionic charges of species analyzed by the mass spectrometer were z =1. Raw signal intensity (ion counts per second) was collected for the mass to charge (m/z) ratios of interest (Table 8) and the mass resolution was approximately 1 amu (atomic mass unit).

Table 8. Plutonium m/z ratios used for ICP-MS analysis for both aqueous and CeF_3 co-precipitated samples.

Radionuclide	Mass-to-Charge (M/z) Ratio
^{140}**Ce***	140.116
^{238}**Pu**	238.049
^{239}**Pu**	239.052
^{240}**Pu**	240.054
^{241}**Am/**^{241}**Pu**	241.057
^{242}**Pu**	242.059
*Cerium mass analysis for filter samples only.	

Peak analysis for each m/z ratio was performed manually for each sample. Method blanks were prepared in 1% HNO_3 to determine background peak signal for each m/z ratio analyzed and were run between each pair of samples. The calculations used to determine net signal intensity are described in Chapter 6.

2.9.4 Analyte Interferences

The primary objective of the experiments in Chapter 6 was to determine the relative isotopic abundance (Table 2) of a Pu standard with respect to the dominant isotope, ^{239}Pu. Potential spectral interferences include the formation of the doubly charged actinide (An^{2+}), the actinide-oxide ($An\text{-}O^{2+}$) and the hydride ($An\text{-}H^{+}$). The first two species result in a decrease in the observed m/z ratio and the latter results in an increased m/z+1 ratio. The ICP-MS used for these experiments had a high background signal for the 238 m/z ratio. It was suspected that the elevated signal was due to the presence of natural or depleted U from previous sample analyses or from possible U contamination in the nitric acid used for sample preparation.

CHAPTER 3

EXTRACTION CHROMATOGRAPHY PERFORMANCE - AMERICIUM SEPARATIONS

3.1 Abstract

In this work, physical and chemical parameters associated with extraction chromatography separation procedures to facilitate the development of an automated radioanalytical separations platform are investigated. A vacuum box system was designed in-house, which incorporated a digitally controlled vacuum regulator, multiple valves for optimum evacuation conditions and a stackable lid that can accommodate 15 resin cartridges per lid for discrete sample processing. The vacuum box system was characterized in terms of flow rate reproducibility, matrix effects on flow rate for sequential elution, and actinide separation efficiency using two different types of resin, TRU and DGA. Efficiency characterization included reproducibility at various activity concentrations and in the presence of common matrix interference ions. Results indicate that the columnar kinetics of the resins are sufficiently rapid to run high purity Am samples through the unit over a wide range of flow rates for both resin types. Single matrix interferences at a metal ion ratio of $1:10^6$ relative to Am have little effect on separation efficiency at varied flow rate conditions. It was determined that DGA resin has better sorption/desorption characteristics in terms of Am recovery but is also more sensitive to the presence of Zr and PO_4^{3-} matrix contaminants than the TRU resin. This preliminary data has been used to

develop a modularized actinide analysis procedure that can be transferred to an automated solid phase extraction unit.

3.2 Introduction

A persistent challenge in both the nuclear forensic and environmental sciences is the accurate and timely determination of isotopic information in samples containing a mixture of actinides. Many rapid analysis methods have been developed over the last few years, with most incorporating commercially available extraction chromatography resins for the chemical separation and purification of actinides in aqueous samples (14, 46-50). These resins are preferred by some experimenters over more traditional separations methods such as co-precipitation, solvent extraction and ion exchange chromatography because of the high degree of selectivity of the resin for actinides in the presence of other matrix constituents (15,34,51).

Several automated separation methods have also incorporated these resins into on-line or continuous process monitoring systems for trace analysis in bioassay, environmental and medical isotope applications (16-23). These systems are designed for sequential sample processing, meaning that batch samples are run through the system one at a time. The major disadvantage of this type of system is the increased risk of cross-contamination between samples, especially when non-routine samples are being processed**.** As an example, soil samples collected from areas where nuclear testing/accidents have occurred contain actinide concentrations from trace levels to several milligrams

due to the inhomogeneous distribution of debris and radioactive particulates in the environment (52-56). Under these conditions, it is important to keep each sample isolated - if cross-contamination occurs within the analysis system, critical information that can be used for remediation efforts or source term identification may be compromised. In this respect, many radioanalytical laboratories continue to develop rapid (less than 8 hours) manual methods for time-sensitive samples.

Recent publications (10-12, 25-28) have demonstrated the utility of vacuum-assisted separations for a wide range of sample matrices. A vacuum box system was used to accelerate chemical separations and to process multiple samples simultaneously. This discrete approach to batch sample analysis reduces the risk of cross-contamination between samples and decreases experimental variability within a given batch. In comparison with pressurized extraction chromatography systems, vacuum extraction techniques promote more uniform column performance. Forced flow from a pressurized system can lead to the diminution of column loading capacity. As an example, an over-pressurized column can lead to resin compaction or channeling (formation of preferential flow paths) resulting in a decrease in the number of theoretical plates available for chemical exchange.

Although vacuum-assisted separations are efficient for batch processing, sample through-put is limited by the labor force and individual skill sets. It is the goal of this research to develop automated vacuum-assisted chemical separation methods. Custom built robotic platforms using off-the-shelf laboratory

components are ideal for large scale sample analysis and individual components already exist for portions of the radioanalytical process. Translating manual methods into automated methods requires a greater understanding of the physical and chemical parameters that are important from an engineering standpoint. Each step must be evaluated first on a basic level to determine which portions of the process are critical for achieving acceptable results. Once the fundamental chemical reactions are understood, each step can then be approached from an engineering perspective to optimize the procedure for automation.

Two extraction chromatography resins are discussed in this work, TRU and DGA (Eichrom Industries, Inc.). The extraction properties of these resins are described (30,31) and are used primarily for the isolation of transuranics from various acidic matrices. The parameters that govern actinide extraction efficiency include flow phenomena, diffusion, and extraction kinetics (57). These chemical/physical properties are influenced by the matrix constituents, the extractant loading and mobile phase velocities, the column length, bead size and the operating temperature (24). Each of these factors presents a unique challenge for developing an automated separations method. Pre-packed, 2 mL dry resin cartridges manufactured by Eichrom Technologies, Inc. (Darien, Il, USA) are used in this work. These cartridges reduce column preparation time, minimize variations associated with in-house column packing, provide an efficient way of separating multiple radionuclides from matrix interferences with stackable

cartridges, and provide a working foundation for a modular vacuum box automation platform.

This work evaluates a mixed actinide separations procedure for potential automation. A digitally regulated vacuum box was developed and various physical/chemical parameters were evaluated to establish method boundary conditions. These parameters included engineering controls, such as evacuation rate, pressure regulation, flow rate reproducibility, and cartridge failure. Method efficiency is characterized in terms of flow rate regulation, yield reproducibility at various concentrations, and versatility using aqueous samples containing ^{241}Am. Americium was selected for preliminary study based on its tendency to exist in a single trivalent oxidation state in acid solution and well-characterized extraction behavior on both DGA and TRU resins under the given matrix conditions (30,31). Efficiency characterization studies were performed on high purity ^{241}Am solutions and solutions containing matrix interferences such as Mg, Mn, Zn, Fe, Al, Zr, Ca, and PO_4^{3-}. These interferences are found in natural and anthropogenic matrices and are problematic for current radioanalysis protocols (30,58).

3.3 Materials and Methods

3.3.1 Vacuum Extraction System

The vacuum extraction unit developed for this project is made from acid-resistant polyvinyl chloride (PVC) plates, held together with a PVC adhesive and coated stainless steel screws, (Figure 1, Chapter 2). The box configuration consists of 3 rows, each accommodating 5 resin cartridges for the ability to

process 15 samples simultaneously. The unit is connected to an acid vapor trap and a digital vacuum regulator (DVR, J-Kem Scientific, Inc.) which controls the atmospheric pressure within the box. The vacuum line connecting the rotary vane vacuum pump (Edwards, Model No. EW-79303) to the DVR is split and a ball valve and precision needle valve have been added with the inlets of each valve terminating at the DVR outlet. The ball valve allows for rapid evacuation of the vacuum box with loss of DVR fidelity, the precision needle valve limits the evacuation rate of the system but improves the fidelity of the DVR. This combination of valves allows for rapid evacuation of the system and increased pressure stability over the course of the separation experiment.

3.3.2 Reagents

Nitric and HCl acid solutions were prepared from reagent grade acids (ACS reagent grade, Merck KGaA, Darmstadt, Germany) and DI water (18 MΩ·cm, Millipore, Billerica, MA, USA). Aluminum nitrate nonahydrate crystals (ACS, reagent grade, Merck KGaA) are added to the sample solution to increase the NO_3^- concentration for enhanced Am uptake on the TRU resin (30).

Extraction chromatographic resins were obtained from Eichrom Technologies, Inc. (Darien, IL, USA) in 2 mL pre-packed polypropylene cartridges. Two resins, TRU and DGA were chosen for experimental evaluation. TRU resin (50-100 µm), contains a mixed octylphenyl-N, N-di-isobutyl carbamoylphosphine oxide (CMPO) and tri-n-butyl phosphate (TBP) stationary phase and is primarily used for isolating and separating tri-, tetra- and hexavalent actinides (30). DGA is a diglycolamide-based extraction chromatographic resin (DGA- normal, 50-100 µm,

40% w:w) that is also effective for actinide separations (31). Each pre-packed 2 mL cartridge is shipped dry and therefore must be pre-treated with the acid matrix prior to use. This step serves several purposes – 1) the surfaces of the beads are wetted, establishing the interface for chemical exchange, 2) it equilibrates the resin for the nitrate system, 3) it washes the cartridge of any fines or residual impurities and 4) it allows the NO_3^- to fill voided or dead space to maximize the working capacity of the cartridge and provide a more uniform flow.

3.3.3 Radionuclide Standards

Americium stock solutions were prepared from traceable standard solutions. An ^{241}Am stock solution (1198-21-4, 01-Jul-06, Isotope Products, Valencia, CA, USA) was prepared in 3 M HNO_3· 1 M $Al(NO_3)_3$ with activity concentrations from 5 to 50 Bq/mL of stock solution. Aliquots of the original sample matrix and each subsequent fraction were taken and the activity of each was measured by liquid scintillation counting, LSC (Tri-carb 3100, Perkin Elmer, Boston, MA, USA) with 10 mL of Ultima Gold AB cocktail (Perkin Elmer, USA) as the counting medium. The LSC samples were counted for 60 minutes or until the counting error reached 2S% (2% of the 2σ standard deviation of the total counts) in the CPMB energy window (200-2000 keV). The 2S% is a standard protocol option that serves as a normalization parameter for the comparison of multiple sample measurements, i.e. the error reported for each measurement represents 2% of twice the standard deviation of the counts collected in the CPMB region of the spectrum. The average background count rate in the CPMB window was 8.83 ± 0.77 (1σ) cpm for method blanks.

3.3.4 Flow Rate Characterization

The relationship between vacuum setting and flow rate was evaluated in terms of precision and accuracy using a 3 M HNO_3 solution. The vacuum set point was programmed into the DVR and 10 mL of acid solution was added to each of the sample reservoirs. The DVR activation switch was set to “Run Program” which opens the solenoid valve to allow the box to draw down to the specified vacuum set point. The times required for the vacuum box to reach the set point and for the sample reservoirs to empty were recorded for each resin cartridge. Once the reservoirs emptied, the DVR activation switch was returned to the neutral position and the box was allowed to return to equilibrium with ambient conditions. The experiment was repeated under the same conditions at various vacuum settings to determine flow rate vs. vacuum setting relationship for an average cartridge. Additionally, the matrix effects vs. flow rate were evaluated for each method fraction, i.e. column preparation, sample loading, column rinse and elution matrices.

3.3.5 Americium Separation

A sample reservoir (30 mL polypropylene Luer-lock syringe, B-D, NJ, USA) was connected to the top of the 2 mL resin cartridge. The resin bed was pre-treated with 5 mL of the HNO_3 sample matrix solution prior to sample loading, followed by 10 mL of the ^{241}Am stock solution. These two eluate solutions were collected together in a labeled 50 mL centrifuge tube. Sequential column elutions were performed to rinse the Am in place and/or strip it from the resin bed. The sample loading and unloading matrices and volumes for the TRU and DGA

resins were chosen based on the optimum parameters (K' values) for Am (31,34). The loading matrices for TRU and DGA were 3 M HNO_3 ·1 M $Al(NO_3)_3$ and 5 M HNO_3, respectively. Americium was selectively removed from the resin with 4 M HCl for TRU and 0.5 M HCl for DGA. A summary of the elution matrices is provided in Table 9**.** Each fraction was collected in a 50 mL centrifuge tube and aliquots were counted by LSC to verify activity concentration.

Table 9. Method elution matrices used for ^{241}Am separation.

Resin	TRU	DGA
Resin Preparation	3 M HNO_3	5 M HNO_3
Sample Load	3 M HNO_3 $Al(NO_3)_3$	5 M HNO_3
Rinse	3 M HNO3	5 M HNO_3
Elution 1	4 M HCl	0.5 M HCl
Elution 2	4 M HCl	0.5 M HCl

3.3.6 Elemental Matrix Interference Effects

The interference species were evaluated on both TRU and DGA 2 mL pre-packed resin cartridges at various vacuum settings. Ionic solutions were prepared in a HNO_3 loading matrix based on the sample loading conditions listed in Table 9. Total ion concentration for all experiments was approximately 2.5 mM, which is approximately one to two orders of magnitude higher than the theoretical resin capacity for Am (or Eu surrogate) (30,31,34). Iron, Ca, and Mn were

chloride salts, and Al and Zr were nitrate salts. Potassium phosphate salt was used for the PO_4^{3-} ion studies. Solutions were equilibrated at least 1 week prior to use. All chemicals and reagents used were of analytical grade or better.

Each single ion matrix solution (10 mL) was run through a row of pre-treated (wetted) resin cartridges (n = 5) on the 3x5 vacuum box system and collected in 50 mL centrifuge tubes. Total ion concentration was determined by inductively coupled plasma absorption emission spectrometry, ICP-AES (iCAP 6000 Series Thermo Scientific, Cambridge, UK). The solutions were diluted by a factor of 10 with DI water prior to analysis. Calibration curves were run for each ion based on 0-10 mM standard solutions gravimetrically prepared in 1 % HNO_3 solution. The wavelengths used for determining signal intensity were chosen from the instrument software database based on relative signal intensity and minimized spectral interferences, listed in Table 10. The nitrogen signal was collected for baseline intensity to monitor the stability of the apparatus during analysis. The manufacturer-recommended analytical parameters were used. Three replicate measurements were taken for each sample with a sample flush time of 30 seconds in Precision analysis mode and a sample integration time of 15 seconds.

Americium separation and efficiency experiments (Section 3.3.5) were repeated with each of the 2.5 mM single ion solutions at two separate vacuum settings – 275 and 575 torr. Each matrix solution was spiked with ^{241}Am at an activity concentration of 50 Bq/mL of solution. Aliquots of each sequential elution

were counted by LSC to determine the Am separation efficiency of the TRU and DGA resins in the presence of the selected ions.

Table 10. Matrix ion photon wavelengths used to determine signal intensity on the ICP-AES.

Counter Ion	Photon Wavelength (nm)
Nitrogen	174.2
Calcium	393.3
Manganese	257.6
Magnesium	279.5
Zirconium	339.1
Silicon	251.6
Phosphorus	177.4
Iron	259.9

3.4 Results and Discussions

3.4.1 Vacuum Extraction System Characterization

The vacuum box developed for this project is modeled after an automated solid-phase synthesis unit currently used in biotechnology research (59,60). The in-house design (Figure 1, Chapter 2) included a viewing window (clear PVC front panel) for flow observations, recessed cartridge inserts for increased stability for separation procedures requiring stacked cartridges, and a recessed

channel lid with a low viscosity, self-leveling silicon gasket. The lock-tight lid was designed for secure, reproducible placement (movement only in the z-axis, up-down) and contamination control purposes. The box was coupled to a digital vacuum regulator (DVR) and characterized in terms of control and reproducibility of the internal pressure of the box, which affects the flow rate of the system. The time required to reach the pre-selected set-point was dependent on the absolute difference between the initial/ambient pressure inside the vacuum box and the evacuation end point. The high degree of reproducibility of the time required to evacuate the box can be used as a performance indicator for the system.

The evacuation rates for the vacuum system using 15 pre-packed 2 mL TRU resin cartridges are provided (Figure 8). The error bars represent a 1σ standard deviation for the evacuation rate assuming a 5 torr variability in the DVR readout, a 3 torr variability in the ambient pressure (once the box is in use the ambient pressure adjusts slightly) and 0.5 second variability in the recorded time. At vacuum settings close to ambient conditions, i.e. > 625 torr, it is believed that the DVR read out does not accurately reflect the draw down pressure conditions in the box. During the initial draw down phase, the large solenoid valve is used to maximize the volume of air removed from the box. This solenoid valve is controlled by the digital “open/close” response. This response time (~0.1 seconds) is slow compared to the time required to evacuate a small volume of air (61). Once the vacuum set-point is established, the variability in the set-point is controlled via the precision needle valve. In the middle range of vacuum settings, the mean evacuation rate, 30 ± 2 (1σ) torr/sec, is fairly constant. As the vacuum

pressure decreases below 275 torr, the evacuation rate decreases, therefore the optimal operating range for the current vacuum system was set for 275 and 575 torr, to monitor the system fidelity in subsequent experiments.

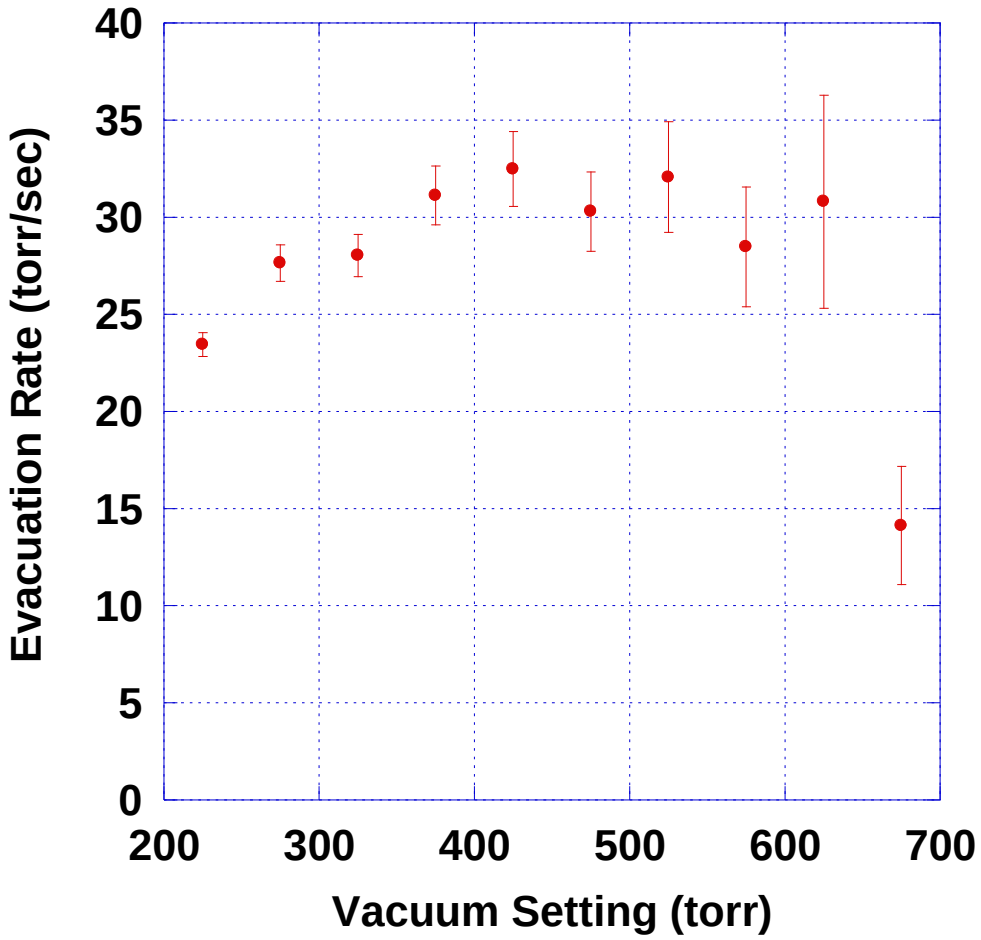

Figure 8. The rate of evacuation of the vacuum system based on ambient pressure conditions and pre-programmed vacuum set points using the 2 mL TRU cartridges and a HNO_3 matrix.

The relationship between flow rate and the DVR pressure settings for the vacuum system with 3 M HNO_3 as the loading matrix system is linear and reproducible (Figure 9).

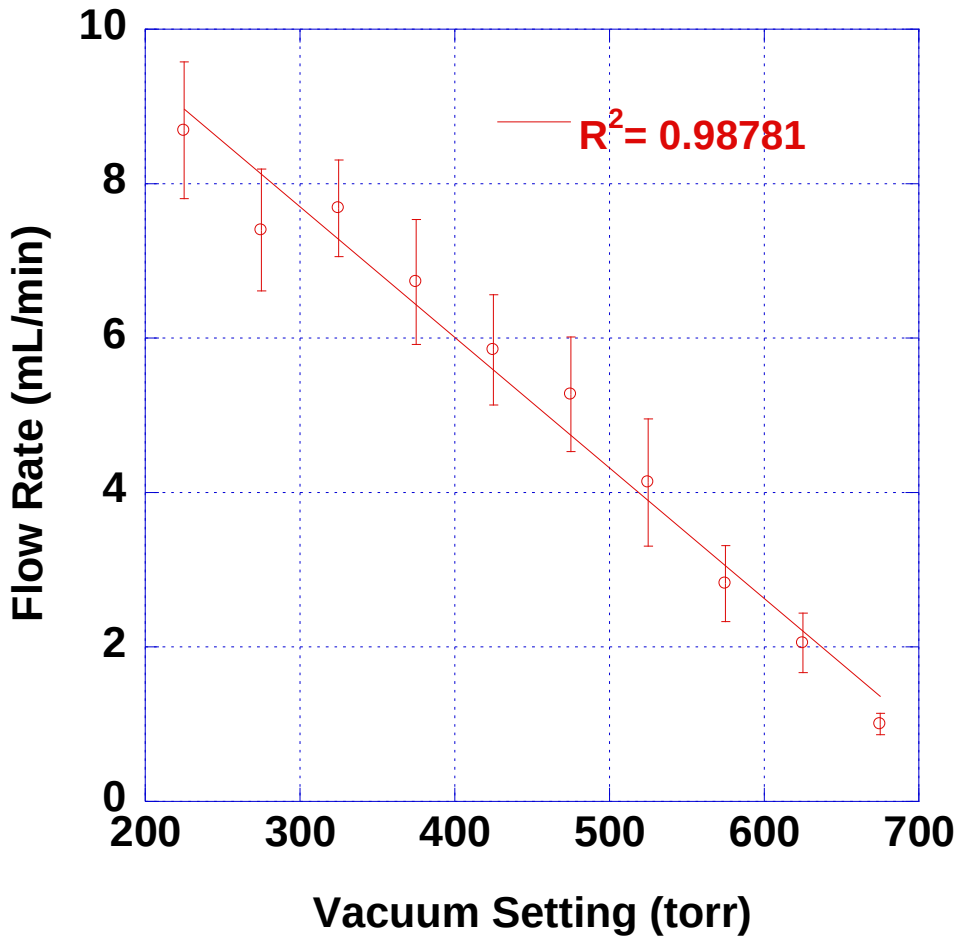

Figure 9. The relationship between flow rate and vacuum setting for the 3x5 vacuum box using a 3M HNO_3 matrix solution. Each data point represents the average flow rate taken over 5 trials for 5 separate 2 mL pre-packed TRU resin cartridges.

Cartridges were tested at various x-y locations in the lid and no positional dependence associated with preferential flow rate was observed. Slight variations in the physical packing characteristics of the resin cartridges can also influence the rate of flow (57).While using pre-packed (batch produced) cartridges reduces packing variations, there are observable differences in flow rate ($0.4 \leq 1\sigma \leq 0.9$ mL/min) within a given batch of resin cartridges. The cause of this variation was not studied in detail; however, the end result is that in a given batch of samples, some resin cartridges run dry during the procedure. In chromatography experiments, this is considered unfavorable. Data presented herein indicate that the flow rate variation does not affect the separation efficiency of Am (see Section 3.4.2).

For a given separation procedure, various matrices are used in sequence to control the isolation of the actinide(s) of interest from other constituents. The matrices used for the selective removal and recovery of ^{241}Am for both TRU and DGA resins (Table 9) and their influence on flow rate are presented (Figure 10 and Figure 11). There is a significant difference in the resin preparation step between the two resins. In this step, the resin cartridges are wetted with 5 mL of the nitric acid solution. The wetting characteristics of the resin can have an effect on the porosity and mobile phase velocity (57). Initial characterization work for the DGA resin (31) observed that the resin did not readily wet in nitric acid solutions. In addition to wetting characteristics, viscosity and ionic strength can have an effect on flow rate. The sample loading solution for the TRU resin contains 1 M $Al(NO_3)_3$, which is added as a salting agent to increase the free

NO_3^- concentration in solution (30). The $Al(NO_3)_3$ increases the viscosity of the solution, resulting in a slower flow rate as compared to the fractions using only nitric acid.

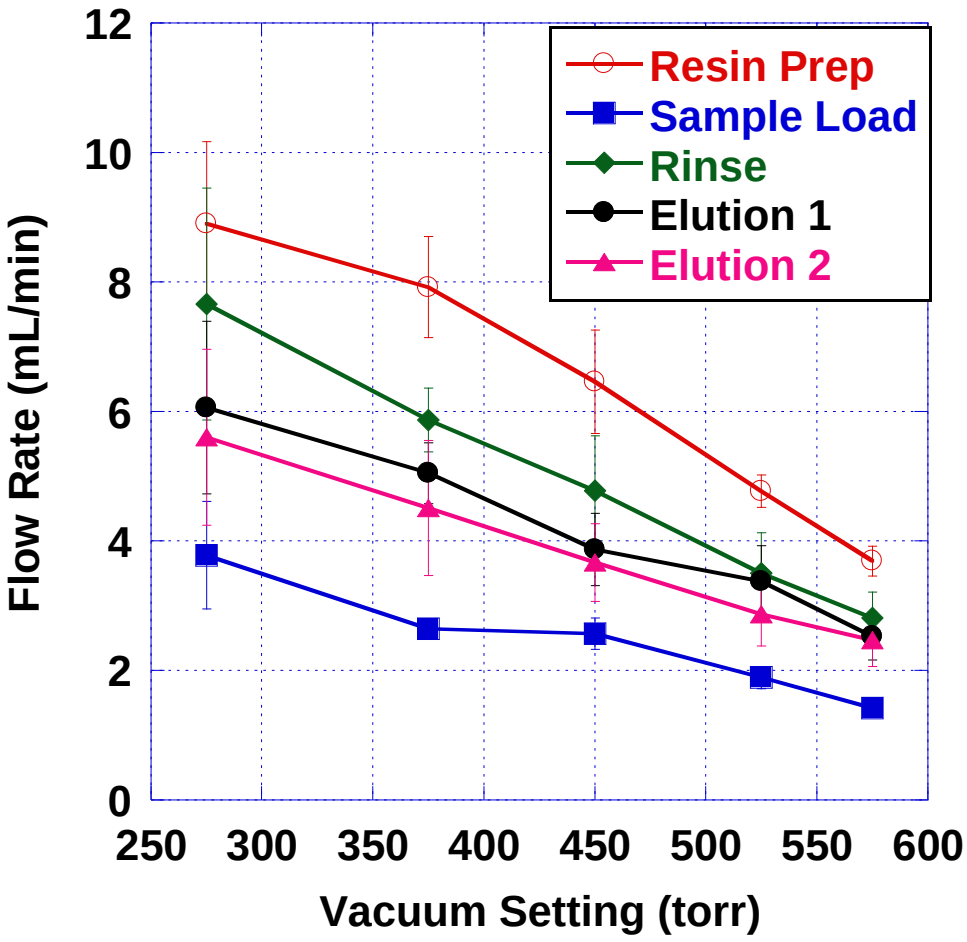

Figure 10. Elution matrix effects on flow rate for the 2 mL pre-packed TRU resin cartridges at various vacuum settings. Each data point represents the average flow rate over a row of resin cartridges (n=5), for 5 separate trials, with new resin cartridges used for each trial.

The data presented establish clear differences in flow rate based on the type of resin, the elution matrix and resin packing variability. These parameters result in non-uniform elution rates, therefore optical sensors will be required to monitor evacuation of the sample reservoir for an automated method.

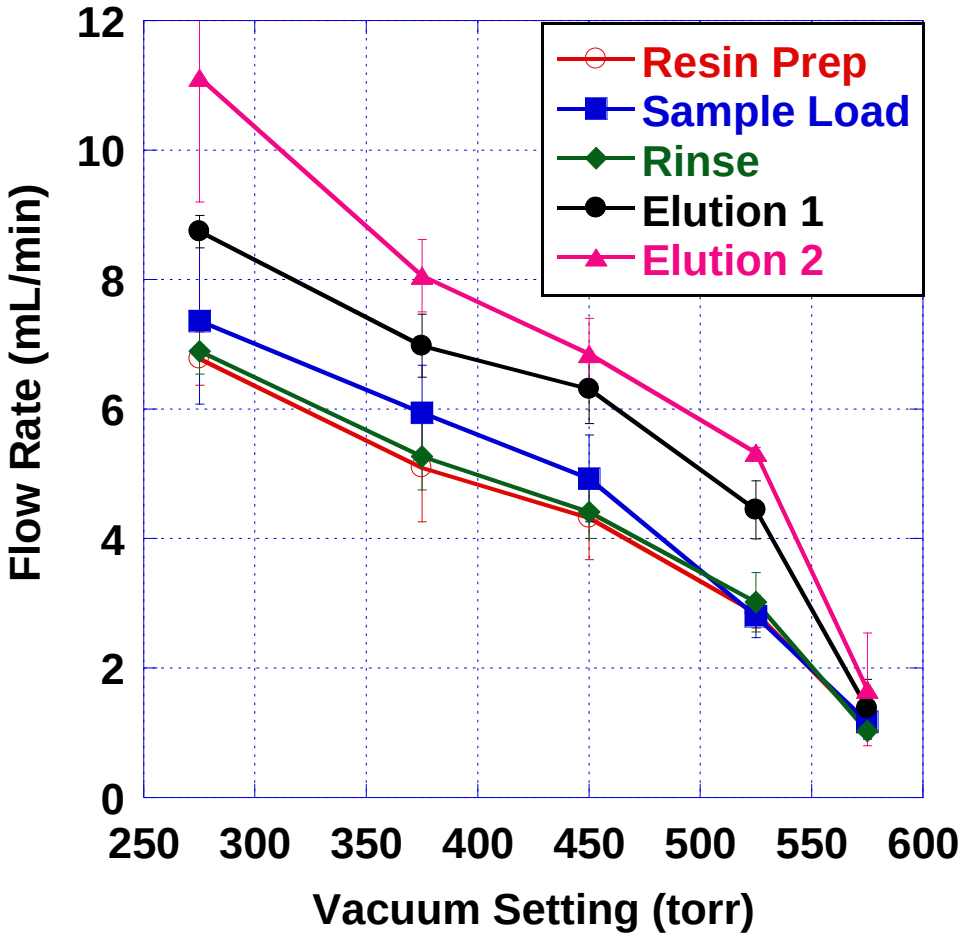

Figure 11. Elution matrix effects on flow rate for the 2 mL pre-packed DGA resin cartridges at various vacuum settings. Each data point represents the average flow rate over a row of resin cartridges (n=5), for 5 separate trials, with new resin cartridges used for each trial.

3.4.2 Effects of Flow Rate on Americium Extractions

The influence of flow rate on the loading and unloading efficiencies of Am solutions was evaluated for both TRU and DGA resins (Figure 12and Figure 13).

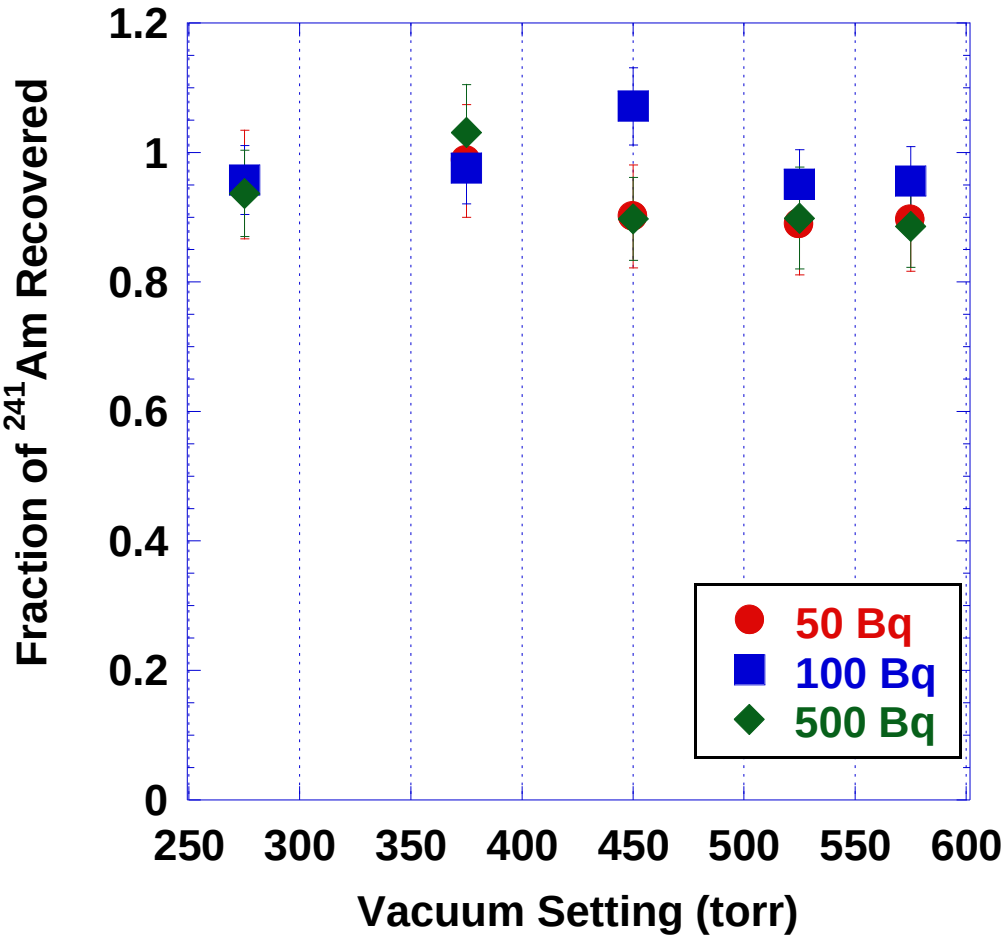

Figure 12. Extraction efficiency of ^{241}Am on 2 mL TRU cartridges at various activity concentrations. The average extracted fraction is 0.92 ± 0.04 (±1σ). Each data point represents the average value for a row of 5 cartridges at a given vacuum setting.

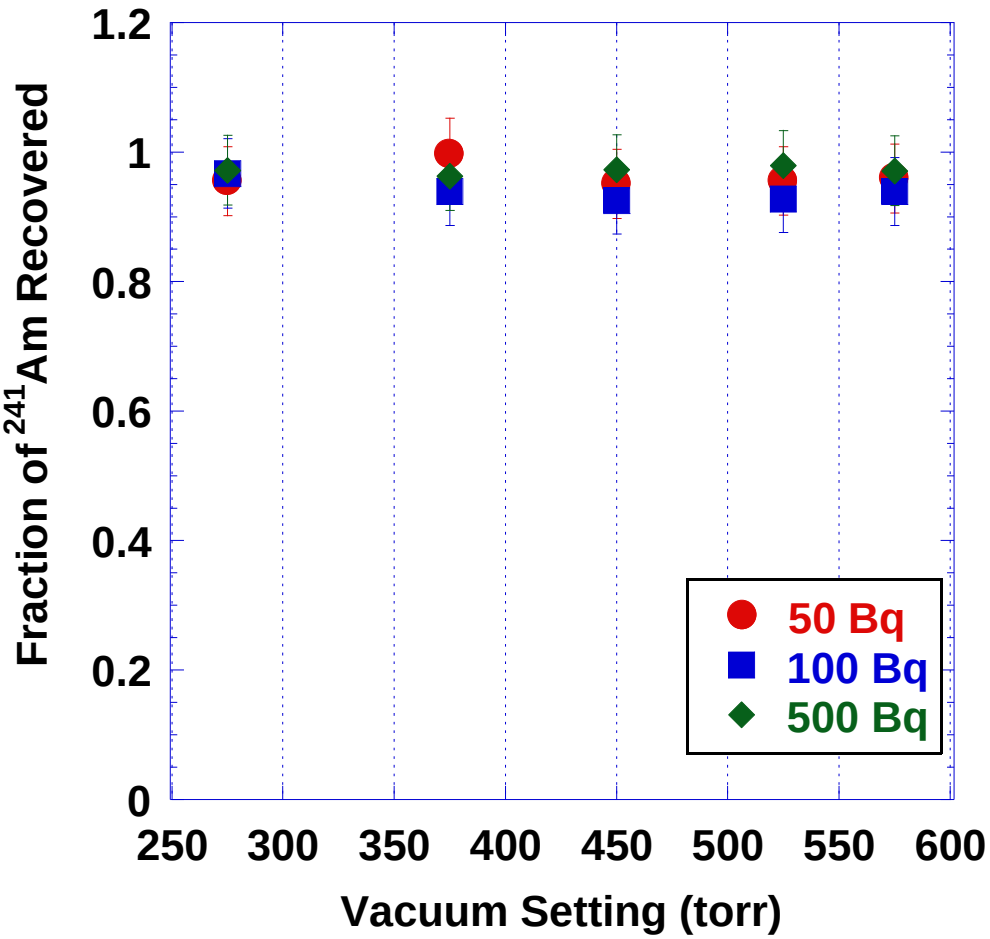

Figure 13. Extraction efficiency of ^{241}Am on 2 mL DGA cartridges at various activity concentrations. The average extracted fraction is 0.96 ± 0.02 (±1σ). Each data point represents the average value for a row of 5 cartridges at a given vacuum setting.

These studies were conducted with various activity levels of ^{241}Am; 50, 100 and 500 Bq. Trials (n = 5 resin cartridges per trial) were completed for each resin type at each of the activity levels mentioned above at vacuum settings of 275, 375, 450, 525 and 575 torr. The extraction kinetics are fast enough to maintain Am elution efficiencies of greater than 80% for both types of resin over a wide range of flow rates (1-10 mL/min). These data provide valuable information for

the development of the automated procedure in that fine control or continuous monitoring of the flow rate is not necessary.

3.4.3 Sorption of Elemental Matrix Interferences

Extraction chromatography efficiency is governed by the electromechanical properties of the resin, the metal ion species formed in solution, and the sorption/desorption kinetics of the metal species with the resin (15). The presence of matrix contaminants in solution can influence actinide speciation and, at higher concentrations, other metal-ion species can saturate the resin binding sites. In addition, some of the matrix contaminants may persist throughout the separations procedure and become problematic for sample analysis measurements. Actinide analysis is usually preceded by a sample pre-treatment step to remove potential matrix interferences for optimized separation efficiency; however, trace levels of contaminants may remain in solution. For high purity samples, Am sorption/desorption kinetics are rapid for both TRU and DGA resins, therefore residence time (flow rate) does not need to be closely monitored. These experiments were conducted to determine how single ion contaminants interact with the resin at various flow rates and what effect the ion has on americium separation efficiency. Bulk sorption characteristics of the matrix contaminant ions on the TRU resin versus vacuum setting are presented in Figure 14. Each bar represents the mean fraction of matrix ion retained on the resin (n = 5) after sample loading (total volume = 10 mL). It should be noted that the error reported is representative of the relative standard deviation for n=5 samples, to highlight reproducibility.

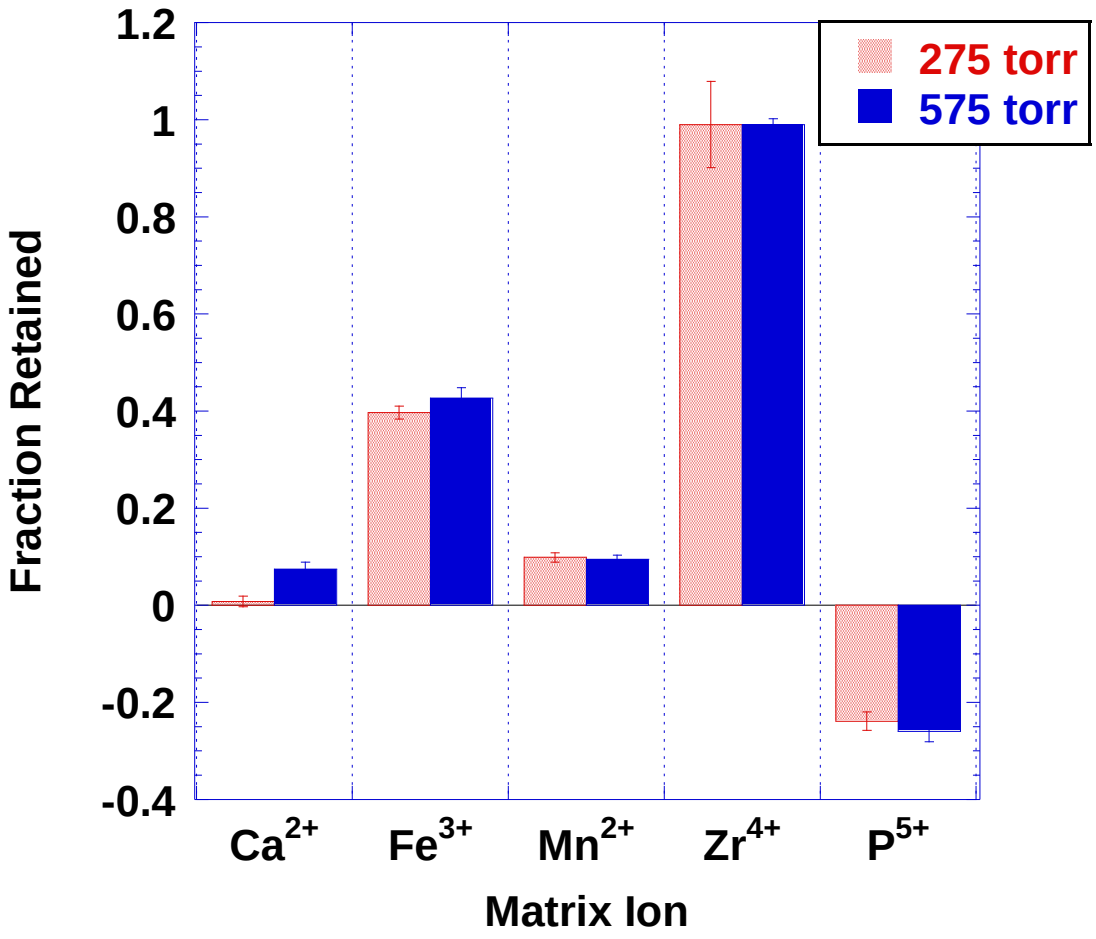

Figure 14. Sorption of interference ions at various vacuum settings using 2 mL TRU resin cartridges (n = 5). Ion concentration is 2.5 mM in a 3M HNO_3· $Al(NO_3)_3$ loading matrix.

Counter ion retention on the TRU resin occurred in the following order Ca < Mn < Fe < Zr. The excess P signal, resulting in a negative retention fraction is due in part to the TBP loss during sample loading. These results are in agreement with studies on the initial characterization of the TRU resin (30). Longer residence time (slower flow rate, higher vacuum setting) slightly enhances Ca and Fe uptake, but does not significantly influence the other ions.

Ion sorption studies were also conducted with the DGA resin. The sample matrix contained 2.5 mM of the ion in 5 M HNO_3. Calcium and Zr strongly sorb to the DGA resin, while the rest of the matrix ions show no affinity (Figure 15).

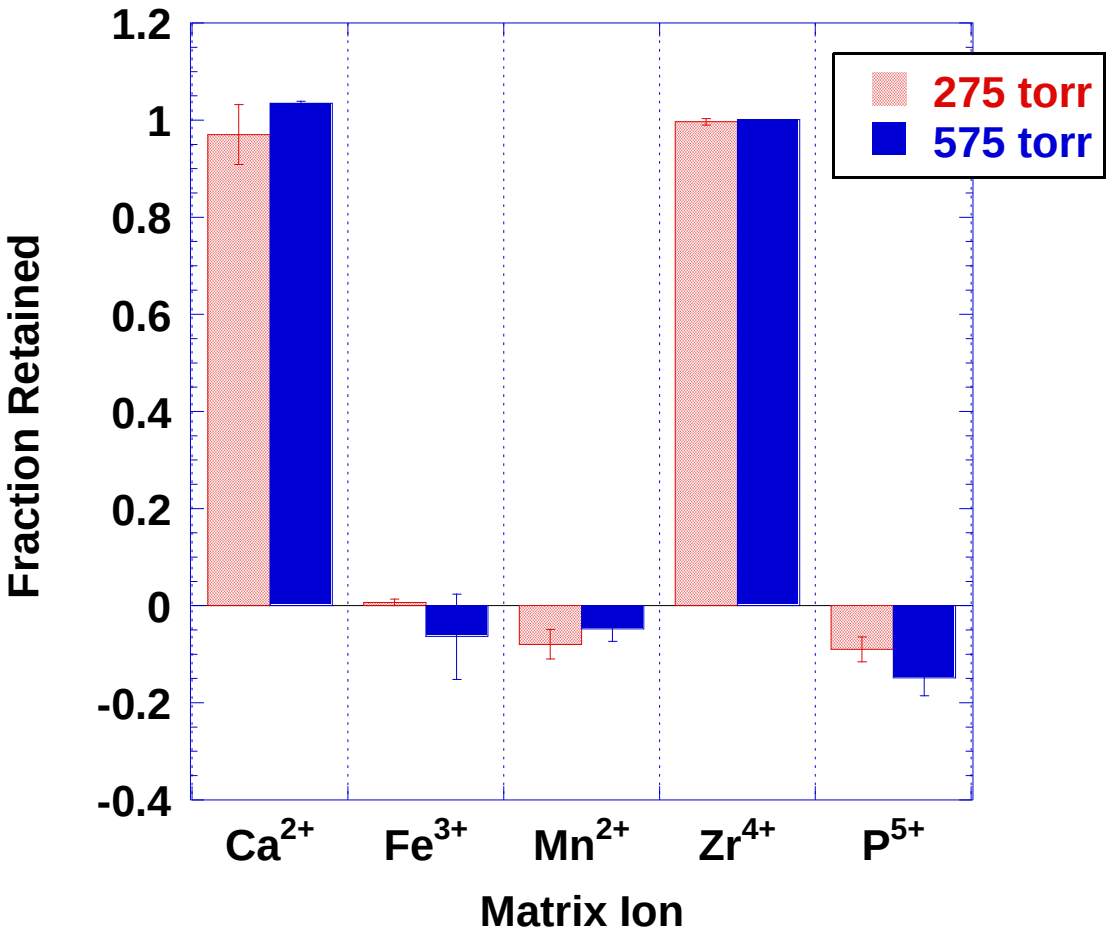

Figure 15. Sorption of interference ions at various vacuum settings using 2 mL DGA resin cartridges (n = 5). Ion concentration is 2.5 mM in a 5 M HNO_3 loading matrix.

Iron and Mn are presented for comparison with the TRU results; however, it should be noted that the experimental error is greater than the reported fraction

values for these ions. An excess of P^- in the post-separated sample is observed, which cannot be accounted for by extractant stability, as with the TRU resin. This may be attributable to non-spectral chemical or physical interferences (62). The results agree with the batch uptake experiments (31). In comparing the sorption characteristics under high and low flow rates, there are no observed differences in ion uptake.

3.4.4 TRU Resin Capacity of Selected Metal Ions

Initial characterization studies (30) experimentally determined the TRU resin metal ion capacity using neodymium nitrate ($Nd(NO_3)_3$). The resin capacity value was experimentally determined as 4.1 mg of Nd/mL of resin. This value is less than the mathematically derived value of 5.49 mg/mL of resin; therefore, the manufacturer of the resins provides a working capacity value which conservatively estimates the operational resin capacity to be half the calculated capacity. The manufacturer also provides the working capacity for Am as determined from the molar equivalence of Nd and Am in the extraction equilibrium equations:

$$Nd^{3+} + 3NO_3^- + 3E \leftrightarrow Nd(NO_3)_3 \cdot E_3 \qquad \text{Equation 8}$$

$$Am^{3+} + 3NO_3^- + 3E \leftrightarrow Am(NO_3)_3 \cdot E_3 \qquad \text{Equation 9}$$

The extractant molecule (CMPO) is represented by E in equations 1 and 2. Therefore, the TRU resin capacity of Am can be calculated using the following formula:

$$\frac{\text{mass capcity (Nd)}}{\text{MW(Nd)}} \times \text{MW(Am)} = \text{mass capacity (Am)} \qquad \text{Equation 10}$$

For the pre-packed 2 mL resin cartridges, the working capacity (50% of theoretical capacity) is expected to be approximately 9.2 mg of the Am metal ion. The early TRU resin characterization studies (30) also evaluated the elution behavior of selected cations from TRU and determined that the lanthanides and Zr exhibited a high affinity for the resin. In the current work, the mass loading of Zr is 2.5 mg/sample. The theoretical capacity of Zr can be derived from the resin capacity for Nd and the extraction equilibrium equations from literature (63-68):

$$\text{Zr}^{4+} + \ 4\text{NO}_3{}^- \ + \ 2\text{E} \leftrightarrow \text{Zr(NO}_3)_4 \ \cdot \text{E}_2 \qquad \text{Equation 11}$$

$$\text{Zr(NO}_3)_2{}^{2+} + \ 2\text{NO}_3{}^- \ + \ 2\text{E} \leftrightarrow \text{Zr(NO}_3)_4 \ \cdot \text{E}_2 \qquad \text{Equation 12}$$

The theoretical capacity of the TRU resin for the Zr metal ion is approximately 5.21 mg /mL of resin. This is also the operational working capacity for the 2 mL resin cartridge (i.e. 50% of 5.21 mg Zr/mL of resin bed * 2 mL of resin per cartridge). It can be assumed that Zr mass loading in the current work is less than TRU working capacity; therefore, Am adsorption should not be affected by the presence of Zr in solution.

Iron is also retained by the TRU resin cartridge under the given experimental conditions. The resin loading capacity of Fe^{3+} can be qualitatively determined as previously described for Am and Zr (65,69,70).

$$\text{Fe}^{3+} + \ 3\text{NO}_3{}^- \ + \ 3\text{E} \leftrightarrow \text{Fe(NO}_3)_3 \ \cdot \text{E}_3 \qquad \text{Equation 13}$$

The theoretical capacity of the TRU resin for the Fe^{3+} metal ion is approximately 2.13 mg/mL of resin, and the operational working capacity of the 2 mL TRU resin cartridge is 2.13 mg. The mass loading of Fe in the samples tested ranged from 5.47 to 7.43 mg. From Figure 14, it is evident that 40% of the Fe present in the sample sorbed to the TRU resin, which equates to 2.2 to 3.0 mg of Fe, in agreement with the calculated column capacity. If it is assumed that the TRU resin is saturated with Fe^{3+} nitrate species, then adsorbed Am is effectively out-competing the Fe species for the extractant. This assumption is supported by the initial characterization studies of the TRU resin (30) where the Am:Fe capacity (K') ratio is approximately 100:1, and by solvent extraction studies of actinide recovery with CMPO /TBP from high level nuclear waste matrices (65,69). Increased Fe^{3+} concentrations of greater than 1 mM affect Am sorption to the TRU resin and in most procedures, the experimenter reduces the Fe to the divalent oxidation state prior to running the column.

3.4.5 DGA Resin Capacity for Selected Metal Ions

The extractant and metal ion loading capacity of the DGA resin was determined (31). The extractant loading capacity was 0.246 mmol of N,N,N',N'-tetraoctyl-3-oxapentanediamide per mL of resin bed or 0.592 mmol per 2 mL resin cartridge. Metal ion capacity was evaluated with europium nitrate, $Eu(NO_3)_3$ on the DGA resin column and was equivalent to 0.077 millimoles (11.7 mg) of Eu per mL of resin bed, with the extraction equilibrium equation:

$$Eu^{3+} + 3NO_3^- + 3E \leftrightarrow Eu(NO_3)_3 \cdot E_3 \qquad \text{Equation 14}$$

where E now represents the diamide extractant molecule.

The elemental sorption characteristics of selected ions to the DGA resin is provided (Figure 15). Both Ca and Zr have a high affinity for the DGA resin. These data are supported by previous extraction studies with N,N,N',N'-tetraoctyl-3-oxapentanediamide (TODGA) for both liquid-liquid and chromatography methods (31, 71-73). In these studies, the ion to extractant molar ratio is 1:2 and 1:4, for Ca and Zr, respectively. Using this information and the extractant loading capacity, the metal loading capacities of Zr and Ca on DGA can be determined using the following equation:

$$\frac{E\ capacity}{mL\ of\ resin} \times \frac{ion}{E} \times MW_{ion} = Mass\ Capacity \qquad \text{Equation 15}$$

where *E capacity* is the extractant loading capacity (0.246 mmol), *ion/E* is the metal ion to extractant molar ratio (1/4 for Zr and 1/2 for Ca) and *MW* is the molecular weight of the Ca or Zr ion. The Zr loading capacity is approximately 5.61 mg Zr/mL of DGA resin, which is also the working capacity for the 2 mL cartridge (i.e. 50% of 5.61 mg Zr/ mL of resin bed * 2mL of resin per cartridge). In the current study, approximately 2.45 mg of Zr is loaded onto the column. This mass value is below the working capacity of the 2 mL DGA resin cartridge. Both Zr and Am show high affinity for the DGA resin, therefore, decreased Am extraction efficiency in the presence of Zr may be a result of direct competition for the coordination of DGA. Calcium mass loading per sample is 1.00 mg and the working capacity for the 2 mL DGA resin cartridge is approximately 4.93 mg. Under these mass loading conditions, Am efficiency is not expected to be influenced by the total adsorption of Ca to the resin.

3.4.6 Effects of Elemental Matrix Interferences on ^{241}Am Separation Efficiency

A summary of the matrix ion effects on the method efficiency for Am on both the TRU and DGA resins is provided (Table 11).

Table 11. ^{241}Am separation efficiency for TRU and DGA resins in the presence of selected ions.

Matrix Ion[a]	275 torr	575 torr	275 torr	575 torr
	DGA[b,c]		TRU[b,c]	
Calcium	104 ± 3	100 ± 1	101 ± 6	100 ± 1
Iron	100 ± 2	99 ± 2	96 ± 2	100 ± 1
Manganese	103 ± 3	100 ± 3	118 ± 8	103 ± 3
Zirconium	90 ±3	87 ± 4	93 ± 3	100 ± 1
Phosphate	83 ± 3	99 ± 1	100 ± 2	103 ± 1
None	97 ± 3	97 ± 3	94 ± 2	89 ± 3

[a] [Matrix Ion] = 2.5 mM

[b] ^{241}Am Activity = 500 Bq/sample, verified by LSC

[c] Efficiency standard deviation (n=5, ±1σ)

Studies were conducted at fast flow rates (6-8 mL/min, 275 torr) and the manufacturer recommended flow rate (1-2 mL/min, 575 torr). The TRU resin method efficiency is not affected by flow rate in the presence of single matrix contaminants. This indicates that the kinetics of the interactions between the extractant and metal ligand are sufficiently rapid to be run over the range of flow

rates tested. In comparison with the trials conducted with the high purity Am solution, the method efficiency for DGA resin decreased by ten percent in the presence of Zr and PO_4^{3-}. Flow rate effects on method efficiency are not observable in the Zr spiked matrix. From the loading capacity calculations, the uptake parameters presented in (31) and discussions earlier in this work, the presence of Zr should not affect Am retention.

The presence of Zr in the sample matrix contributes to Am elution band spreading, which leads to the decreased column efficiency (Figure 16). In ideal, high purity solutions, Am is eluted from DGA with 0.5M HCl within the first 23 free column volumes (FCV, where 1 FCV = mobile phase volume =0.66 mL) or 15 mL solution for the 2 mL DGA resin cartridge, with less than 0.5% of the activity remaining on the column. In the presence of macro-quantities of Zr, greater than 7% of the Am activity remains on the column after 20 mL elution volume and is eluted in the second elution matrix fraction (Elution 2, with total volume = 15 mL).

The presence of PO_4^{3-} decreases the DGA separation efficiency for Am more significantly at the higher flow rate. The organic extractant on the DGA resin is a tridentate ligand with two carbonyl and one ether oxygen donor groups that form chelated rings around the metal-ligand species (31,74,75). The carbonyl groups are less likely to attach to the metal ion if it is has already formed phosphoryl or mixed nitrato- phosphoryl complexes with the PO_4^{3-} ions in the matrix. This decrease in efficiency in the presence of PO_4^{3-} is not seen in the TRU resin studies. The organic extractant on the TRU resin is a monodentate ligand, with a

phosphoryl donor group; therefore it should successfully compete with the PO_4^{3-} metal species in solution.

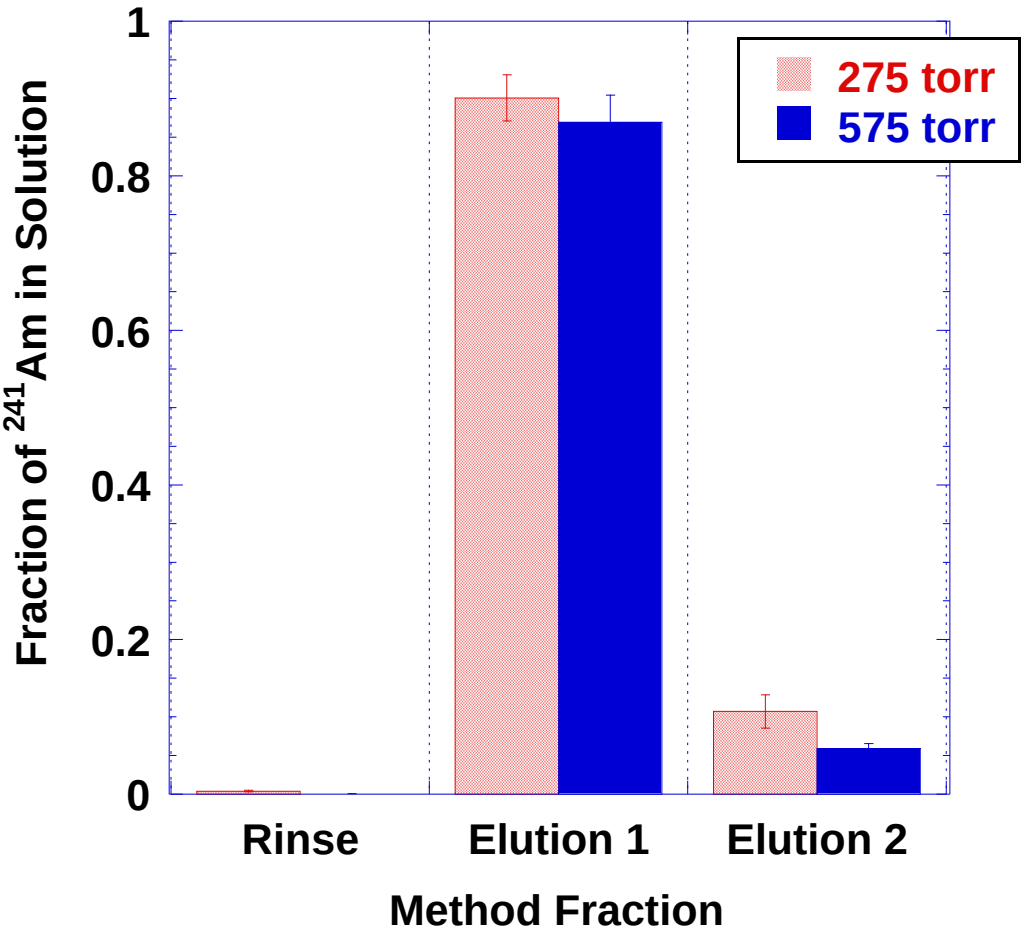

Figure 16. Fraction of ^{241}Am present in each method fraction, with original loading matrix containing 2.5 mM Zr in solution. The fraction matrices are defined in Table 9. The fraction labeled Rinse is the rinse fraction immediately following sample loading (total volume = 8 mL). Elution 1 is the primary Am stripping fraction (total volume = 20 mL) and Elution 2 is the second stripping fraction (for residual Am collection). Trials were conducted at 575 and 275 torr vacuum settings with n = 5 cartridges or samples per trial.

3.5 Concluding Remarks

Vacuum-assisted extraction chromatography is ideal for discrete, simultaneous batch processing; however, the methods currently used with this system require further parameterization to determine which aspects of the procedure need to be monitored. Establishing boundary conditions with regards to precision, versatility and reproducibility provide valuable information from both an economical and engineering standpoint. In this work, we have shown that precision flow rate is not required for reproducibility using two different separation procedures and resins for Am isolation from other matrix constituents. Sample evacuation rates vary between resin cartridges resulting in some resin beds running dry. This parameter is important from an automation standpoint, in that each sample reservoir will need to be monitored with optical sensors for total evacuation. From a chemistry standpoint, this parameter does not affect Am separation efficiency under the conditions tested. Studies are continuing with other resins and actinides to develop an automated mixed actinide separations procedure based on these preliminary data.

CHAPTER 4

EXTRACTION CHROMATOGRAPHY PERFORMANCE -PLUTONIUM SEPARATIONS

4.1 Abstract

The effects of columnar flow rate on the sorption/desorption efficiency of Pu to TEVA extraction chromatography resin has been characterized in both high purity aqueous systems and in aqueous systems containing common matrix ion interferences. This study is part of the continued effort to develop an automated vacuum extraction chemistry unit that is suitable for rapid actinide separations. Previous work demonstrated that columnar kinetics in DGA and TRU resins had little effect on the separation efficiency of americium when present in high purity solutions and solutions with selected interference ions. In this work, the Pu system is evaluated in terms of redox reagent addition, sample aging, columnar kinetics, and the influence of matrix ions on extraction efficiency. The results of this work showed that Pu extraction with TEVA resin is insensitive to flow rate for high purity systems; however, in the presence of other common matrix ions, separation efficiency was greater for those experiments run at lower flow rates.

4.2 Introduction

Automation of radioanalytical procedures can lead to increased productivity, which becomes of particular importance in emergency response situations where thousands of samples may need to be analyzed for contamination control and public health concerns (4, 52-56,76,77). These procedures must provide highly

accurate, reproducible results for a wide range of sample matrices and analyte concentration levels, especially in cases where information can lead to suppositions about the source term and ultimately affect policy decisions. In the last decade, there have been several publications demonstrating the use of continuous flow-through radioanalytical systems, where each sample is processed consecutively (16-18,22,47). The major disadvantage of a flow-through automation system is that samples are processed sequentially. If a sample does not fully dissolve, or has higher than expected analyte concentration, there is increased risk of contamination or blockage of the flow-through system. The goal of this project is to develop an automated radioanalytical platform, where each sample in a given batch is processed simultaneously, in a discrete, isolated fashion thereby eliminating potential cross contaminations or process failures.

Radioanalytical methods can be sub-divided into modules for platform automation development, sample dissolution/pre-treatment, chemical separation, source preparation, and analysis/data processing. Each of these components must be evaluated in terms of the physical/chemical parameters to determine the engineering specifications of the automated system. In this work the chemical separation module for automated analysis is examined - where the unit consists of a vacuum box modeled after a commercially available automated solid-phase synthesis unit.

Extraction chromatography (EC) methods are well-suited for automated chemical separations as demonstrated in various continuous flow-through

separation units (16-23). The EC resins have high analyte selectivity, simplistic elution schemes, rapid kinetics, and they can be stored dry prior to immediate use (24). The manufacturer, Eichrom Technologies, Inc. packages the resin into cartridges, which reduces preparation time and minimizes variations associated with in-house packing. The cartridges are stackable, providing an efficient way of separating multiple radionuclides based on analyte affinity for different extractant compounds. There are manual EC methods available that use vacuum box technology to accelerate the separation procedure; however, these methods are not optimized for an automated unit.

In previous work, engineering controls, such as evacuation rate, pressure regulation, flow rate reproducibility, and cartridge failure were established (Chapter 3). The method investigated in this communication is the mixed actinide separation procedure recommended by the manufacturer (78). The mixed actinide sample is loaded onto two stacked resin cartridges, TEVA and TRU (or DGA). Actinides in the tetravalent oxidation state (i.e. Pu^{4+}, Np^{4+}, Th^{4+}) are retained on the TEVA resin. Actinides in the tri- and hexavalent oxidation states (i.e. Am^{3+}, Cm^{3+}, UO_2^{2+}) are retained on the TRU (or DGA) resin.

Preliminary studies focused on the characterization of the separations unit using TRU and DGA resins and Am to establish some of the chemical and engineering boundary conditions associated with the manual separation method (Chapter 3). Method efficiency was characterized in terms of flow rate regulation, yield reproducibility, and versatility using aqueous samples containing various concentrations of ^{241}Am solutions. Results indicate that the columnar kinetics of

the resins are sufficiently rapid to run high purity americium samples through the unit over a wide range of flow rates for both resin types. Method efficiency was also evaluated with single matrix interferences present in solution. It was determined that the matrix interferences (molar ratio of $1:10^6$ for Am:Interference) have little effect on separation efficiency at varied flow rate conditions. Americium was selected for initial study based on its single trivalent oxidation state in acid solution and well-characterized extraction behavior on both DGA and TRU resins under the given matrix conditions.

The focus of this study is the Pu system. Pu sorption/desorption studies have a greater degree of complexity due the presence of multiple species in an aqueous solution. This diversity is based largely on the fact that the various oxidation states of Pu have similar redox potentials, yet different reaction kinetics (79-81). For separation procedures utilizing extraction chromatographic resins, redox agents, such as sulfamic acid, hydroxylamine, ascorbic acid, peroxide, Fe^{2+} and sodium nitrite are used to force the Pu into the desired or most extractable oxidation state (58). The reagents are added sequentially to enhance separation from matrix contaminants and to control the kinetics of metal complex formation. From an automation perspective, these reagents introduce parameters that must be characterized for the automation platform. This work describes the efficiency characterization studies performed on high purity ^{239}Pu solutions and solutions containing common matrix interferences on TEVA resin.

4.3 Materials and Methods

4.3.1 Vacuum Extraction System

The vacuum extraction unit developed for this project has been described in detail in Chapter 3. The unit is attached to a digital vacuum regulator (DVR) that controls the evacuation rate and pressure setting within the unit. The box can process 15 samples simultaneously. Sample vials with 50 mL volume are placed in a removable tray within the unit and are replaced after each method fraction is collected.

4.3.2 Reagents

Nitric and hydrochloric acid solutions were prepared from reagent grade acids (ACS reagent grade, Merck KGaA, Darmstadt, Germany) and de-ionized water (18 MΩ·cm, Millipore, Billerica, MA, USA). Aluminum nitrate nonahydrate crystals (ACS reagent grade, Merck KGaA) are added to the sample solution to increase the nitrate concentration. Redox agents added to the sample solution include sulfamic acid, ascorbic acid and sodium nitrite, each prepared from reagent grade solids (Mallinckrodt Baker, Phillipsburg, NJ USA) and de-ionized water. Sodium nitrite was prepared within 30 minutes of use. Ascorbic acid was prepared and used within two weeks of initial preparation. Pu was selectively removed from the TEVA resin using a mixture of hydrofluoric/hydrochloric acids, 20% $TiCl_3$ solution (ACS reagent grade, Merck KGaA, Darmstadt, Germany), and de-ionized water. The $TiCl_3$ solution was added to the HCl/HF mixture within thirty minutes of use.

Extraction chromatographic resins were obtained from Eichrom Technologies, Inc. (Darien, IL, USA) in 2 mL pre-packed polypropylene cartridges. TEVA resin (50-100 µm) was chosen for experimental evaluation and contains an aliphatic quaternary amine as the extractant compound for the stationary phase and is primarily used for isolating and separating tetra-valent actinides from tri- and hexa- valent actinides and fission products (34). Each pre-packed 2 mL cartridge is shipped dry and therefore must be pre-treated with the acid matrix prior to use. This step reconstitutes and equilibrates the resin, promotes uniform flow and maximizes the working capacity of the cartridge.

4.3.3 Radionuclide Standards

Plutonium stock solutions were prepared from traceable standard solutions (Isotope Products, Valencia, CA, USA) in 3M HNO_3·1M $Al(NO_3)_3$ with activity concentrations from 50 to 200 Bq per mL of stock solution. Aliquots of the original sample matrix and each subsequent fraction were taken and the activity of each was verified by liquid scintillation counting (LSC) (Tri-carb 3100, Perkin Elmer, Boston, MA, USA) with 10 mL of Ultima Gold AB cocktail (Perkin Elmer, USA) as the counting medium. The LSC samples were counted for 60 minutes or until the counting error reached 2S% (2% of the 2σ standard deviation of the total counts) in the CPMB energy window (50-1000 keV). The 2S% is a standard protocol option that serves as a normalization parameter for the comparison of multiple sample measurements, i.e. the error reported for each measurement represents 2% of twice the standard deviation of the counts collected in the CPMB region of

the spectrum. The average background count rate in the CPMB window was 8.83 ± 0.77 (1σ) cpm for method blanks.

4.3.4 Flow Rate Characterization

Initial flow rate characterizations relating vacuum set point (for the digital vacuum regulator, DVR) and cartridge flow rates are provided in Chapter 3. The TEVA resin cartridges were characterized for flow rate in terms of matrix effects based on each method step, i.e. resin preparation, sample loading, column rinse and elution matrices. The vacuum set point was programmed into the DVR and the sample solution (or subsequent elution/rinse solutions) was added to each of the sample reservoirs. The DVR activation switch was set to “Run Program” which allows the box to draw down to the specified vacuum set point. The times required for the vacuum box to reach the set point and for the sample reservoirs to empty were recorded for each TEVA cartridge. Once the reservoirs emptied, the DVR activation switch was returned to the neutral position and the box was allowed to return to equilibrium with ambient conditions.

4.3.5 Plutonium Separation

A sample reservoir (30-mL polypropylene Luer-lock syringe, B-D, NJ, USA) was connected to the top of the 2 mL TEVA resin cartridge. The resin bed was pre-treated with 5 mL of the 3 M HNO_3 matrix solution prior to sample loading, then 10 mL of the ^{239}Pu stock solution was added. These two eluates were collected together in a labeled 50 mL centrifuge tube. Sequential elutions were performed to rinse the resin (removes interferences) and strip Pu from the resin bed. The sample loading and elution matrices and volumes were chosen based

on the recommended method of manufacture for mixed actinide separations (78). A summary of the sequential elution matrices used in the method is provided (Table 12).

Table 12. Method elution matrices used for ^{239}Pu separation on TEVA resin

Method Fraction	Fraction Matrix	Load Volume
Resin Prep	3 M HNO_3	5 mL
Sample Load	3M HNO_3· 1M $Al(NO_3)_3$ · 1.5M Ascorbic and Sulfamic Acids · 3.5 M $NaNO_2$	12.75 mL
Rinse 1	3 M HNO_3	8 mL
Rinse 2	3 M HNO_3	10 mL
Elution 1	0.1 M HCl/ 0.05 M HF/ 0.03 M $TiCl_3$	20 mL
Elution 2	0.1 M HCl/ 0.05 M HF/ 0.03 M $TiCl_3$	20 mL

The loading matrices contained 10 mL of 3 M HNO_3 ·1 M $Al(NO_3)_3$. Several additional reagents were added to the load solution in sequential order - 0.5 mL of 1.5 M sulfamic acid, 1.25 mL of 1.5 M ascorbic acid and 1 mL of 3.5 M sodium nitrite. The sulfamic acid is added to each sample as a ‘holding’ agent and reductant. It reduces Pu that may be present in solution in the higher oxidation states to the trivalent oxidation state and helps sustain this oxidation state (58). Nitric acid produces some nitrous acid as a by-product. Nitrous acid can rapidly

oxidize Pu to the tetravalent oxidation state. The sulfamic acid reacts with HNO_2 to prevent Pu oxidation. Ascorbic acid is used to reduce Fe and Mn contaminants that may be present in the sample solution, which are also problematic for Pu oxidation (58). The final addition of sodium nitrite oxidizes Pu to the tetravalent state. Plutonium is removed from TEVA with a 0.1 M HCl/ 0.05 M HF/ 0.03 M $TiCl_3$ solution. Each fraction was collected in a labeled 50 mL centrifuge tube and aliquots were counted by LSC to verify activity concentration.

4.3.6 Elemental Matrix Interference Effects

The interference species were evaluated on TEVA 2-mL pre-packed resin cartridges at 2 vacuum settings, 275 and 575 torr, corresponding to the upper and lower boundaries of the flow rates tested. Ionic solutions were prepared in the sample loading matrix with the redox agents. The concentration of interfering ions for all experiments was approximately 2.5 mM, which is 1 to 2 orders of magnitude higher than the working capacity of Pu for TEVA resin (34). Iron, Ca, and Mn were chloride salt forms, and Al and Zr were nitrate salts. Potassium phosphate salt was used for the phosphate ion studies. Solutions were equilibrated at least one week prior to use. All chemicals and reagents used were of analytical grade or better. Each matrix solution was 10 mL and was run through a row of pre-treated resin cartridges and collected in 50 mL centrifuge tubes. Total ion concentration was determined by inductively coupled plasma absorption emission spectroscopy, ICP-AES (iCAP 6000 Series Thermo Scientific, Cambridge, UK). The solutions were diluted by a factor of 10 with de-ionized water prior to analysis. Calibration curves were run for each ion based on

0-10 mM standard solutions gravimetrically prepared in 2% HNO_3 (by volume). The wavelengths used for determining signal intensity (Table 13) were chosen based on relative signal intensity and minimized spectral interferences from the instrument software database.

Table 13. Matrix ion photon wavelengths used to determine signal intensity on the ICP-AES.

Counter Ion	Photon Wavelength (nm)
Nitrogen	174.2
Calcium	393.3
Manganese	257.6
Magnesium	279.5
Zirconium	339.1
Silicon	251.6
Phosphorous	177.4
Iron	259.9

The nitrogen signal was collected for baseline intensity to monitor the stability of the apparatus during analysis. The analytical parameters recommended by the manufacturer were used. Three replicate measurements were taken for each

sample with a sample flush time of 30 seconds in Precision analysis mode and a sample integration time of 15 seconds.

Plutonium separation and efficiency experiments (Section 2.5) were repeated with 2.5 mM solutions of each of the interfering ions. Each matrix solution was spiked with ^{239}Pu at an activity concentration of 200 Bq/mL of solution. Aliquots of each sequential elution are counted by LSC to determine the separation efficiency in the presence of the selected ions.

4.4 Results and Discussions

4.4.1 Vacuum Extraction System Characterization

Vacuum system characterization data from previous work with TRU and DGA resins showed a linear relationship between flow rate and the DVR set point. Variations in flow rate for the method matrices at different vacuum settings were also observed (Chapter 3). These variations are attributed to differences in ionic strength and viscosity of the elution matrices, and the packing and wetting characteristics of the resin. Pre-packed TEVA 2 mL resin cartridges were evaluated for the method matrix affects on flow rate (Figure 17). Three vacuum settings, 275, 425 and 575 torr, were chosen based on a high, medium and low flow rates. Resin prep was the first step in the method, where the dried resin cartridges are wetted with nitric acid. In comparison with studies run on the TRU resin cartridge, the flow rate versus vacuum setting was equivalent. From an engineering perspective, this is an indication that, under the same matrix

conditions the vacuum system does not differentiate between the TEVA and TRU resin cartridges.

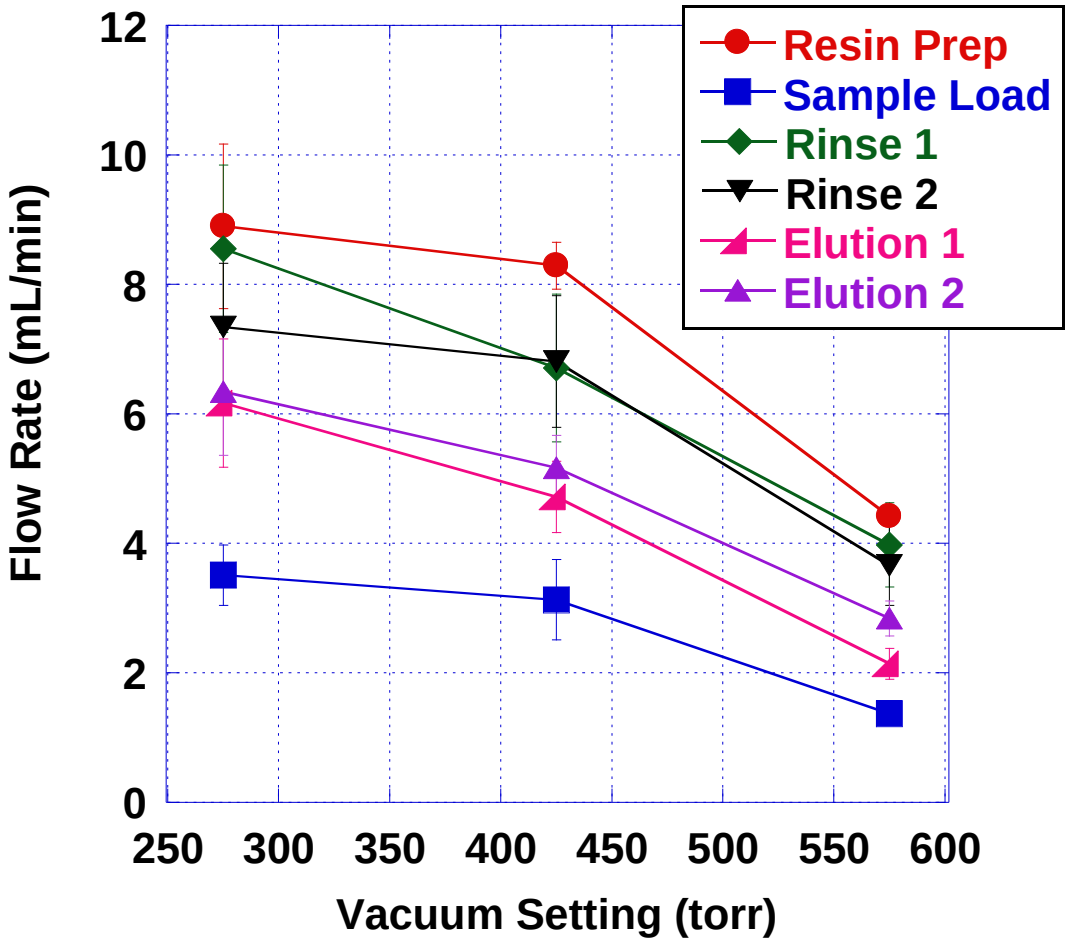

Figure 17. Elution matrix (Table 12) effects on flow rate for the 2 mL pre-packed TEVA resin cartridges at various vacuum settings. Each data point represents the average flow rate over a row of resin cartridges (n=5), for three separate trials, with new resin cartridges used for each trial.

4.4.2 Effects of Flow Rate on Plutonium Extractions

Residence time effects on Pu sorption/desorption efficiency for the TEVA resin were determined at the manufacturer recommended flow rate of

approximately 1 mL/minute (575 torr vacuum setting) for sample loading and at faster flow rates corresponding to the 425 and 275 torr vacuum settings. The vacuum setting rather than flow rate was kept constant throughout the separation procedure therefore the elution flow rate was twice as fast as the initial sample loading flow rate (Figure 17).

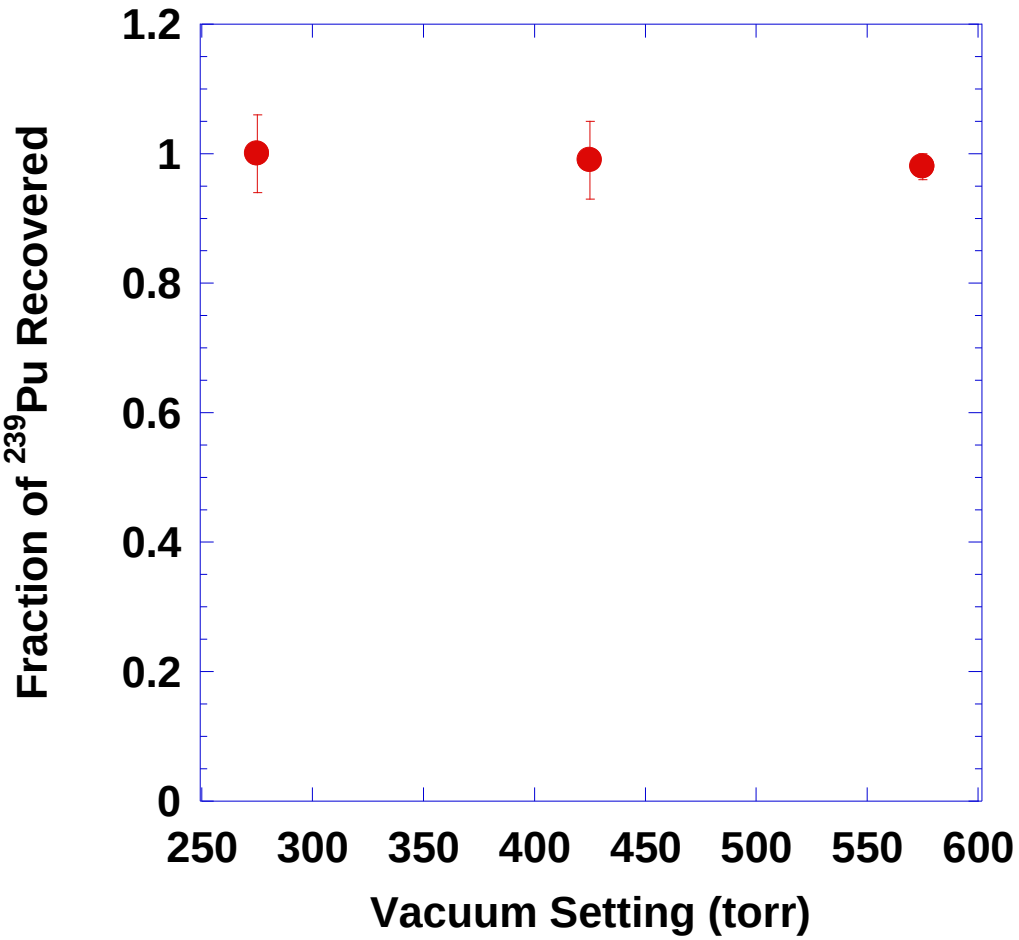

Figure 18. Extraction efficiency of ^{239}Pu on 2 mL TEVA cartridges at 2000 Bq/sample activity concentrations. The average extracted fraction is 0.99 ± 0.01 (±1σ). Each data point represents the average value for three trials (n=5 resin cartridges per trial) at a given vacuum setting.

These studies were conducted with high purity ^{239}Pu standard solutions with activity concentrations of 200 Bq/mL of solution, or 2000 Bq per sample. Three trials were conducted at each vacuum setting with n = 5 samples per trial. The extraction kinetics were rapid enough under the given conditions that the method efficiency was not affected by flow rate (Figure 18). Average Pu recovery was 99 ± 1% (±1σ) across the range of vacuum settings tested (Figure 18**)**. These data were similar to studies conducted with ^{241}Am on the TRU and DGA resin (Chapter 3), and recent EC optimization studies conducted with TRU resins (47). From an automation perspective, these data suggest that flow rate monitoring and precision control during the chemical separations procedure is not critical for high purity samples.

4.4.3 Optimization of Redox Reagent Addition

Reagent addition for an automation platform must be considered in terms of preparation requirements, solution equilibration, and sample aging time. Under the current method, the manufacturer recommends that the ascorbic acid solution be replaced after two weeks shelf time. Plutonium efficiency experiments were conducted with aged ascorbic acid (1 week < age ≤ 2 weeks) or with freshly prepared ascorbic acid. Table 14 provides the Pu recovery yields with the freshly prepared ascorbic acid and the aged ascorbic acid for the high purity Pu stock solution with 2000 Bq/sample activity concentration at 575 and 425 torr vacuum settings. Plutonium recovery decreased by half with the older solution. Ascorbic acid degradation studies have shown that the oxidation of ascorbic acid to

dehydro-ascorbic acid (DHAA) and other products can occur rapidly, with significant degradation occurring within the first 24 hours (82,83).

The effect of ascorbic acid degradation on Pu sorption/desorption efficiency to TEVA resin has not been previously reported in the literature. In this study, the decomposition of ascorbic acid was not evaluated; however, the activity present in each collected fraction provided some evidence of the underlying causes for decreased Pu separation efficiency.

Table 14. Redox reagent aging effects on Pu efficiency on TEVA resin.

Vacuum Setting (torr)	Aged Ascorbic Acid[a]	Fresh Ascorbic Acid[b]
	Pu Recovered from TEVA Separation Method[c]	
425	55 ± 19 % (±1σ)	99 ± 4% (±1σ)
575	41 ± 5 % (±1σ)	98 ± 1 % (±1σ)

[a] Ascorbic acid aged for 1-2 weeks prior to use

[b] Ascorbic acid preparation and use < 1 day

[a, b] Values reported as average activity percent recovered in the Pu fraction for all trials

[c] Based on a sample activity concentration of 2000 Bq (high purity)

For the studies conducted with aged ascorbic acid, the fractions containing measurable activity as determined by LSC included the first fraction (13.75 mL total volume), the Pu stripping fraction (20 mL) and the residual fraction (retained on the column). The total Pu yield in the first collected fraction ranged from 0 to

27% and was not consistent across samples in a given trial. Plutonium yield in its elution fraction ranged from 33 to 70% (average yield reported in Table 14). The Pu elution fraction was not repeated with these samples; however, the resin was counted in LSC cocktail to determine the residual activity sorbed to the resin. This technique was not ideal for estimating the residual activity because the resin settled to the bottom of the plastic vial during counting. The estimated residual activity percent sorbed to the TEVA resin was 35 ± 10% (1σ). Decreased Pu efficiency with aged ascorbic acid could be the result of incomplete reduction/oxidation of the Pu to form the doubly charged anionic species, $Pu(NO_3)_6^{2-}$, Pu complexation with the ascorbic acid by-products, and/or affinity of the by-products to the active resin sites. Further studies must be conducted to determine how ascorbic acid degradation affects Pu yield recovery.

Based on this information and the low recovery yield of Pu from high purity solutions, it is recommended that ascorbic acid be prepared fresh daily for optimal recovery. Aging of sulfamic acid solutions did not influence method efficiency. As $NaNO_2$ is prepared immediately prior to use, solution aging was not evaluated.

4.4.4 Sorption of Elemental Matrix Interferences

The overall performance of the EC resin cartridge is governed by the selectivity of the extractant compound to the species of interest, the extraction kinetics, diffusion/ flow phenomena and the extractant capacity (32,33). The presence of other ions in the sample solution can enhance or diminish uptake of the actinides by the resin. As an example, aluminum (hydrated nitrate salt) is

added to the initial sample loading solution to increase the free nitrate anion concentration and to scavenge potential interferences such as fluoride and phosphate anions. In this particular case, the aluminum is added to enhance the formation of the $Pu(NO_3)_6^{2-}$ species in solution for higher sorption on the TEVA resin (34).

Several common matrix ion contaminants were selected for characterization on TEVA resin based on their abundance in environmental matrices and nuclear material. Additionally, actinide enrichment for aqueous samples is often performed by precipitation with $Fe(OH)_3$, $Ca_3(PO_4)_2$, or MnO_2. Calcium, Fe, Zr and Mn were only slightly retained by the TEVA resin under the given testing conditions (Figure 19). These results were similar to those obtained during the initial TEVA resin characterization studies (34).

In our previous work, it was determined that Zr showed a high affinity for both the TRU and DGA resins (Chapter 3). The sample loading conditions used in this study for the TEVA resin were equivalent to those used in the TRU studies. The Zr present in solution exists as the $Zr(NO_3)_4$ charge neutral species (84,85) which is not extractable by the TEVA resin. In samples where Pu is present with high (or unknown) Zr concentrations, it may be beneficial to use TEVA resin versus TRU resin for separation and purification. This is of particular importance for samples originating from the nuclear fuel cycle as Zr is likely to be present as a fission product or a component of the cladding material.

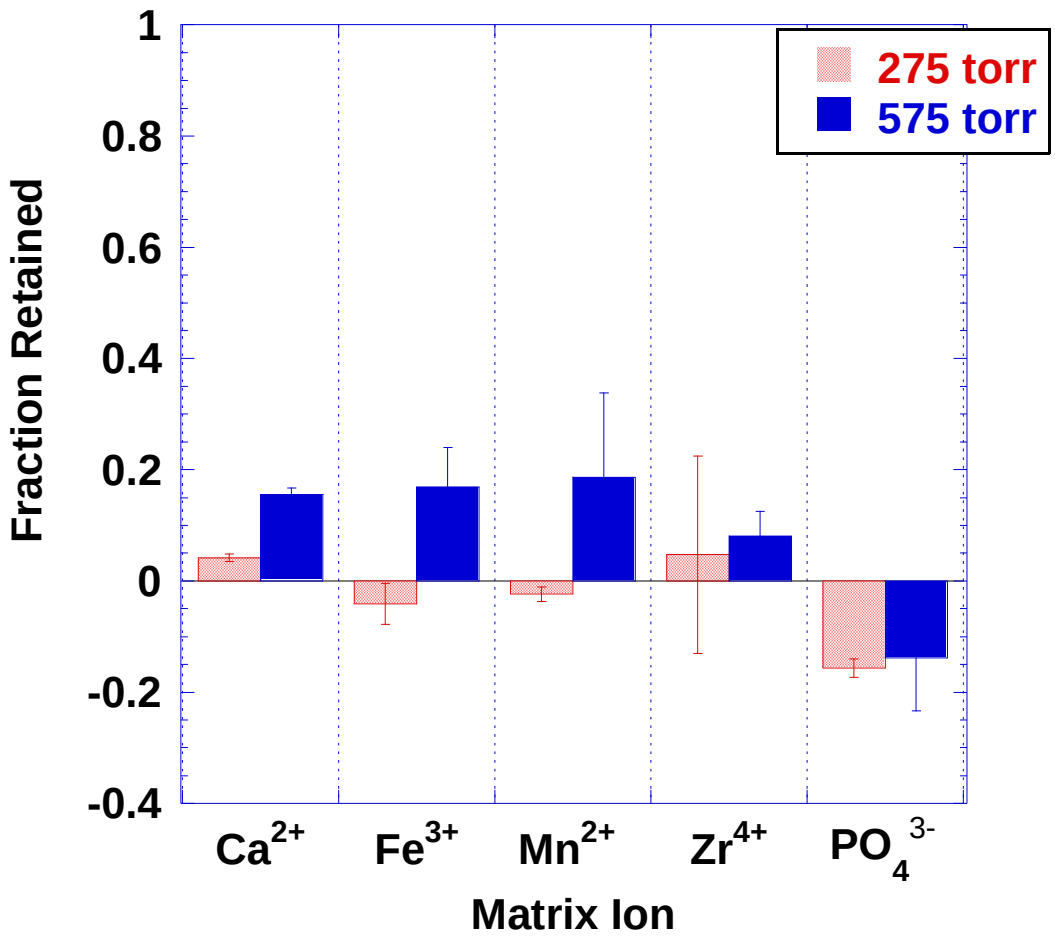

Figure 19. Sorption of interference ions at various vacuum settings using 2 mL TEVA resin cartridges (n = 5). Ion concentration is 2.5 mM in a 3 M HNO_3 · 1 M $Al(NO_3)_3$ loading matrix.

4.4.5 Effects of Elemental Matrix Interferences on ^{239}Pu Separation Efficiency

Plutonium extraction experiments were repeated in the presence of selected ions. The method extraction efficiency for Pu at both the fast and slow flow rates (275 and 575 torr, respectively) is provided (Figure 20). The fraction of Pu recovered in the presence of all matrix ion interferences decreased at the faster

flow rate, indicating that the TEVA extraction kinetics were sensitive to the mobile phase velocity under non-ideal matrix conditions.

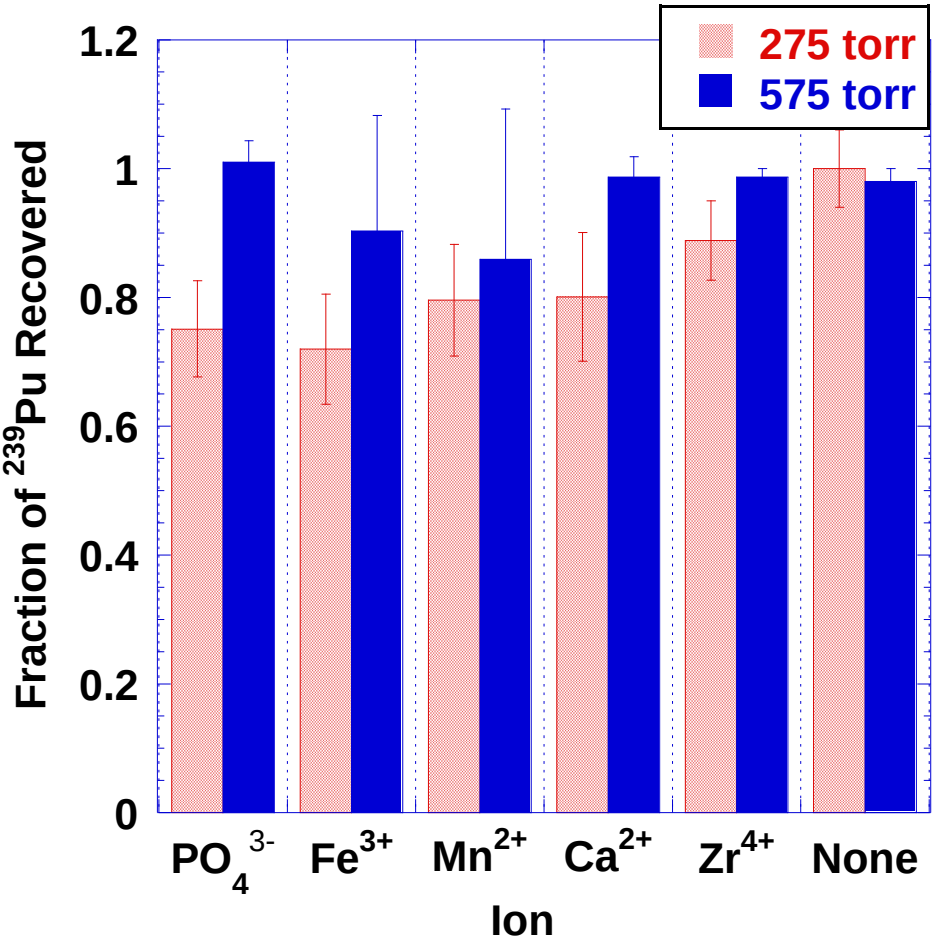

Figure 20. Fraction of Pu recovered at various vacuum settings using 2 mL TEVA resin cartridges (n=5 cartridges/ion per vacuum setting). Pu activity concentration was equivalent to 2000 Bq per sample, verified by LSC. Counter ion concentration is 2.5 mM in a 3 M HNO_3·1 M $Al(NO_3)_3$ loading matrix. Error bars represent the recovery reproducibility at 1σ.

The average activity percent collected for each method fraction from experiments run at the faster flow rate (275 torr vacuum setting) is provided (Table 15). Losses occurred in all of the collected fractions for each of the

solutions spiked with matrix ion contaminants. The degree of loss in each collected fraction was not ion specific, and could be a result of preferential flow path formation within the column.

Table 15. Plutonium activity percent recovered in each collected method fraction determined by LSC counting in the presence of selected ions

Method Fraction	Load/ Elution Volume	PO_4	Fe	Mn	Ca	Zr	None
Sample Load + Rinse 1	20.75	3.6 (± 0.1)	3.8 (± 0.2)	3.9 (± 0.1)	3.1 (± 0.2)	5.8 (± 0.5)	1.1 (± 0.7)
Rinse 2	10	1.5 (± 0.1)	1.5 (± 0.1)	1.5 (± 0.1)	1.2 (± 0.1)	1.5 (± 0.1)	0
Elution 1	20	75 (± 7)	72 (± 9)	80 (± 9)	80 (± 10)	89 (± 6)	99 (± 3)
Elution 2	20	2.9 (± 0.2)	3.0 (± 0.1)	3.0 (± 0.1)	2.6 (± 0.1)	3.0 (± 0.3)	0
Total Activity % Recovered		83 (± 7)	80 (± 9)	88 (± 9)	87 (± 10)	99 (± 6)	100 (± 3)

275 torr vacuum setting was used for all collected fractions.

In column chromatography, plug flow (or non-turbulent flow) of the mobile phase is desired because more of the active sites (or theoretical plates) on the resin are sampled for sorption/desorption interactions. Fingered flow, also called

turbulent flow results in the formation of preferential flow paths and effectively decreases the number of theoretical plates in the column. The introduction of matrix ions in solution may increase the effects of preferential flow by decreasing Pu adsorption efficiency.

It is unclear if the decreased efficiency is a result of flow restriction or due to changes in the Pu species in the mobile phase when the matrix ions of interest are present. Neither Ca nor Zr affects Pu recovery at the slower flow rate (575 torr). The presence of Fe and Mn in the sample matrix can affect the oxidation state and speciation of Pu. Under the current separation method, Mn and Fe are reduced using ascorbic and sulfamic acids to prevent premature oxidation of Pu. The final addition of $NaNO_2$ oxidizes Pu to the tetravalent state as well as Fe to the trivalent state. Manganese is expected to remain in the divalent state (58).

In these studies, the Pu stock solutions (with interfering ionic species) were prepared for both the 575 torr and 275 torr vacuum setting experiments. The lower flow rate (575 torr vacuum setting) experiments were conducted first, followed by the faster flow rate (275 torr) experiments approximately 1 hour later. It was unclear if the difference in method efficiency was due to the mobile phase velocity alone or if the difference in sample rest time (t= 1hour for 275 torr study) affected Pu speciation. A separate set of experiments were conducted to determine the effects of sample aging on Pu recovery and the method efficiency. Plutonium samples were prepared with the single matrix interferences as previously discussed and loaded on the column within five minutes of preparation. The results of this study are presented in Figure 21. Sample aging

time does affect Pu recovery, with the greatest effect seen with the phosphate and Fe matrix ions present in solution.

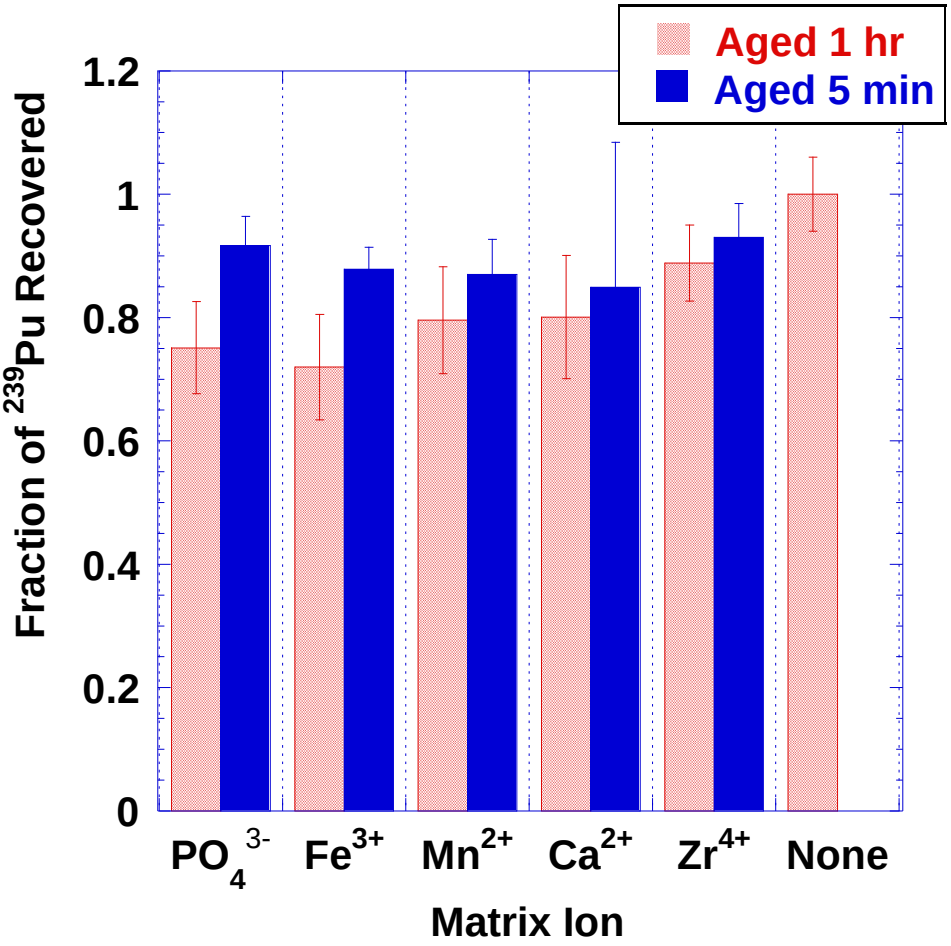

Figure 21. Fraction of Pu recovered at 275 torr vacuum settings using 2 mL TEVA resin cartridges (n=5 cartridges/ion per vacuum setting) for various sample aging times. Pu activity concentration equivalent to 2000 Bq per sample, verified by LSC. Counter ion concentration is 2.5 mM in a 3M HNO_3·1M $Al(NO_3)_3$ loading matrix. Error bars represent the recovery reproducibility at 1σ.

4.5 Concluding Remarks

The focus of this work is to optimize extraction chromatography procedures for an automated platform procedure where mixed actinide samples are

processed in a discrete, simultaneous fashion. Our previous work focused on the development of a prototype vacuum extraction system that is based on a commercially available automated solid-phase extraction unit. Initial characterization studies were completed with americium and two types of EC resins, TRU and DGA. The results of this initial study concluded that flow rate monitoring is not critical for reproducible method extraction efficiency and that specific vacuum settings can be used throughout the separation procedure. In this study, it was determined that Pu extraction is affected by the mobile phase velocity in the presence of isolated matrix interferences such as phosphates, calcium, manganese and iron. From an automation standpoint, these data suggest that maintaining a lower flow rate, or fixed vacuum setting equivalent to 1-2 mL/min is favored if TEVA resin cartridges are used for Pu separations. We are continuing this work with mixed matrix ions solutions for both americium and Pu.

CHAPTER 5

HOT PARTICLE DISSOLUTION AND PLUTONIUM ISOTOPIC ANALYSIS

5.1 Abstract

A persistent challenge in both the nuclear forensics and environmental sciences is the rapid and accurate determination of isotopic ratios of Pu in samples containing a mixture of actinides. This process of determining Pu isotopic ratios can be enhanced by its chemical separation from an actinide matrix using a simplified sequential extraction chromatography method. This work focuses on the dissolution of weapons grade Pu particles using HNO_3/HF acid digestion, vacuum assisted sequential extraction chromatography for chemical separation and alpha spectrometry sample preparation using CeF_3 micro-precipitation. Isotopic analysis was obtained by a combination of radiometric methods (e.g. alpha/gamma spectrometry). The results of these experiments were compared to both the historical record surrounding the source of the particles as well as the non-destructive techniques used during the preliminary characterization of the particles.

5.2 Introduction

Historical incidents that have resulted in the release of radioactive materials from different sources into the environment are well documented (86-92). Once the material is incorporated into the surrounding environment, understanding the link between source term and nuclide speciation is of fundamental importance for remediation efforts, dose modeling and attribution science. Particles created

during the release incident containing elevated levels of radioactivity are referred to as ‘hot particles’ (3). The United States Defense Threat Reduction Agency (DTRA) further specifies that hot particles are “discrete point sources” with a diameter greater than or equal to 45 μm and an activity concentration greater than 5000 Bq per particle (93). These particles have been collected from event sites around the world and characterized in terms of surface morphology and elemental composition using various non-destructive imaging techniques. This information has been used to predict environmental impact in terms of bioavailability and mobility.

Recent studies have shown that the size, oxidation state, and crystalline structure of the particle are dependent on the type of release scenario (2,7,8,88,94,95). While advancements in technology have given scientists the tools to study the surface and structural characteristics of these hot particles, the interpretation of the data remains the most challenging part. Non-destructive techniques mainly provide qualitative characterization of hot particles. To substantiate the effect of the hot particle on an environmental system and link the material back to a particular source, total dissolution studies are required.

Dissolution studies provide more detailed isotopic information about the radionuclide content of the sample. This information can be used to determine the relationship between the sample matrix constituents and the radionuclides of interest from a speciation perspective and also provides substantive forensic evidence with regards to source term identification (95). As an example, the relative abundance of Pu and U in a hot particle can be determined using non-

destructive imaging techniques; however, the isotopic content cannot be fully determined. The relative isotopic abundance of Pu and U can help determine if the material of interest originated from defense or civilian based sources (5,96).

In this work, particles with elevated gamma-ray activity were manually isolated from soil cores obtained from a military base where a fire involving a Boeing Michigan Aeronautical Research Center (BOMARC) surface-to-air missile occurred over forty years ago. In this incident, the high explosive warhead caught fire and burned uncontrollably. The pit assembly containing weapons grade Pu, WGPu (^{239}Pu enrichment ≥ 93% by mass), ^{238}U and ^{235}U burned, causing the release of these materials into the environment during initial fire suppression and subsequent decontamination and site remediation efforts. A detailed summary of the incident is provided in (97) and (98), and references therein. Isolated hot particles (n = 20) were characterized, in terms of size, morphology and depth distribution, and elemental composition by non-destructive means (6). The results obtained from these studies provided evidence of particle heterogeneity in terms of elemental composition and surface morphology.

As part of the non-destructive analysis, gamma spectrometry data was also collected for intact particles and small soil core sections with elevated gamma activity. The spectral results provided some isotopic information based on the photons associated with the decay of ^{241}Am, a daughter product of ^{241}Pu decay; however, its presence is not particularly useful in terms of source term characterization and material dating (5). A better understanding of the material can be gained from the relative ratios of the minor Pu isotopes in WGPu to the

dominant ^{239}Pu isotope. Information about the type of reactor, the hardness of the neutron spectrum, and the initial fuel enrichment used in material production can be extrapolated from these relative ratios (5,99).

Table 16. Plutonium isotopic composition of the nuclear missile in 1958.

Radionuclide	Half-Life (yr)	[1]Mass %	Activity %	Alpha Activity %
^{238}Pu	8.770E+01	0.0099	0.31	2.3
^{239}Pu	2.410E+04	93.7	10.4	80.1
^{240}Pu	6.560E+03	5.6	2.3	17.6
^{241}Pu	1.440E+01	0.47	87.0	0.0
^{242}Pu	3.750E+05	negligible	--	--
^{241}Am	4.327E+02	not reported	--	--

[1]Pu isotopic composition as reported in Air Force Institute for Environment, Safety and Occupational Health Risk Analysis report IERA-SD-BR-SR-2001-0006 (101).

Evaluating Pu isotopic composition is confounded by the presence of ^{241}Am. Americium is particularly useful from a remediation point-of-view in that the 59.54 keV gamma ray emitted by the decay of ^{241}Am can be easily detected with common field instrumentation. However, in terms of mass and radiometric

analysis, ^{241}Am is a spectral interference for ^{241}Pu (m/z ratio), ^{238}Pu (alpha energy analysis) and ^{240}Pu (gamma energy analysis).

The focus of this work was to chemically isolate Pu from other matrix constituents to determine the isotopic composition of each dissolved particle. Seven particles were dissolved individually in nitric/hydrofluoric acid and the Pu was purified using extraction chromatography resins. Plutonium was isolated on TEVA resin (Eichrom Technologies, Inc., Darien, Il, USA) and isotopic analysis was performed with gamma and alpha spectrometry using a cerium fluoride sample preparation method. The observed isotopic ratios were compared to those provided in the site remediation reports (92,100,101). The reported Pu isotopic composition of the weapon is provided in Table 16. Elemental analysis of each hot particle solution was also performed to determine the variances in particle composition.

5.3 Materials and Methods

5.3.1 Reagents

Nitric, hydrochloric and hydrofluoric acid solutions were prepared from reagent grade acids (ACS reagent grade, Merck KGaA, Darmstadt, Germany) and de-ionized (DI) water (18 MΩ·cm, Millipore, Billerica, MA, USA). Hydrogen peroxide (30.0-32.0%, ACS reagent grade, Mallinckrodt Baker, Inc., Phillipsburg, NJ, USA) was added to the nitric/hydrofluoric acid solution during particle digestion. Aliquots of each dissolved hot particle solution were diluted with the nitric/hydrofluoric acid and aluminum nitrate nonahydrate crystals

($Al(NO_3)_3 \cdot 9H_2O$, ACS grade, Merck KGaA) were added to each sample to remove excess fluoride ions. Plutonium was selectively extracted using a mixture of hydrofluoric/hydrochloric acids, 20% $TiCl_3$ solution (p.a. grade, Merck KGaA, Darmstadt, Germany), and de-ionized water. The $TiCl_3$ solution was added to the HCl/HF mixture within thirty minutes of preparation.

TEVA and DGA extraction chromatography resins (Eichrom Technologies, Inc., Darien, Il, USA) were used for Pu, U and Am isolation from other matrix constituents and radionuclide purification. The active component of the TEVA resin (50-100 µm particle diameter) is an aliphatic quaternary amine that is selective for tetra-valent actinides over tri- and hexa- valent actinides and fission products (34). DGA is a diglycolamide-based extraction chromatographic resin (DGA- normal, 50-100 µm, 40% w:w) that is also effective for actinide separations (31). When used in combination, TEVA extracts the tetra- valent actinides and the tri- and hexa-valent actinides are retained by DGA. Each resin type is self-contained in a pre-packed polypropylene cartridge that contains approximately 2 mL of resin. The resin cartridges are stackable, allowing for sequential isolation of the actinides of interest during sample loading. The cartridges are then separated and subsequent elutions are carried out for each resin type for actinide purification.

5.3.2 Particle Dissolution

Isolated particles were placed in labeled 50 mL wide mouth Teflon bottles (Sigma-Aldrich, St. Louis, MO, USA), covered with 5 mL of 7 M HNO_3-0.05 M HF and approximately 0.5 mL of H_2O_2. Teflon stir bars were added to each vial for

continuous mixing (lowest setting) and the solutions were heated to 120-160 °C until complete evaporation of the acid solution was observed. The dissolution process was repeated twice with a total dissolution time of approximately 2 hours. Each dissolved particle solution was filtered through a 0.45 µm polytetrafluoroethylene (PTFE) filter and collected in a 50 mL centrifuge tube. The PTFE filter was washed three times with 5 mL of nitric/hydrofluoric acid, with each wash collected in separate vials. After the final wash, each filter was placed on a sodium iodide (NaI) detector to determine if any residual gamma activity remained on the filter.

Aliquots of each dissolved particle solution and filter wash were taken for total activity verification by liquid scintillation counting, (LSC, Tri-carb 3100, Perkin Elmer, Boston, MA, USA) with 10 mL of Ultima Gold AB cocktail (Perkin Elmer, USA) as the counting medium. The LSC samples were counted for 60 minutes or until the counting error reached 2S% (2% of the 2σ standard deviation of the total counts) in the energy window (50-1000 keV) labeled CPMB. The 2S% is a standard protocol option that serves as a normalization parameter for the comparison of multiple sample measurements, i.e. the error reported for each measurement represents 2% of twice the standard deviation of the counts collected in the CPMB region of the spectrum. The average background count rate in the CPMB energy window was 8.83 ± 0.77 (1σ) cpm for method blanks.

5.3.3 Chemical Separations

An aliquot of the dissolved particle solution equivalent to 2000 Bq of total activity was placed in a labeled 50 mL centrifuge tube. The volume was adjusted

to 10 mL with 7 M HNO_3- 0.05 M HF. Aluminum nitrate (0.05 M) was added to remove excess fluoride anions from solution and the sample was allowed to rest for at least 1 hour before performing separations. Plutonium, U and Am were chemically isolated from other matrix constituents using stacked TEVA/DGA extraction chromatography resin cartridges. Five samples solutions were prepared for sequential extraction from each filtered hot particle solution. Samples were transferred to holding reservoirs that were attached to the stacked resin cartridges. The lower cartridge (DGA) was secured in the lid of a vacuum extraction unit that was developed in-house. Sample loading and average elution flow rate were controlled by a digital vacuum regulator (J-Kem Scientific, Inc., St. Louis, MO, USA). For each elution step, the vacuum box was maintained at a constant pressure of 575 torr, resulting in an average flow rate of 1 to 3 mL/min (per 2 mL resin cartridge). All experiments were performed at room temperature (20.2 ± 1.8 °C). Prior to sample loading, the resin cartridges were wetted and equilibrated with 5 mL of 7 M HNO_3. The sample loading solution was added immediately after the pre-treatment of the resin. Tetravalent Pu was sorbed to the TEVA resin and Am^{3+} and UO_2^{2+} were sorbed to the DGA resin (31,34). Both pre-treatment and sample loading solution volumes were collected in a centrifuge tube (total volume ~15 mL). After sample loading, the vacuum on the extraction unit was released, the TEVA and DGA cartridges were unstacked and the collection tubes were exchanged for the next extraction step. Each subsequent elution fraction was collected and reserved for liquid scintillation counting and cerium fluoride precipitation sample preparation. Plutonium was eluted from the

TEVA resin using a mixture of hydrochloric/hydrofluoric acids and $TiCl_3$, which reduces Pu^{4+} to Pu^{3+}. Uranium and Am were eluted from the DGA resin with dilute nitric acid and dilute hydrochloric acid, respectively. The method separation diagram is provided (Figure 22).

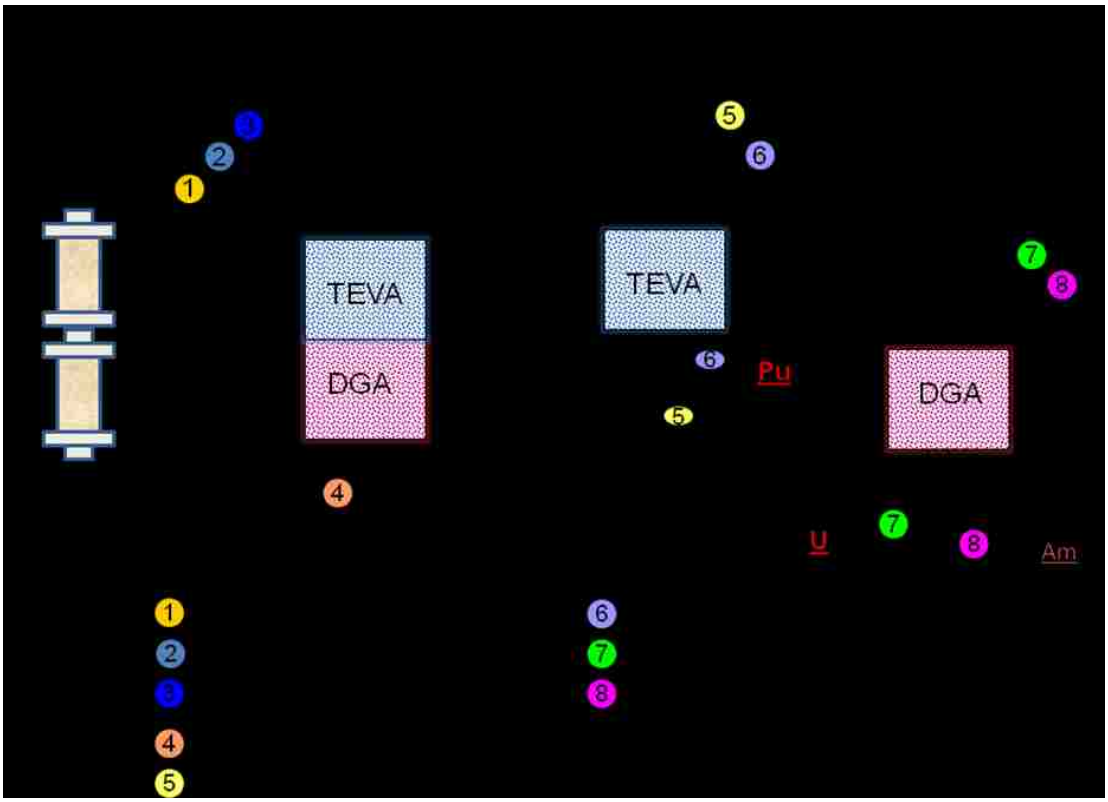

Figure 22. Chemical separation flow sheet for dissolved hot particle solutions. Five aliquots of the filtered dissolved particle matrix solution equivalent to 2000 Bq total activity were taken and total sample volume normalized to 10 mL (7 M HNO_3· 0.05 M HF· 0.05 M $Al(NO_3)_3$).

5.3.4 Sample Preparation for Plutonium Isotopic Analysis

Chemical recovery and actinide separation efficiency were determined using various radiometric techniques. Cerium fluoride (CeF_3) co-precipitation was

chosen for sample preparation based on its utility for both radiometric and mass analysis methods. A Ce carrier was added to the sample solution followed by an excess of concentrated HF to force precipitate formation. The sample was allowed to rest for 30 minutes and was then filtered through a Resolve filter (polypropylene, 0.1 µm pore size, 25 mm diameter, Eichrom Technologies, Inc.). The precipitate was collected on the filter and air dried for approximately 20 minutes. A more detailed explanation of the CeF_3 precipitation procedure is available from the filter manufacturer (29).

5.3.5 Plutonium Isotopic Analysis – Gamma and Alpha Spectrometry

The detection methods used for hot particle isotopic analysis were primarily alpha and gamma spectrometry. The CeF_3 filters were counted for 24 hours on a broad energy spectrum germanium detector (BEGe, Canberra Industries, Inc., Meriden, CT, USA) to collect the gamma spectrum for the Pu fraction. Three photon energies were used for determining ^{239}Pu content, 38.7 keV (0.0105% yield), 51.6 keV (0.0271% yield) and 129 keV (6.31×10^{-3}% yield). The lower energy photons were chosen based on the relative proximity to the photon energies chosen for ^{240}Pu and ^{238}Pu evaluation, 45.1 keV (0.045% yield) and 43.8 keV (0.0392% yield), respectively. The 129 keV photon associated with ^{239}Pu decay, whose attenuation caused by the intervening sample matrix is considerably less than that of the lower-energy photons, was used as a third reference point for determining the absolute amount of ^{239}Pu in each sample. The relative ratios of ^{239}Pu to ^{240}Pu and ^{238}Pu were determined based on the following relationship:

$$\frac{\left[\frac{C_{\gamma,239}}{\varepsilon_{\gamma,239} \times Yield}\right]}{\left[\frac{C_{\gamma,240(238)}}{\varepsilon_{\gamma,240(238)} \times Yield}\right]} = R_{239/240(238)} \qquad \text{Equation 16}$$

where C_γ was the net counts in the photopeak, ε_γ was the BEGe detection efficiency, and *Yield* was the yield associated with a given emitted photon. Gamma detection efficiency was initially determined using various certified gamma point sources. By using closely spaced gamma lines, corrections due to finite source size and source self-attenuation tend to cancel one another. A CeF_3 precipitated Pu source was prepared for use as a calibration standard with approximately 2000 Bq total activity.

The aqueous standard (Isotope Products, Valencia, CA, USA) contained approximately 98 atom% ^{239}Pu in 4 M HNO_3 solution. The remaining 2% contained a mixture of ^{238}Pu, ^{240}Pu, ^{241}Pu, ^{242}Pu and ^{241}Am. Americium was not separated from the standard solution prior to precipitation, but accounted for less than 0.001% of the total atom percent in solution. Gamma spectra were analyzed using Genie 2000 Gamma Acquisition and Analysis and Interactive Peak Fit (IPF) software (Canberra Industries, Inc., Meriden, CT, USA). Peaks were located and an energy calibration established using the unidentified second differential option in the analysis software with a significance threshold of 3.00 and a tolerance of 1.00 keV (default settings). Peak area was first determined using the Sum/Non-linear Least Squares Fit setup. A step continuum function was performed across the entire energy interval, (0- 515 keV), over all channels (1 - 4096). Once general peaks were identified, IPF filters were applied for more

accurate peak integration. An example of the CeF_3 precipitated standard spectrum is provided in Figure 23.

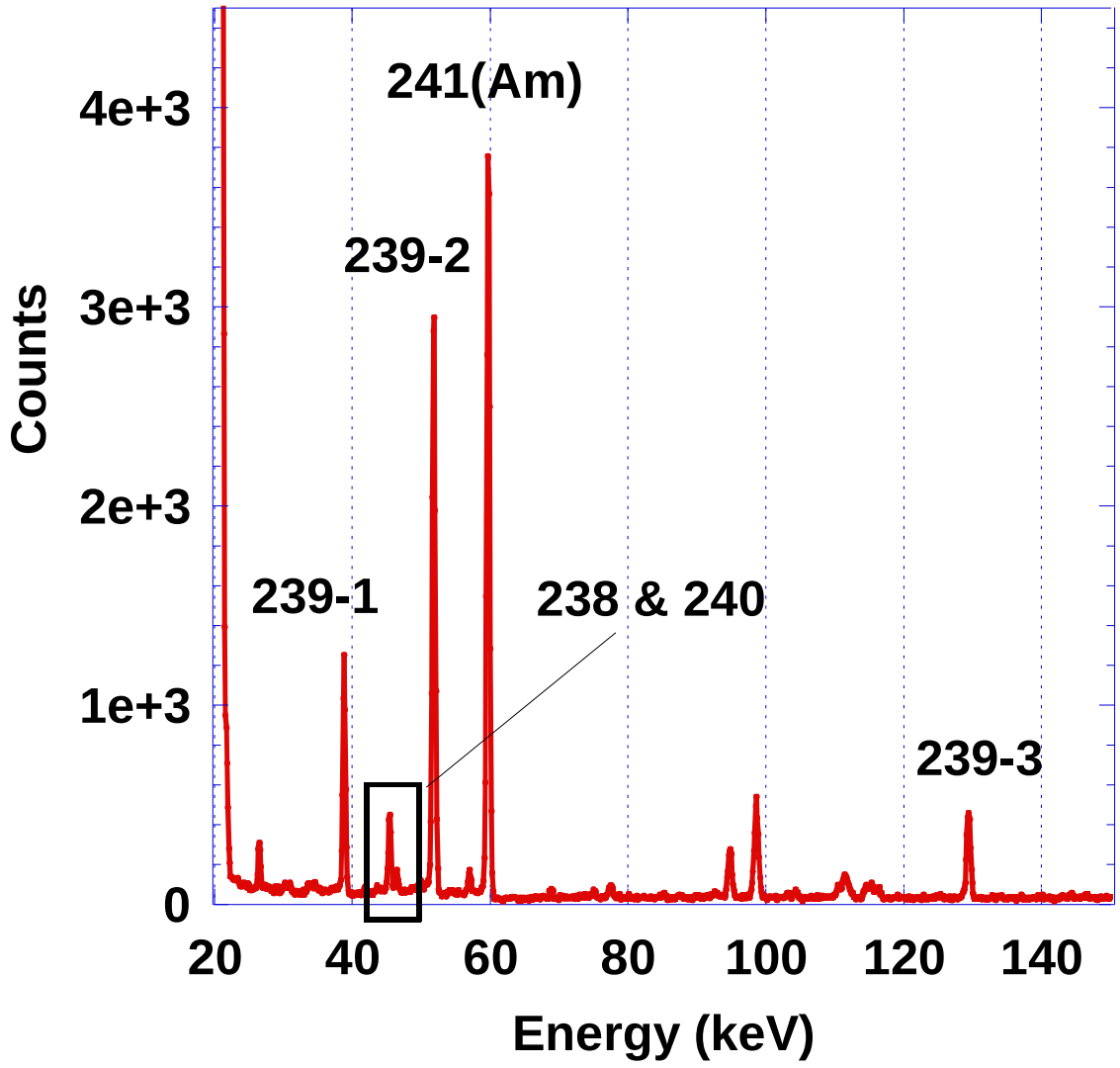

Figure 23. Gamma spectrum collected for the ^{239}Pu calibration standard prepared in-house by CeF_3 precipitation. The 38.9 (^{239}Pu), 43.5 (^{238}Pu), 45.2 (^{240}Pu), 51.9 (^{239}Pu), 59.5 (^{241}Am) and 129 (^{239}Pu) photopeaks were used for determining relative Pu isotopic composition.

This analysis method was used for both the standard and experimental sample filters. The BEGe gamma spectrometry system detection efficiencies for the photons of interest are listed in Table 17.

Table 17. Detection efficiency for selected photons using the broad energy germanium (BEGe) spectrometry system.

Radionuclide	Photon Energy (keV)	Detector Efficiency[1,2]	Plot ID
^{239}Pu	38.7	0.23	239-1
^{238}Pu	43.5	0.23	238
^{240}Pu	45.24	0.23	240
^{239}Pu	51.9	0.24	239-2
^{241}Am	59.5*	0.24	241(Am)
^{239}Pu	129	0.18	239-3

[1] The detection efficiency for the 59.5 keV photon is estimated from the efficiency fitting function determined by the analysis software (Genie 2000). The concentration of ^{241}Am in the aqueous Pu standard used to prepare the calibration standard filter was not provided by the source manufacturer.

[2] The uncertainty associated with the detection efficiency value is ±5% of the value.

Alpha spectra were collected on an Alpha Analyst spectrometer (Canberra Industries, Inc., Meriden, CT, USA). The solid state detectors used for all experiments had an active area of 450 mm^2 and the sample position was fixed at 16 mm from the detector face. A 24 hour background count was obtained for each chamber prior to sample analysis and a 1000 second background count was taken prior to and immediately after sample counting.

The activity of each filter was first assessed with a hand-held analog alpha/beta count rate meter (Model 2360, Ludlum Measurements, Inc., Sweetwater, TX, USA). Filters containing less than 50 Bq total activity were counted in low background chambers and those with activity greater than 50 Bq per filter were counted in "high activity" designated chambers to minimize cross-contamination effects. Filters were counted for 1000 seconds to 24 hours on the alpha spectrometry system, depending on the activity concentration. Filters that were prepared from the minor elution fractions collected (i.e. sample load and rinse fractions) were counted for 24 hours to determine if any residual alpha activity was present. The CeF_3 filters that contained the isolated Pu and Am were counted for 1000 seconds. Each Pu and Am filter was counted three times.

Alpha spectrum analysis was performed with Genie 2000 and Alpha Analyst software (Canberra Industries, Inc.). Alpha detection efficiency for the CeF_3 filters was approximately 9.2 ± 1.1%, independent of alpha-decay energy. Peak integration was performed by manually defining the alpha peak region of interest (ROI). The combined $^{240+239}Pu$ alpha peak ROI was set between 4.96 MeV and 5.21 MeV. The $^{238}Pu/^{241}Am$ peak ROI was set between 5.31 MeV and 5.57 MeV.

The tailing associated with the $^{239+240}$Pu peak was also evaluated for each sample to monitor peak area losses associated with peak broadening. The lower energy tail was not used for determining the peak ratio for ^{238}Pu (^{241}Am):$^{239+240}$Pu because of the presence of ^{237}Np (decay product of ^{241}Am and ^{237}U). For the chemical separation method used, Np was retained on the TEVA resin and co-eluted with Pu. There was approximately 1% difference in peak area integration with and without the lower energy tail. In comparison to the values obtained over 5 trials per hot particle, this error was three times lower than the average uncertainty of the population mean, so it was ignored.

5.3.6 Elemental Analysis

The dissolved particle solutions were also characterized in terms of additional matrix constituents. A 1 mL aliquot of each of the filtered hot particle solutions was delivered to a weighed 15 mL centrifuge tube. The mass of the solution was recorded and the solution was evaporated to dryness in an oven at 90 °C. The samples were reconstituted in 10 mL of 1% HNO_3 and analyzed by inductively coupled plasma atomic emission spectrometry (ICP-AES, iCAP 6500 series, Thermo Scientific, Inc., Cambridge, UK). Elements of interest included Pb, Pt, Al, Cd, Fe, Ga, Fe, Rb, Si, Ti and U. Calibration curves were established for each of these elements prior to sample analysis using ICP standard solutions (BDH Aristar, UK) at concentrations between 0 and 1 mM.

Wavelengths used for element identification and concentration were chosen based on relative intensity and potential analyte interference by the instrument software spectral line database (Table 18).

Table 18. Photon wavelengths used to determine signal intensity for the ICP-AES

Counter Ion	Photon Wavelength (nm)	Relative Intensity
Nitrogen	174.2	1.8×10^4
Silicon	251.6	6.0×10^5
Iron	259.9	2.0×10^6
Aluminum	167.0	1.83×10^6
Rubidium	424.4	2.5×10^4
Cadmium	228.8	2.0×10^6
Lead	220.3	1.2×10^5
Gallium	294.3	4.0×10^5
Platinum	214.4	1.5×10^5
Titanium	334.9	5.0×10^6
Uranium	367.0	5.0×10^4

The relative intensity value is based on the detector sensitivity for the element over other elements with similar photon wavelengths.

5.4 Results and Discussion

5.4.1 Plutonium Isotopic Composition – Historical Record

Several unclassified reports have been published on the incident that occurred on 7 June 1960 involving the BOMARC weapon (97,98,101,102) regarding site monitoring and remediation efforts. Following the incident, explosive ordinance disposal personnel filled containers with the warhead debris at which time it was shipped to various secure storage facilities (92,102). Analysts from the Los Alamos National Laboratory (LANL) performed nuclear measurements on the containers and determined that most of the WGPu was recovered.

The exact amount of Pu and U present during the fire was not provided; however, it was estimated that approximately 60-300 g of WGPu was released into the environment as a result of fire suppression, response activities and routine activities that occurred post-accident (92). It was also assumed that most of the Pu released into the environment was in the dioxide form, PuO_2. This assumption was supported by site remediation efforts, where in-situ survey measurements and soil core analysis suggested that activity was not uniformly distributed, but isolated in ‘hot-spots’ around the site (92). Data from the United States Air Force (USAF) remediation efforts and the characterization studies conducted at LANL collectively provide information regarding the estimated isotopic composition of the WGPu used in the BOMARC missile, listed in Table 16.

5.4.2 Particle Dissolution

All that was known about particle composition was based on the historical record and the information obtained from non-destructive analysis studies. Data collected by extended x-ray absorption fine structure (EXAFS) and x-ray absorption near edge spectroscopy (XANES) indicated that the particle matrix was in a mixed oxide form (6). Elemental mapping using micro x-ray fluorescence (μ-XRF) and energy dispersive spectroscopy (EDS) indicated that Pb, Fe, Ga, Al and Si were also present on the surfaces of the particles (6). In addition to the particle matrix components, mounting adhesives that were used for non-destructive particle characterization were also present, which included organic polymers and gold coating. In terms of isotopic analysis and relative radionuclide abundance, total dissolution is critical. The 7 M HNO_3/0.05 M HF acid digestion procedure with H_2O_2 added as a catalyst was chosen based on preliminary work described in (103) regarding Pu recovery from WGPu disposition for incorporation into mixed oxide fuel (MOX). In this method, Pu metal is converted to PuO_2, which is then dissolved for the chemical separation of Ga by ion exchange prior to production of the purified Pu dioxide needed for the MOX fuel.

The particles used for the dissolution experiments varied in size, shape and morphology, but all were within a 50 to 500 μm size range and could be seen with the naked eye prior to dissolution. After the first acid treatment, smaller particles were noticed in the Teflon vial. These particles varied in color and size and it was unclear if they were from the breakdown of the particle or from the

digestion of the mounting adhesives. After the third acid treatment, light brown flakes floated on the surface. These flakes were only observed in particles that were gold coated. A flake was isolated, rinsed with DI water and placed under a lead-shielded NaI detector that was attached to a count rate meter. No counts were distinguished over background, indicating the sample did not contain gamma emitting isotopes. After the dissolved sample was evaporated, a total of 5 to 10 mL of 7 M HNO_3/0.05 M HF was added to the vial in 0.5 mL increments. Each addition was transferred to a polypropylene syringe that was fitted with a 0.45 µm PTFE filter.

The Teflon container used for dissolution was checked for activity with the NaI detector after each 0.5 mL rinse. The rinse process was repeated until the residual activity in the container was less than 1% of the total count rate observed prior to rinsing. Initial particle mass was not measureable with the instrumentation available in the laboratory, therefore, a quantitative assessment of the total dissolved solids was not possible. The total activity in solution was determined by LSC and these data were qualitatively compared to the original activity estimates determined by non-destructive gamma spectrometry analysis (Table 19). The non-destructive analysis consisted of peak integration of selected photons associated with the decay of ^{239}Pu, ^{241}Am, and ^{235}U. Total activity was extrapolated from relative peak ratios and the information provided in Table 16. The particle activity estimates from both non-destructive and dissolution experiments were within a factor of 2 for most of the hot particles. The exceptions were the two highest activity particles, labeled HP-10 and HP-18. The LSC data

estimated a total particle activity that was more than twice the gamma estimated total activity.

Table 19. Activity recovered from hot particle dissolutions vs. estimated activity from non-destructive gamma spectrometry analysis.

Analysis	HP 3	HP 7	HP 9	HP 10	HP 17	HP 18	16-D
Gamma Spectrometry	2.5	1.3	1.4	63.1	2.2	44.4	N/A
Dissolved Particle (LSC)	2.9	2.0	1.7	153.3	2.9	97.5	1.4

Units = KBq per hot particle

Gamma data obtained pre-isolation of hot particle in 2-20 g soil from ^{241}Am (59.5 and 125 keV), ^{239}Pu (129 keV), ^{235}U (185 keV) peak integration.

There are several possible explanations for this discrepancy. LSC is extremely effective for determining total alpha/beta activity concentration because all of the energy is deposited within the counting medium. Most of the radioactive constituents present in the particle (parent and progeny) decay by alpha or beta emissions and therefore are likely to be counted by LSC. In contrast, gamma spectrometry counting efficiency is highly dependent on the

photon energy, the absorber matrix (i.e. soil and sample containment), and the sample geometry.

The positional dependence of the particle or a given point source with respect to the detector face can decrease the counting efficiency. Table 20 illustrates the positional dependence of a point source on detection efficiency (6).

Table 20. Sample geometry dependence on high resolution gamma spectrometry detection efficiency.

Particle Position Relative to the Center of the Detector Face	Δ Efficiency[1]
10 mm	-3.1 %
20 mm	-14.2 %
25 mm	-26.6 %

The change in efficiency is reported as the net decrease in peak counts as the particle is moved away from the center of the detector face. Measurements were collected on a Canberra BE3830 broad energy germanium detector.

These values were determined by placing a standardized ^{241}Am gamma button source on the detector face and counting the source at various distances from the center of the detector face. In the non-destructive gamma analysis studies, the hot particles were in 2 to 20 g of soil. Additional efficiency losses were attributed to photon absorption within the sample matrix and sample container. These values can be derived from the relationship between the

incident photon energy (i.e. 60 keV for the photon released by the decay of ^{241}Am), the type and thickness of the material the photon interacts with prior to reaching the detector (i.e. the soil and container) and the particle position with respect to the detector face. The fractional loss of photon intensity can be estimated using the following simplified formula (35):

$$\frac{I}{I_0} = e^{-\mu t} \qquad \text{Equation 17}$$

where I/I_o is the fraction of photons that reach the detector, μ is the attenuation coefficient for the 60 keV photon in soil (or plastic for sample containment) and t is the thickness of the soil sample/containment with respect to the hot particle location within the sample, assuming that the particle is a discrete point source. In the case of the BOMARC soil samples used for initial gamma analysis, the soil was primarily composed of silicon dioxide, most likely in the form of $Al_2Si_2O_5$ (density, $\rho \approx 2.4$ g/cm^3). The attenuation coefficient for the 60 keV photon in the soil is approximately 0.226 cm^2/g. If the particle was located on the top layer of the soil and centered over the detector face, the photon intensity would be reduced by approximately 18% and 46% for soil depths of 3.5 mm and 10 mm, respectively.

5.4.3 Bulk Activity Ratios

Prior to chemical separation, an aliquot of each of the hot particle solutions was co-precipitated with CeF_3 to determine the bulk alpha activity ratio of ^{238}Pu and ^{241}Am to $^{239+240}$Pu using alpha spectrometry (Figure 24). Values ranged from 0.15 to 0.26, with an average bulk alpha activity ratio of 0.20 ± 0.04. This mean value agreed with earlier reports (100,104).

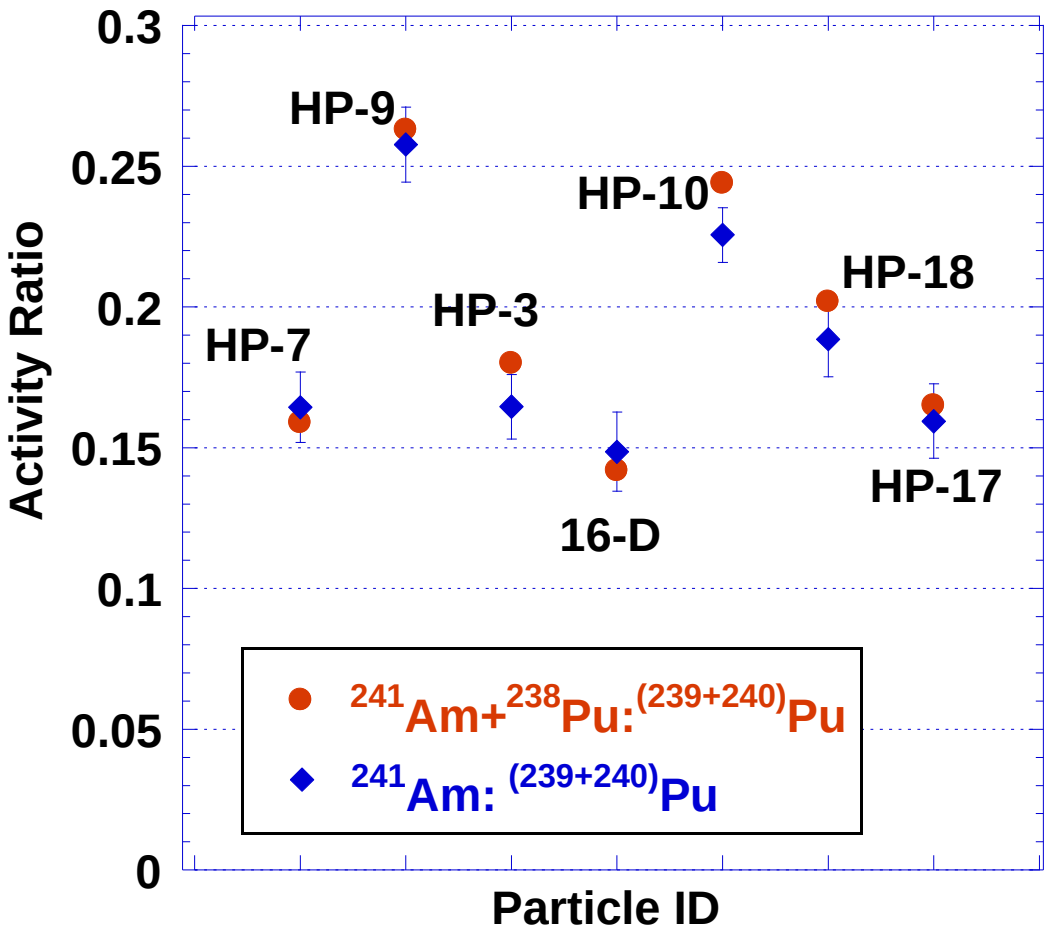

Figure 24. Activity characterization (^{238}Pu + ^{241}Am to $^{239+240}$Pu) of dissolved hot particle solutions as determined by alpha spectrometry. The red circles represent the bulk activity ratio prior to chemical separation and the blue diamonds represent the Am to $^{239:240}$Pu ratio after chemical separation. Each sample was counted for 1000 seconds. Error bars are representative of the reproducibility of the activity ratios at n= 5 samples per hot particle solution at 1 σ.

5.4.4 Chemical Separations

The hot particle solutions were run through the separations procedure (Figure 22) and the total activity collected in each elution fraction was determined by LSC (Figure 25). The activity was concentrated in 2 major fractions, the Pu fraction (TEVA E1) and the Am fraction (DGA E1 Am). The total activity recovered in

these two fractions was 98±3%, indicating that the separation procedure successfully isolated the bulk of the activity from solution.

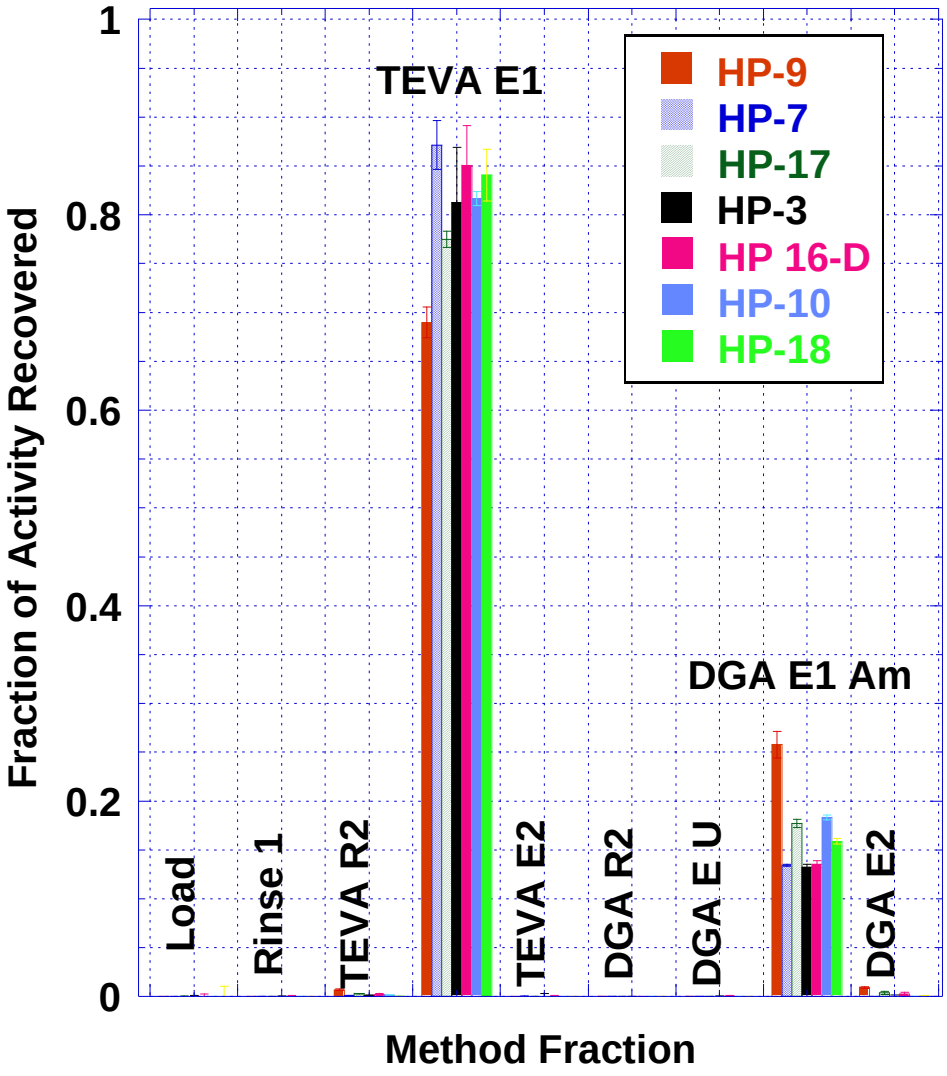

Figure 25. Bulk activity distribution of dissolved particles (in 7 M HNO_3 ·0.05 M HF· 0.05 M $Al(NO_3)_3$ sample loading matrix) using TEVA and DGA resins for chemical separations. TEVA E1 and DGA E1 Am correspond to the Pu and Am elution fractions, respectively. The values given for HP-9 were later revised (see text).

While LSC analysis cannot provide information about the radioactive contributors in each of the collected fractions, it is useful to compare the activity collected in the designated Pu and Am fractions for gross activity ratios. The activity ratios of DGA E1 Am: TEVA E1 ranged from 0.154 to 0.374, with an average activity ratio of 0.21 ± 0.08 (Figure 25). The particle identified as HP-9 had a two-fold increase in activity in the Am fraction. Some Pu breakthrough occurred during separation, which was confirmed with alpha spectrometry analysis. The average activity ratio of the DGA E1 Am to TEVA E1 reduced to 0.19 ± 0.03 upon omission of HP-9. This value was in good agreement with the expected ^{241}Am:$^{238+239+240}$Pu ratio (0.195) based on the Pu isotopic composition of the original material, corrected from the time of the historical assay to the present day.

After the dissolved particle solutions were run through the chemical separations procedure, the CeF_3 co-precipitated Am fraction was compared to the co-precipitated Pu fraction. The activity ratio of ^{241}Am:$^{239+240}$Pu ranged from 0.16 to 0.26, with an average of 0.18± 0.06. These ratios are also plotted in Figure 24 for comparison with pre-separation ratios. The expected ratio for ^{241}Am:$^{239+240}$Pu was 0.198 based on the information provided in Table 16 and decay calculations. The mean ratio observed in this study was lower than the expected ratio and this observation has also been noted in other reports (6,104).

5.5 Plutonium Isotopic Composition

5.5.1 Relative Abundance of ^{240}Pu

High resolution gamma spectra that were collected for an isolated hot particle prior to dissolution and after dissolution and chemical separation are provided (Figure 26).

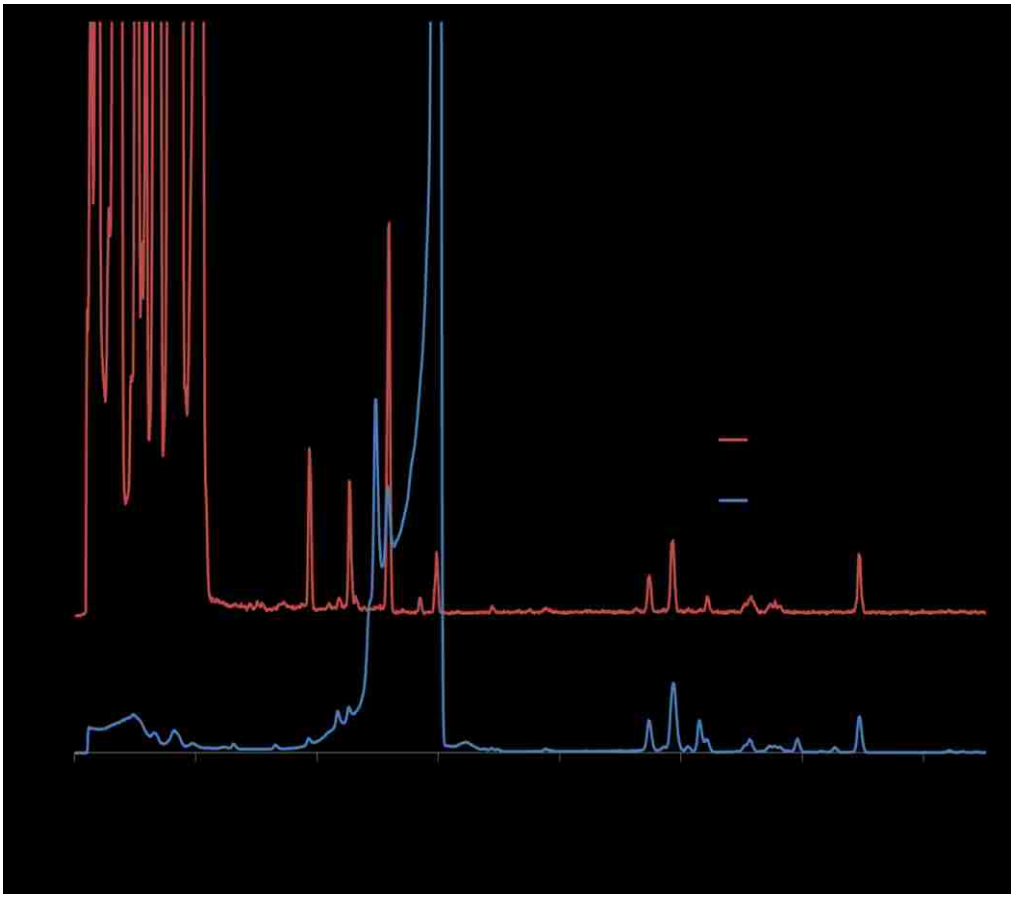

Figure 26. High resolution gamma spectrum of an isolated hot particle (prior to dissolution) and after chemical separation. Samples were counted on a BEGE detector for 24 hours. The post separation spectrum (Am Removed) was shifted upward by a constant value (i.e. 10,000 counts were added to the counts in each channel to raise the baseline).

The ^{241}Am peak at 60 keV had a large tail or continuum that masked the peak energies used for determining ^{240}Pu:^{239}Pu activity ratios. After ^{241}Am removal from the system, the lower energy peaks that were hidden under the tail could be used for determining ^{240}Pu:^{239}Pu isotopic ratios. The ^{240}Pu: ^{239}Pu ratios are plotted in Figure 27.

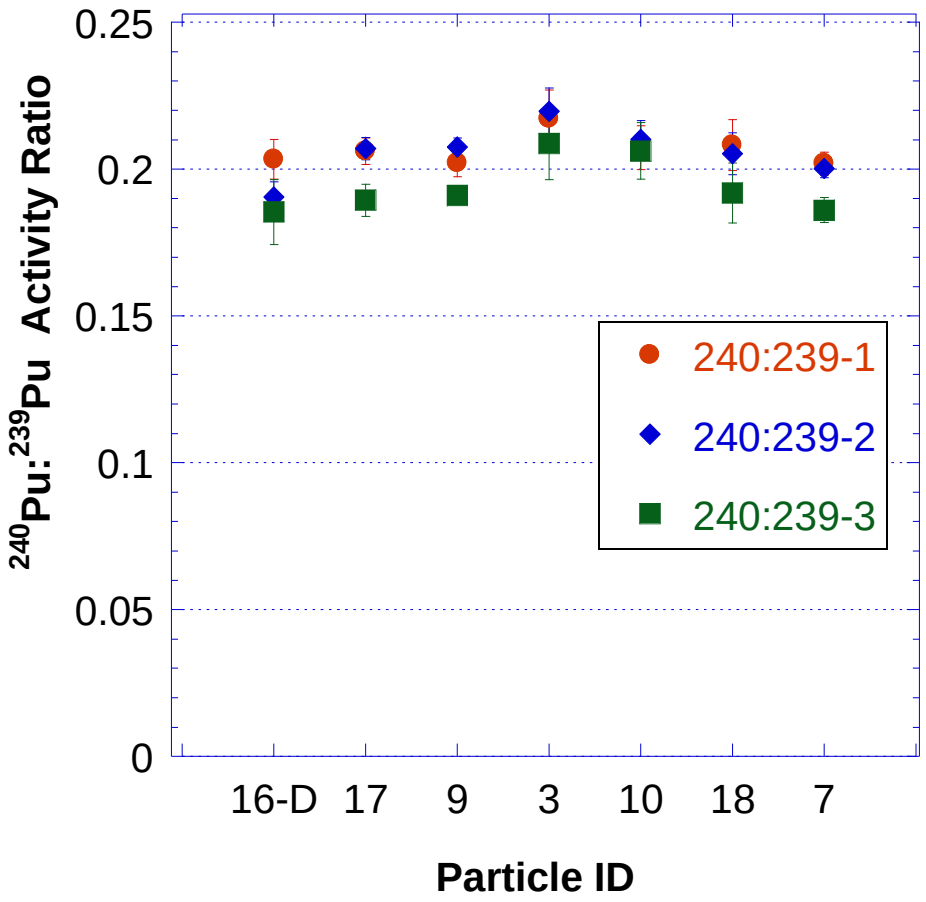

Figure 27. Collective $^{240:239}$Pu activity ratios as determined by gamma spectrometry. Each sample was counted for 24 hours. ^{239}Pu peaks selected for analysis include 38.6 keV (γ yield = 1.04E-4, 239-1), 51.6 keV(γ yield = 2.72E-4, 239-2), and 129 keV(γ yield = 6.31E-5, 239-3). Data are consistent with 0.20 ± 0.01, in reasonable agreement with expectations from the literature. The peak selected for ^{240}Pu analysis was at 45.6 keV (γ yield = 4.474E-4). As expected, the less attenuated line in ^{239}Pu at 129 keV resulted in a lower 240:239 value than did the others.

The 43.5 keV photon associated with the decay of ^{240}Pu was compared to three different ^{239}Pu photon energies (Table 17). The mean ^{240}Pu:^{239}Pu ratio was 0.20 ± 0.01. This ratio was in good agreement with the expected ratio of 0.22 derived from the information in Table 16 and published values (104).

5.5.2 Relative Abundance of ^{238}Pu

After chemical separation, the relative isotopic ratio of ^{238}Pu was determined by alpha and gamma spectrometry. The ^{238}Pu:$^{239+240}$Pu alpha activity ratio was consistent across the hot particle population, with a mean activity ratio of 0.0151 ± 0.001 (Figure 28). This value was lower than the expected ^{238}Pu:$^{239+240}$Pu ratio of 0.0161. Each Pu filter was also counted by gamma spectrometry to determine the ^{238}Pu to ^{239}Pu activity ratio. A low yield photon (43.5 keV) produced by the decay of ^{238}Pu was used to determine the ^{238}Pu:^{239}Pu ratio for each hot particle. The mean ratio for ^{238}Pu:^{239}Pu across all particles was 0.0193 ± 0.003, which agreed with the expected ratio of 0.020. It is of particular interest that the gamma ratio for ^{238}Pu:^{239}Pu was in good agreement with the reported value, but the alpha ratio of ^{238}Pu to $^{239+240}$Pu was lower than expected.

5.5.3 Relative Abundance of ^{241}Pu

The isotope ^{241}Pu primarily decays by beta emission. The beta associated with ^{241}Pu decay has an average energy of 5.23 keV and an endpoint energy of 20.78 keV and can be difficult to detect in a high alpha field. Many studies have used LSC to determine the ^{241}Pu isotopic content relative to the total alpha-emitting Pu isotopes due to the relatively high beta counting efficiency.

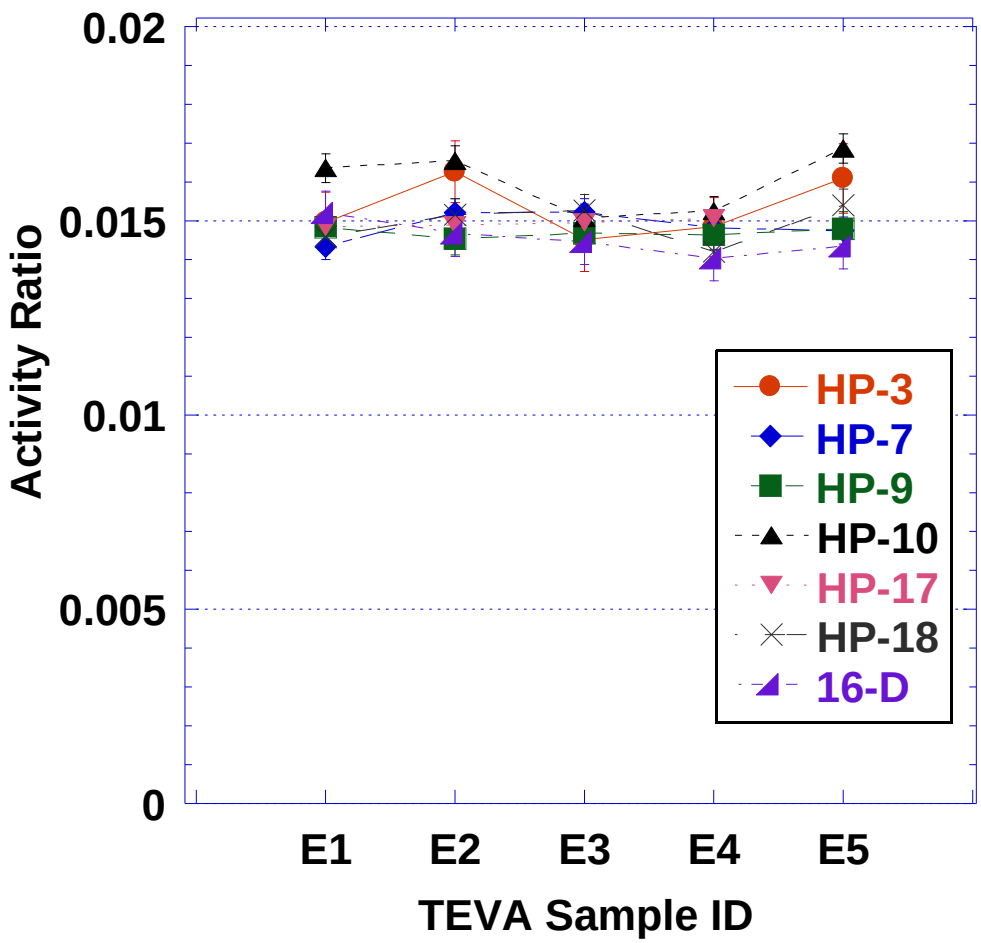

Figure 28. ^{238}Pu to $^{239+240}$Pu activity ratios for the dissolved hot particle solutions after chemical separations. E1-E5 on the x-axis represent the 5 Pu elution fractions collected for n= 5 trials per dissolved hot particle. Error bars represent the counting error associated with each activity ratio at 1 σ. Data are consistent with a value of 0.0151 ± .001, somewhat lower than the value of 0.0161 expected from a decay calculation of the data in the literature (Table 16).

In this study, energy discriminator settings were used to separate the low energy region of the LSC spectrum from the high energy spectrum. The ^{241}Pu energy region (CPMA) was set between 0-50 keV and the alpha energy region (CPMB) was set between 50-1000 keV. Average alpha decay energies are between 4 and 6 MeV; however, all but approximately 1/10 of the energy is lost

to the counting medium prior to signal collection. This results in an LSC spectral shift of the alpha signal into the 400-600 keV energy range. It was assumed that the alpha spill over signal into the low energy window was insignificant relative to the expected ^{241}Pu activity present in the dissolved hot particle solutions.

The low energy ^{241}Pu beta signal was compared to the total alpha Pu signal after chemical separation of the Pu in the hot particle solutions using the following relationship:

$$\frac{CPMA(post)}{CPMB(post)} \times \frac{\varepsilon_\alpha}{\varepsilon_\beta} = \frac{^{241}Pu}{^{238+239+240+242}Pu} \qquad \text{Equation 18}$$

where CPMA and CPMB represent the counts per minute in the respective energy windows, ε_α and ε_β are the alpha and beta decay LSC detection efficiencies. It was assumed that the alpha detection efficiency was 100%. The ^{241}Pu beta efficiency was determined using a Pu standard (Isotope Products, Valencia, CA, USA). The Pu standard was diluted to 200 Bq/mL in the method sample loading matrix, 7 M HNO_3 · 0.5 M HF · 0.5 M $Al(NO_3)_3$, and counted by LSC prior to and after chemical separation with the TEVA resin. The ^{241}Pu detection efficiency was determined using the following relationship, derived from Equation 18:

$$\frac{CPMA}{CPMB} \times \frac{A_{Pu-total\ \alpha}}{A_{241}} \times \varepsilon_\alpha = \varepsilon_\beta \qquad \text{Equation 19}$$

where $A_{Pu\text{-total}\alpha}$:$A_{241}$ was the activity ratio of ^{241}Pu to $^{238+239+240+242}$Pu in the standard, and CPMA, CPMB, ε_α and ε_β are defined above. The average ^{241}Pu beta efficiency was 36 ± 9%. The large variance in the counting efficiency was due to the relatively low activity concentration of ^{241}Pu relative to alpha emitting

Pu isotopes (activity ratio = 0.0797). Studies conducted with high purity Pu standards with higher ^{241}Pu concentrations have shown similar LSC detection efficiencies (105-109).

Using Equation 18, the average observed ^{241}Pu to $^{238+239+240}$Pu ratio was 0.533 ± 0.05 across all hot particle samples and the expected ratio was 0.55. It should be noted that this method was a qualitative approach to ^{241}Pu isotopic analysis and should only be used in combination with the alpha and gamma spectrometry data so that chemical separation efficiency can be accounted for in the calculations.

5.5.4 Elemental Analysis

Aliquots of the dissolved, filtered hot particle solutions (in the 7 M HNO_3 - 0.05 M HF matrix) were taken for elemental evaluation. Each aliquot was evaporated to dryness and reconstituted with 1% nitric acid for ICP-AES analysis. Lead, Fe, and Ti were present in all hot particle solutions at concentrations ranging from 0.01 to 0.1 mM. Aluminum was the most abundant element with concentrations ranging from 0.1 mM to 10 mM (Figure 29).

After the samples were evaporated to dryness, a clear residue developed on the bottom of the vial. The residue was treated with concentrated nitric acid (100 µL) and aged in this solution for 30 minutes prior to the addition of de-ionized water. The residue did not fully dissolve; therefore, the 1% HNO_3 solution was heated in a warm water ultrasonicator bath for 2.5 hours, but still did not dissolve in this time.

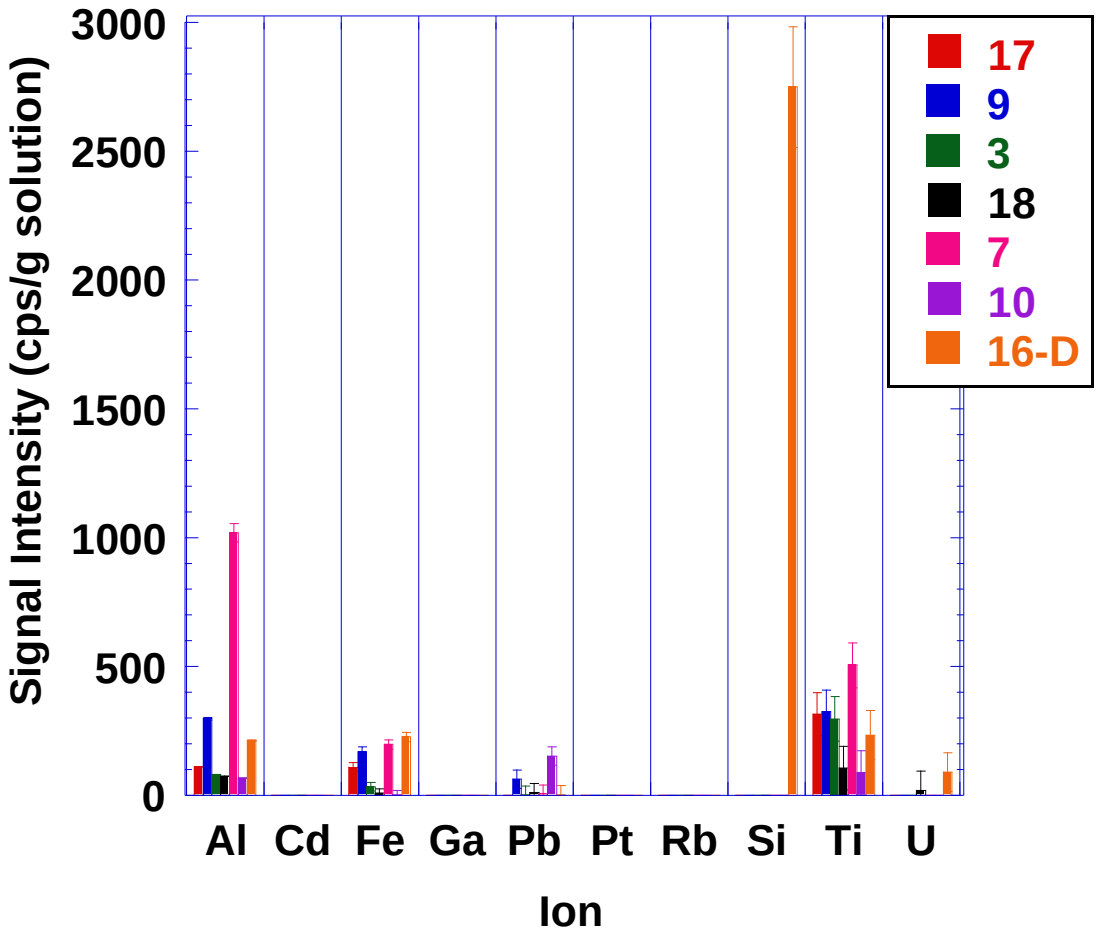

Figure 29. Hot particle elemental analysis. Original sample matrix solution (7M HNO_3· 0.05M HF) was evaporated and samples were reconstituted first in 100 µL of concentrated HNO_3 and diluted with 9.9 mL of DI water. Analysis was performed by ICP-AES.

It was believed that the residue was an insoluble silicate formed during evaporation. However, evaporation of HNO_3/HF solutions can lead to loss of Si; as seen from Figure 29, only sample 16-D contained an observable concentration of silicon. Another possibility is that evaporation of titanium-bearing solutions in the absence of halides leads to the formation of rutile (TiO_2) which is very resistant to redissolution; rutile is not a very good carrier of the light

actinides. Several of the hot particle samples were tested for elemental analysis without evaporating the original sample matrix solution. The elemental analysis results for one of the hot particle solutions (HP-9) were compared to the results obtained from evaporation (Figure 30).

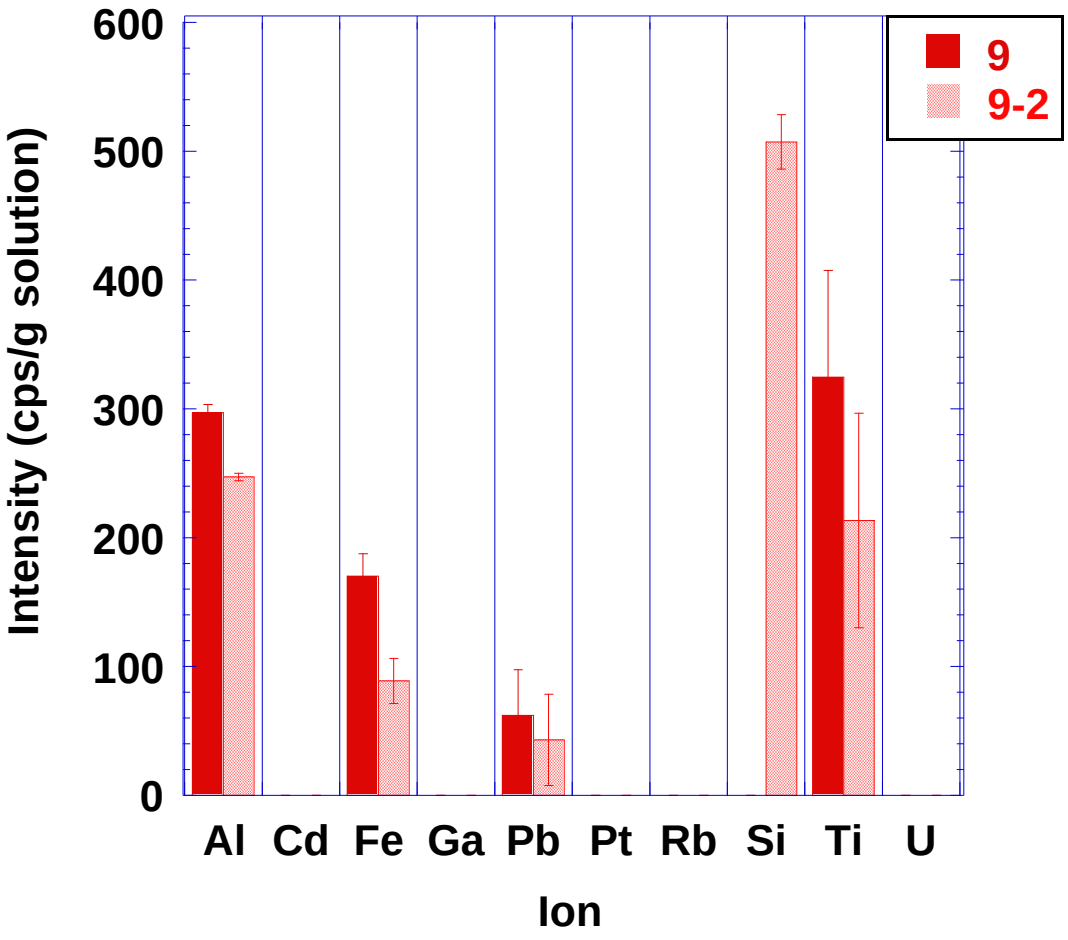

Figure 30. A comparison of the elemental analysis of hot particle (HP-9) with samples evaporated at 90 °C (solid bar) prior to analysis and samples not pre-treated prior to ICP-AES analysis (hatched bar).

Aluminum, Si and Fe were the elements most affected by sample evaporation pre-treatment when compared to no pre-treatment. Silicon was present in samples that did not undergo evaporation, but not detectable in the samples that were evaporated. This supports the assumption that the insoluble residue that was observed after evaporation was most likely silicate based, but could also contain rutile. Iron and Al concentrations were higher in the evaporated samples.

5.6 Concluding Remarks

High-fired WGPu particles that have been in the environment for the last 4 decades were characterized by both non-destructive and dissolution techniques. The non-destructive imaging and soil profile characterization studies showed that the Am was heterogeneously dispersed in the soil and that morphology and surface composition were unique for each hot particle (6). Dissolution studies showed that the elemental matrix of each hot particle was unique, but that several key elements were present throughout the particle population. Preferential Am leaching from the particle matrix was supported by the dissolution data, but cannot be confirmed under the confines of this work. Further investigations will be required to determine how particle chemistry in terms of size, source term and microchemistry govern actinide speciation.

From a forensic perspective, the method used in this work was sufficient for separating Pu from other particle matrix constituents for determining relative isotopic ratios. The isotopic abundance for ^{238}Pu, ^{240}Pu and ^{241}Pu relative to ^{239}Pu obtained from LSC and gamma analysis experimentally placed the material

production date between 51 and 54 years ago (assuming the relative Pu isotopic abundance information in Table 16 is accurate). Alpha spectrometry analysis placed the production date at 60 years ago. The discrepancy in the relative abundance of ^{238}Pu from alpha and gamma analysis is of particular interest and has also been observed in previous work (104) which attributed the difference to a satellite accident that occurred in 1964. In this work, hot particles were isolated from the surrounding soil prior to dissolution; therefore, atmospheric fallout was not expected to influence the particle composition. Alpha spectrometry and LSC analysis should provide more accurate isotopic abundance values based on higher radiative yield and detection efficiency compared to gamma spectrometry. If it is assumed that the ^{238}Pu:$^{239+240}$Pu ratio determined by alpha analysis is accurate, it is possible that the original ^{238}Pu abundance was lower than what is reported in Table 16. From historical documents relating to the production of WGPu (110) around the estimated time of production (52 years), the amount of ^{238}Pu in the production stream varied. If the data presented in Table 16 is from stream analysis, which was based on the isotopic content of the Pu coming out of the plant around the time of part manufacture and the weight of the part, and not from a direct assay of the material recovered from the accident site, then the isotopic abundance of the material may have a higher degree of uncertainty.

Future work will need to focus on the minor actinide constituents. High resolution gamma spectrometry analysis of hot particles prior to dissolution showed that the ^{235}U and ^{238}U content varied across the population of particles that were isolated from the soil (6). In the current work, a designated U fraction

was collected from the DGA resin. At this time, U isotopic analysis has not been performed on the U fraction. The U isotopic content of the particle includes ^{234}U, ^{235}U, ^{236}U, ^{237}U (in equilibrium with ^{241}Pu α decay) and ^{238}U and the relative ratios of each could provide further insight into the source term of the particles.

CHAPTER 6

PLUTONIUM ISOTOPIC STANDARD DEVELOPMENT FOR GAMMA, ALPHA AND MASS SPECTROMETRY

6.1 Abstract

After chemical separation and radionuclide purification, Pu samples are usually divided and prepared separately for mass and radiometric analysis. This work focuses on a singular sample preparation method for determining the isotopic abundance of Pu in a NIST-traceable ^{239}Pu standard with a 98% mass purity. Cerium fluoride (CeF_3) co-precipitation was chosen as the sample preparation technique based on quick preparation time, high actinide recovery, and good energy resolution for alpha spectrometry analysis. Precipitated samples were prepared from the standard Pu stock solution with activity concentrations ranging from 0 to 2400 Bq (0 - 1000 ng ^{239}Pu). Samples were analyzed by alpha and gamma spectrometry for radiometric determination of isotopic abundance. Inductively coupled plasma mass spectrometry (ICP-MS) coupled to a laser ablation sample introduction unit was used for mass analysis. Results indicated that CeF_3 sample preparation is well suited for all three types of analysis techniques. The ^{238}Pu to $^{239/240}$Pu ratios determined by alpha and gamma spectrometry were higher than the reported values, indicating that the trace ^{238}Pu concentration in the standard solution was inaccurate. Mass analysis of ^{238}Pu was not possible for these samples due to low relative abundance and the presence of a high background signal in the 238 mass region, which was suspected to be a result of ^{238}U contamination in the acid used for initial sample

preparation. The ^{240}Pu to ^{239}Pu isotopic ratio was consistent for all three techniques. The isotopic abundance of ^{241}Pu and ^{242}Pu were insufficient for mass analysis and alpha energy resolution was not adequate for resolving ^{242}Pu from $^{239+240}$Pu. These preliminary data are presented as a proof-of-concept. The end goal is to develop a rapid, reliable and reproducible method for sample analysis that can be fitted onto a radioanalytical platform for automated analysis that can exploit gamma, alpha, or mass spectroscopy.

6.2 Introduction

The focus of this work up to now has been to characterize the performance of chemical separations of actinides with the intent of developing rapid, reliable methods that are amenable to platform automation. After separation and purification, each sample and many side samples were analyzed in terms of separation efficiency, isotopic identification and total activity. It would be useful to have one preparation method to produce samples that can be used for multiple analysis techniques. Many studies have combined radiometric and mass-based analysis methods for determining isotopic information on samples containing low concentrations of both long- and short-lived actinides, i.e. global fallout, source term and age determination of Pu, and U in the environment (13,111-117). In most of these studies, sample preparation for alpha spectrometry and mass spectrometry has remained separate. Chemical separation procedures have been streamlined so that the resulting actinide elution fractions are suitable for both types of sample preparation methods (118), reducing the total analysis time.

Aqueous samples are prepared for mass analysis and small aliquots of the sample solution are typically electrodeposited on steel planchets for alpha analysis. Recent studies have explored the use of mass spectrometry on the leachate from electrodeposited Pu and U alpha sources (115,119). In these studies, one sample was produced for multiple analysis techniques; however, after alpha counting, the deposited source was converted to an aqueous source for mass analysis.

Several other actinide studies have been conducted with laser ablation inductively coupled mass spectrometry (LA-ICP-MS) on solid surfaces, such as accelerator target material, metal oxides, ceramics and soil particulates (120,121). The clear advantage of LA-ICP-MS analysis is that only a small portion of sample is consumed, while the rest of the sample remains intact, and can be preserved for future analyses. The limitations of LA-ICP-MS analysis are that the results are semi-qualitative, difficult to interpret for materials of unknown origin, and require isotope concentrations in sufficient concentration be evaluated by mass spectroscopy LA-ICP-MS has been successfully coupled with isotope dilution techniques to provide more quantitative results for environmental soil sample characterization (111,120). While direct mass analysis of solids is advantageous for many sample matrices, it is not adequate for isotopic identification in complex actinide samples that contain isobaric interferences. These samples still require sample dissolution and chemical separation for accurate isotopic identification and quantification. Few studies have focused on direct mass analysis from a prepared alpha sample. One recently published

study (122) characterized electroplated samples containing ^{239,240,241}Pu isotopes using high resolution ICP-MS with laser ablation sample introduction. This study isolated Pu from other radionuclides using acid leaching, extraction chromatography and electrodeposition prior to ICP-MS analysis. In their study, the authors looked at samples containing very dilute concentrations or activity levels of Pu that were chemically isolated prior to analysis.

In our previous work, WGPu hot particles were dissolved in a HNO_3/HF acid solution, and the Pu was chemically separated from other matrix constituents using TEVA and DGA extraction chromatography resins. Each sequential elution fraction was collected and prepared for analysis using a CeF_3 co-precipitation method (29). This method was chosen based on short preparation time (12 samples/hr), good energy resolution for alpha analysis (~32 keV), and high actinide recovery as scavenged by the precipitate. Additionally, the filters could be used for mass analysis with the LA-ICP-MS system to confirm the relative isotopic ratios determined from gamma and alpha analysis. The initial focus of this work was to develop CeF_3 co-precipitated ^{239}Pu calibration standards for optimizing gamma and alpha spectrometry measurements. From an analysis perspective, sample matrix, analyte concentration and geometry should be mimicked in the calibration standards.

The aqueous Pu standard used for these experiments contained minor Pu isotopes in concentrations similar to those found in WGPu and, therefore, isotopic analysis could be performed with the calibrations standards produced in-house. This preliminary work demonstrates the utility of CeF_3 precipitation as a

single source sample preparation method for both radiometric and mass-based Pu isotopic analyses.

6.3 Materials and Methods

6.3.1 Reagents

Nitric acid solutions were prepared from reagent grade acid (ACS reagent grade, Merck KGaA, Darmstadt, Germany) and de-ionized water (18 MΩ·cm, Millipore, Billerica, MA, USA). Plutonium was selectively removed from decay products using TEVA extraction chromatographic resin obtained from Eichrom Technologies, Inc. (Darien, IL, USA) in 2 mL pre-packed polypropylene cartridges. TEVA resin (50-100 μm) contains an aliphatic quaternary amine as the extractant compound for the stationary phase and is primarily used for isolating and separating tetra-valent actinides from tri- and hexa-valent actinides and fission products (34).

6.3.2 Radionuclide Standard

Plutonium stock solutions were prepared from a NIST-traceable ^{239}Pu standard solution (Isotope Products, Valencia, CA, USA) in 3 M HNO_3. The total activity of the stock solution was determined by LSC (Tri-carb 3100, Perkin Elmer, Boston, MA, USA) with 10 mL of Ultima Gold AB cocktail (Perkin Elmer, USA) as the counting medium. The LSC samples were counted for 60 minutes or until the counting error reached 2S% (2% of the 2σ standard deviation of the total counts) in the CPMC energy window (0-2000 keV). The 2S% is a standard protocol option that serves as a normalization parameter for the comparison of

multiple sample measurements, i.e. the error reported for each measurement represents 2% of twice the standard deviation of the counts collected in the CPMC region of the spectrum. The average background count rate in the CPMC window was 38 ± 1 (1σ) cpm for method blanks.

According to the source certificate, the isotopic purity of the ^{239}Pu standard was only 98% (atomic percent), with the remaining two percent consisting of ^{238}Pu, ^{240}Pu, ^{241}Pu and ^{242}Pu. The relative abundance of each Pu isotope is summarized in Table 21. The decay corrected activity percent values (Table 21) were applied to the total activity values determined by LSC to determine the expected activity of each Pu isotope in the stock solution and subsequent sample solutions. A portion of the original Pu stock solution (prepared in 3 M HNO_3) was also run through a TEVA extraction chromatography column to remove the various Pu daughter products (i.e. U and Am). The TEVA resin was treated with 2 mL of 3M HNO_3 then 5 mL of the Pu stock solution were loaded onto the wetted column. Under these loading conditions, Pu^{+4} was retained on the column, while Am^{3+} and UO_2^{2+} passed through the column. Five sequential column elutions with 5 mL of 0.01 M HNO_3 were collected and total activity concentration was determined by LSC, to verify that there were no significant losses in chemistry. This solution was used as the chemically purified Pu stock solution and, with the exception of ^{241}Am, the data in Table 21 also apply to this stock solution.

Table 21. Decay corrected plutonium isotopic standard information.

Radio-nuclide	Half-Life (yr)	[1]March-2005		[2]February-2009	
		Atom %	Activity %	Atom %	Activity %
^{238}Pu	8.77E+01	1.40E-03	3.32E-01	1.36E-03	3.21E-01
^{239}Pu	2.41E+04	9.79E+01	8.44E+01	9.79E+01	8.44E+01
^{240}Pu	6.56E+03	2.05E+00	6.50E+00	2.05E+00	6.50E+00
^{241}Pu	1.44E+01	6.10E-03	8.80E+00	5.05E-03	7.29E+00
^{242}Pu	3.75E+05	1.00E-03	5.54E-05	1.00E-03	5.54E-05
^{241}Am	4.33E+02	Not reported	Not reported	1.05E-03	5.03E-02

[1] Isotopic verification date

[2] Experiment date

Relative uncertainty of each minor isotope value is ±15% per discussions with the manufacturer. ^{239}Pu uncertainty provided with certificate is ±3%. It is assumed that ^{241}Am was removed from the sample in March 2005, but this is not supported by the analytical data.

6.3.3 Sample Preparation

Sample solutions were prepared from the Pu stock solutions mentioned above (i.e. the original stock solution and the chemically purified stock solution). Four sets of samples (n=7 per set) were produced for analysis purposes. Two sets of samples were prepared for aqueous ICP-MS analysis and two sets for CeF_3 co-precipitation (Figure 31).

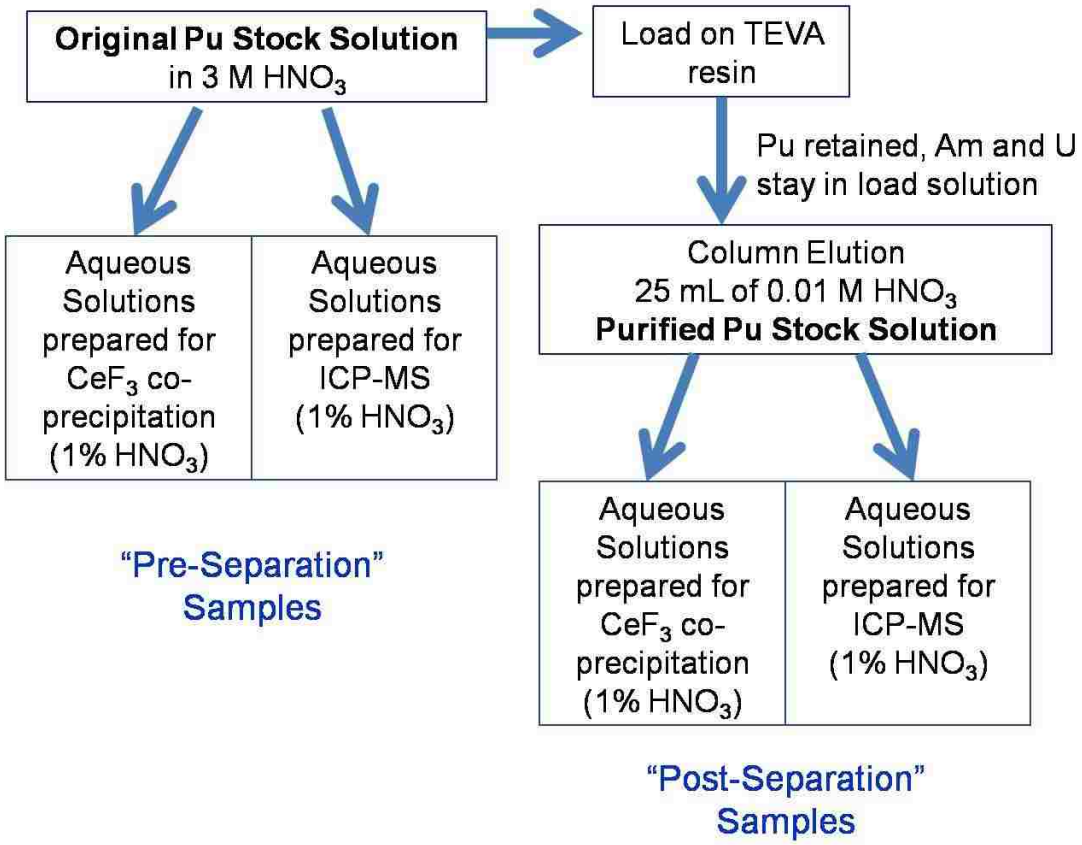

Figure 31. Aqueous sample preparation schematic for ICP-MS and CeF_3 co-precipitation.

Aliquots of the respective Pu stock solutions were taken gravimetrically and diluted with 1% HNO_3 to a normalized solution mass of 10 g for aqueous ICP-MS analysis and 5 g for co-precipitation. The ^{239}Pu mass equivalence and activity concentration of each sample in a set of 7 is provided in (Table 22).

Table 22. Total activity and mass values based on ^{239}Pu for each sample solution within a set of 7. Four sets of aqueous solutions were prepared, 2 for CeF_3 and 2 for ICP-MS.

Sample ID	^{239}Pu Activity (Bq)[1]	Mass (ng of ^{239}Pu)[2]
Method Blank	0	0
1	12	5
2	23	10
3	114	50
4	239	100
5	577	250
6	1168	500
7	2316	1000

[1] Activity per sample prior to co-precipitation.

[2] Total Pu mass in solution. For ICP-MS analysis solutions ranged from 0.5 to 100 ppb (ng ^{239}Pu per g solution, total solution volume = 10 mL)

The net activity in each sample solution (for both ICP-MS and CeF_3 samples) was determined using the following equation:

$$\frac{A_{Pu\ stock\ \ soln}}{g\ stock\ solution} \times m_{aliquot} = A_{net} \qquad \text{Equation20}$$

where *A* is the activity of the Pu stock solution, in Bq/g, determined by LSC and $m_{aliquot}$ is the mass of the stock solution used in each sample.

6.3.4 Cerium Fluoride Co-Precipitation

A Ce carrier aliquot was added to each of the sample solutions from which precipitates were prepared, followed by an excess of concentrated HF to force precipitate formation. The samples were allowed to sit for 30 minutes and were then filtered through a Resolve filter (polypropylene, 0.1 µm pore size, 25 mm diameter, Eichrom Technologies, Inc.). The precipitate was collected on the filter, rinsed with DI water and treated with ethanol for faster drying. Each filter was placed in a protective plastic sample holder and allowed to air dry for approximately 20 minutes before sealing.

A more detailed explanation of the CeF_3 precipitation procedure is available from the filter manufacturer (29). Residual activity in the supernate was assessed to determine co-precipitation efficiency. The supernate for each sample was evaporated to dryness in a 70°C drying oven and reconstituted in 1 mL of 1% HNO_3. The reconstituted solution was placed in a 20 mL plastic vial with 10 mL of Ultima Gold AB cocktail and counted by LSC as described earlier.

6.3.5 Analysis by ICP-MS

6.3.5.1 Aqueous Analysis

Inductively coupled plasma mass spectrometry (ICP-MS) was performed with an ELAN DRC II ICP-MS system (Perkin Elmer, Inc., Shelton, CT, USA) and the ELAN Version 2.4 software provided by the manufacturer. Peak acquisition mode settings included a dwell time of 50 msec, with 15 sweeps per reading, 1 reading per replicate and three replicates per sample. The operation parameters were optimized by the manufacturer upon installation with the radio-frequency power set at 1100 Watts, the plasma gas flow at 15 L/min, the nebulizer gas flow at 0.90 L/min, the argon auxiliary gas flow at 1.2 L/min and the sample uptake rate of 1 mL/min. Prior to analysis, standard instrument optimization procedures provided by the manufacturer were followed.

Aqueous samples were placed in an autosampler (Perkin Elmer, Inc.) with a method blank (1%HNO_3) between each pair of samples. Pre- and post-separation samples were analyzed during the same analysis session with ten method blanks processed between the two sample sets. The analyte was ionized by introducing the sample as an aerosol into the ion source of the instrument. The ionic charges of species analyzed by the mass spectrometer were z=1. Raw signal intensity (ions per second) was collected for the mass to charge (m/z) ratios presented in Table 23. Integrating over the collection period resulted in a spectrum in m/z. Note that the resolution of the spectrometer (1 atomic mass unit, amu) was not sufficient to separate peaks due to isobars (e.g. ^{238}Pu at 238.049 and ^{238}U at 238.051) but little isobaric interference was expected due to

the isotopic composition of the Pu stock solution. Additionally, $^{238}U^{1}H^{+}$ effects from trace U contamination were expected to be < 1% of the 239 m/z signal and therefore, not a significant source of error. The mass bias factor for the 238 to 242 m/z ratios was assumed to be equal to 1 based on previous experiments with U standards and no corrections were made to the Pu isotopic ratios based on mass discrimination. Peak analysis for each m/z ratio was performed manually for each sample spectrum. The background peak signal (obtained from the method blank) for each m/z ratio was subtracted from the appropriate sample signal.

Table 23. Plutonium m/z ratios used for ICP-MS analysis for both aqueous and CeF_3 co-precipitated samples.

Radionuclide	Mass-to-Charge (m/z) Ratio
^{140}Ce*	140.116
^{238}Pu	238.049
^{239}Pu	239.052
^{240}Pu	240.054
^{241}Am/^{241}Pu	241.057
^{242}Pu	242.059
*Ce mass analysis for filter samples only.	

A mass spectrometric measurement results in a set of isotope ratios; to convert these ratios into an absolute number of analyte atoms, a reference concentration must be supplied. The LSC data was utilized for this purpose. Expected mass values for each sample were calculated using the following formulas:

$$\left[\frac{CPMC - CPMC_{BG}}{m_{aliquot}}\right] = \frac{A_{net}}{g\ soln} \qquad \text{Equation 21}$$

where *CPMC* and $CPMC_{BG}$ were the counts per minute collected in the CPMC energy window (LSC analysis) for the stock solution and background, $m_{aliquot}$ was the mass of the Pu stock solution used for activity verification and $A_{net}/g\ soln$ was the net activity per gram of the stock solution; and

$$\frac{A_{net}}{g_{soln}} \times \frac{m_{a,2}}{m_{ICP-MS}} = \frac{A_{total}}{g\ soln_{ICP-MS}} \qquad \text{Equation 22}$$

where $m_{a,2}$ was the aliquot mass of the stock solution used to make the aqueous ICP-MS solution, $m_{ICP\text{-}MS}$ was the mass of the ICP-MS solution (sum of 1% HNO_3 aliquot and stock solution aliquot) and $A_{total}/g\ soln_{ICP\text{-}MS}$ was the total activity per gram of the ICP-MS sample solution. Units of radioactivity were then converted to units of mass:

$$\frac{A_{total}}{g\ soln_{ICP-MS}} \times \frac{Pu\ Activity\%}{100} \times \frac{MW_{Pu}}{\lambda_{Pu}} \times CF = \frac{ng\ {}^{X}Pu}{g\ soln_{ICP-MS}} \qquad \text{Equation 23}$$

where *Pu Activity%* was the percent activity of the Pu isotope compared with the activity of the solution as a whole (Table 1), *MW* was the molecular weight of the

Pu isotope, λ_{Pu} was the decay constant of the Pu isotope, and *CF* was the stoichiometric conversion factor, which was 1.66×10^{-15} ng·mol per g·atoms.

6.3.5.2 Filter Analysis by LA-ICP-MS

The CeF_3 co-precipitated filters were placed inside the laser ablation system (LSX 500, CETAC Technologies, Omaha, NE, USA). The laser used for sample ablation was a frequency quadrupled 266 nm q-switched Nd:YAG (neodymium-doped yttrium aluminum garnet) with an average energy and pulse width of 9.0 mJ and 6 nanoseconds, respectively, and a beam spot with a width of 50 μm. The system included a small enclosed glass sample chamber mounted on an electronically controlled platform. Each filter was placed in the sample chamber and the platform was centered in the laser staging area. Method blanks, consisting of a CeF_3 precipitate prepared in the same manner as the experimental samples, but without incorporation of the Pu standard, were processed before and after each sample filter. Prior to analysis, each filter was mapped using a charge-coupled device (CCD) camera with the manufacturer-provided software DigiLaz II. An example of the filter image before and after ablation is provided (Figure 32).

In the LA-ICP-MS, z=1 ions are produced following ablation of the solid matrix with the laser. The laser ablation system was coupled to the ELAN DRC II ICP-MS. The operational parameters used for sample ablation and ICP-MS analysis are listed in Table 24. Central regions of the filter sample were selected for line scan analysis using the DigiLaz II software and were subsequently irradiated by the laser. The ablated sample matrix was transported with an argon carrier gas to

the plasma ionization chamber where the sample vapor and particulates were atomized and ionized before passing into the reaction cell and mass analyzer. Four sequential line scan analyses were performed for each filter sample.

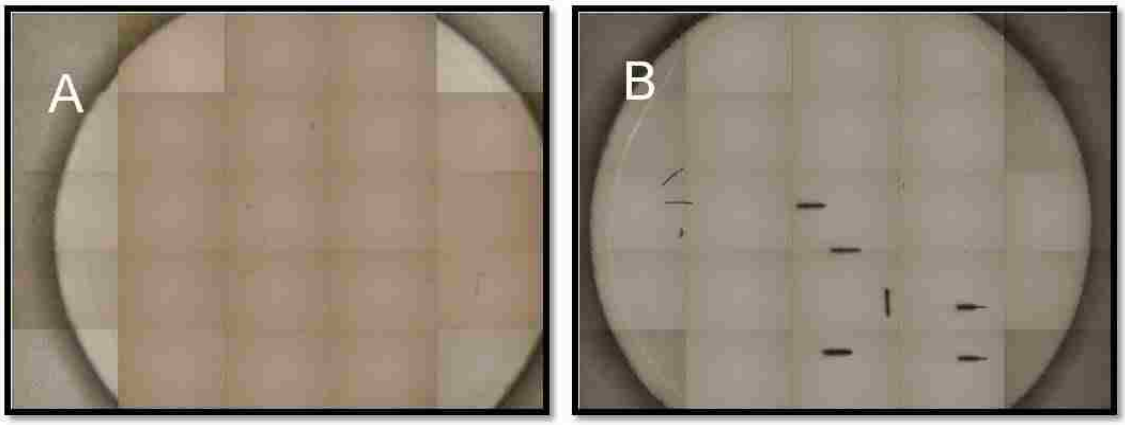

Figure 32. CCD generated image of the CeF_3 filter in the sample chamber of the CETAC laser ablation unit prior to ablation (A) and after ablation of several areas (the dark lines) (B).

Signal integration analysis was performed with GeoPro™ software Version 1.00 (CETAC Technologies) which runs on the Microsoft Excel platform. The m/z ratios analyzed are listed in Table 23. Signal intensity for each m/z ratio was integrated over time from 75 to 150 seconds. The relative m/z peak ratios for 238:239, 240:239, 241:239, and 242:239 were determined using the following equation:

$$\left[\frac{C_x - C_{x,blank}}{C_{239} - C_{239,blank}}\right] = \frac{C_x}{C_{239}} \qquad \text{Equation 24}$$

where C_x and C_{239} represented the integral counts for the m/z ratio of interest

and x = 238, 240, 241 or 242. C_{blank} was the number of counts collected for each respective m/z ratio in the appropriate method blank. Instrument performance at each m/z was determined using the background equivalent concentration (BEC) calculation (123):

$$\frac{I_{BG}}{I_A - I_{BG}} \times C_A = BEC \qquad \text{Equation 25}$$

where *I* is the signal intensity for the background and analyte and *C* is the true analyte mass concentration at the analyte m/z ratio. The BEC is considered a more realistic assessment of the background signal within a given sample set than the instrument limit of detection (LOD), which only represents the background noise. As an example, if the background signal intensity (I_{BG}) in the 140 m/z channel region was 1000 ± 50 cps (1σ) and the analyte signal (I_A) intensity was 3 x10^4 cps for C_A = 20 ng Ce (material ablated during the line scan analysis), the BEC would 0.69 ng of Ce/ line scan.

The LOD would be equal to $3\sigma * C_A/(I_A - I_{BG})$, or 0.10 ng of Ce/ line scan. The Ce signal (m/z=140) was used qualitatively to determine the precipitate homogeneity across each filter. Cerium mass 140 constitutes 88% of the isotopic composition of natural Ce, and was the dominant signal in each mass spectrum. It was assumed that differences in the Ce signal across a given filter would be attributed to inhomogeneous deposition. Mass sensitivity analysis for Ce was not conducted for this preliminary investigation.

Table 24. Operating parameters for the CETAC laser ablation system, LSX500 and ELAN ICP-MS.

CETAC LSX 500	**Experimental Parameter Settings**
Scan Type	Line Scan Single
Laser Energy Level	100%
Pulse Repetition Rate	20 Hz
Spot Size	50 μm
Time per Scan	~ 2 min, 30 sec
Scan Rate	10 μm/sec
Delays Between Scans	0
No. of Times Scanned	1
Gas Blank	30 sec
Shutter Delay	20 sec
ELAN DRC II ICP-MS	
Readings per Replicate	110
Sweeps per Reading	10
Replicates	3

6.3.6 Plutonium Isotopic Analysis – Gamma Spectrometry

The CeF_3 filters with activity concentrations > 100 Bq were counted for 50-140 hours on a broad energy spectrum germanium detector (BEGe, Canberra Industries, Inc., Meriden, CT, USA). Three photon energies were used for determining ^{239}Pu content, 38.7 keV (0.0105% yield), 51.6 keV (0.0271% yield) and 129 keV (6.31 x10^{-3}% yield). The lower-energy photons were chosen based on their relative proximity to the photon energies chosen for ^{240}Pu and ^{238}Pu evaluation, 45.1 keV (0.045% yield) and 43.8 keV (0.0392% yield), respectively. The 59.5 keV (35.9 % yield) photon was used for ^{241}Am evaluation. The 129 keV photon associated with ^{239}Pu decay, whose attenuation caused by the intervening sample matrix is considerably less than that of the lower-energy photons, was used as a third reference point for determining the absolute amount of ^{239}Pu in each sample. The relative ratios of ^{239}Pu to ^{240}Pu and ^{238}Pu were determined based on the following relationship:

$$\frac{\left[\frac{C_{\gamma,239}}{\varepsilon_{\gamma,239} \times Yield}\right]}{\left[\frac{C_{\gamma,240(or\ 238)}}{\varepsilon_{\gamma,240(or\ 238)} \times Yield}\right]} = R_{239/240(or\ 238)} \qquad \text{Equation 26}$$

where C_γ was the net counts in the photopeak, ε_γ was the BEGe detection efficiency, and *Yield* was the radiative yield associated with a given emitted photon. Gamma detection efficiency was initially determined using various certified gamma-ray point sources. By using closely spaced gamma lines, corrections due to finite source size and source self-attenuation tend to cancel one another. Gamma spectra were analyzed using Genie 2000 Gamma

Acquisition and Analysis and Interactive Peak Fit (IPF) software (Canberra Industries, Inc., Meriden, CT, USA).

Table 25. Detection efficiency for selected photons emitted in the decays of the indicated Pu isotopes using the broad energy germanium (BEGe) spectrometry system.

Radionuclide	Photon Energy (keV)	Detector Efficiency[1]
^{239}Pu	38.7	0.23
^{238}Pu	43.5	0.23
^{240}Pu	45.24	0.23
^{239}Pu	51.9	0.24
^{241}Am	59.5*	0.24
^{239}Pu	129	0.18

*The detection efficiency for the 59.5 keV photon is estimated from the efficiency fitting function determined by the analysis software (Genie 2000). The concentration of ^{241}Am in the aqueous Pu standard used to prepare the calibration standard filter was not provided by the source manufacturer.

[1]The uncertainty associated with the detection efficiency value is ±5% of the value.

Peaks were located and an energy calibration established using the unidentified second differential option in the analysis software with a significance threshold of 3.00 and a tolerance of 1.00 keV (default settings). Peak area was first determined using the Sum/Non-linear Least Squares Fit setup. A step continuum function was performed across the entire energy interval (0- 515 keV) and over all channels (1 - 4096). Once the relevant peaks were identified, IPF filters were applied for more accurate peak integration. This analysis method was used for both pre- and post-separation sample filters. The BEGe gamma spectrometry system detection efficiencies for the photons of interest are listed in Table 25.

6.3.7 Plutonium Isotopic Analysis – Alpha Spectrometry

Alpha spectra were collected on an Alpha Analyst spectrometer (Canberra Industries, Inc., Meriden, CT, USA). The solid state detectors used for all experiments had an active area of 450 mm^2 and the sample position was fixed at 16 mm from the detector face. A 24 hour background count was obtained for each chamber prior to sample analysis. Filters were counted for 10 minutes to 2 hours on the alpha spectrometry system, depending on the activity of the sample. Additionally, each filter was counted twice, in two different alpha chambers for improved statistical analysis and to help eliminate any detector-related systematic errors. The detector background count rate was sufficiently low 0.0083 cps) that no background correction was performed.

Alpha spectrum analysis was performed with Genie 2000 and Alpha Analyst software (Canberra Industries, Inc.). Peak integration was performed by manually

defining the alpha peak region of interest (ROI). Activity ratios for ^{238}Pu+^{241}Am and $^{239+240}$Pu relative to the total alpha activity of the sample, and the detector counting efficiency were determined using two different methods. The first method assumed that the low energy tail associated with the ^{239}Pu+^{240}Pu peak was due to lower yield alpha decays and therefore the $^{239+240}$Pu contribution the total alpha energy spectrum was equivalent to:

$$C_{total} - C_{E>5.2\ MeV} = C_{239+240} \qquad \text{Equation 27}$$

where C_{total} was the total number of counts collected across the entire energy spectrum (Emax = 5.6 MeV), $C_{E>5.2\ MeV}$ was the number of counts collected in the 5.3 to 5.6 MeV energy range (associated with decays of ^{241}Am and ^{238}Pu), and $C_{239+240}$ was the number of counts associated with the decay of ^{239}Pu and ^{240}Pu. The ^{238}Pu+^{241}Am to $^{239+240}$Pu ratio was determined using the following formula:

$$\frac{C_{E>5.2\ MeV}}{C_{total} - C_{E>5.2\ MeV}} = R_{Pu-238,Am-241} \qquad \text{Equation 28}$$

This approach is not very accurate, in that there is no way to verify that the low energy tail only contains ^{239}Pu and ^{240}Pu. No information was provided with the standard source regarding the separation efficiency of the daughter products (i.e. ^{234}U, ^{235}U, ^{237}Np and ^{241}Am), most of which have alpha decay energies in the 4-5 MeV energy region of the spectrum. Additionally, an ideal alpha source is a uniformly deposited thin layer of material. As the thickness of the source increases, the alpha particles are attenuated and therefore the energy reaching the active region of the detector may not be representative of the original alpha energy. The uniformity of the CeF_3 deposit on the filter was not evaluated and

therefore, it was possible that lower energy alpha particles were attenuated to a somewhat greater extent than were higher-energy alpha particles. Similarly, the approach assumes that the contribution of degraded-energy alpha particles (associated with the upper energy peak) did not make a significant contribution to the events in the lower energy peak. This approach is supported by the spectra (Figure 33), where the peak separation is complete.

The second method used to determine the isotopic activity ratio set the $^{239+240}$Pu alpha peak ROI between 4.96 MeV and 5.21 MeV, which represented approximately 99.99% of the alpha energies associated with the decay of ^{239}Pu and ^{240}Pu. The ^{238}Pu and ^{241}Am peak ROI was set between 5.31 MeV and 5.57 MeV, which represented approximately 99.99% of the alpha energies produced from the decay of ^{238}Pu and ^{241}Am and includes those higher-energy events caused by summing of conversion-electrons with the main alpha peak of ^{241}Am. Using this method, the low energy tail of the $^{239+240}$Pu peak was neglected, as was any contribution of the tail from the ^{238}Pu+^{241}Am peak to the lower energy peak. This method assumed that > 99% of the $^{239+240}$Pu and ^{238}Pu+^{241}Am decays would fall within the respective ROIs and that the isotopic ratio of ^{238}Pu+^{241}Am to $^{239+240}$Pu would be:

$$\frac{C_{ROI,Pu-238+Am-241}}{C_{ROI,Pu-239+240}} = R_{Pu-238,Am-241} \qquad \text{Equation 29}$$

where C_{ROI} was the number of counts in the low (239+240) and high (238+241) energy ROIs.

The first method potentially under-estimates the isotopic ratio by assigning too many counts to the decay of ^{239}Pu and ^{240}Pu.The second method should lead

to a more accurate isotopic ratio unless there is significant peak broadening. For this work, both analysis methods should yield similar results (i.e. the daughter product contribution to total activity is small). For experiments where the elemental and isotopic composition is unknown, (i.e. Chapter 5) the second method is expected to be more accurate. Detector efficiency was determined from the following relationship:

$$\frac{C_{239+240}}{A_{239+240}} = \varepsilon_{\alpha} \qquad \text{Equation 30}$$

where $C_{239+240}$ is the number of counts per second in the low energy ROI relative to the $^{239+240}$Pu activity of the sample (based on the information provided in Table 21).

6.4 Results and Discussion

6.4.1 Alpha Analysis

Isotopic analysis of the CeF_3 filters was first determined by alpha spectrometry. An example of the spectral data output for the 2316 Bq CeF_3 filter for both pre- and post-separation samples is provided (Figure 33). The observed difference between the spectra was small, indicating that the amount of Am (and other daughter products) in the initial standard solution was small and the samples were of reproducible or negligible thickness.

The isotopic ratios for $^{239+240}$Pu to total alpha activity are presented (Table 26). These values represent the average activity ratio across the two sample sets (n= 7 filters, 10 Bq < Activity <2400Bq, pre- and post-separation). The average $^{239+240}$Pu: total alpha activity ratios for both pre- and post- separation sample

filters were in good agreement with the expected activity ratio (Table 26).

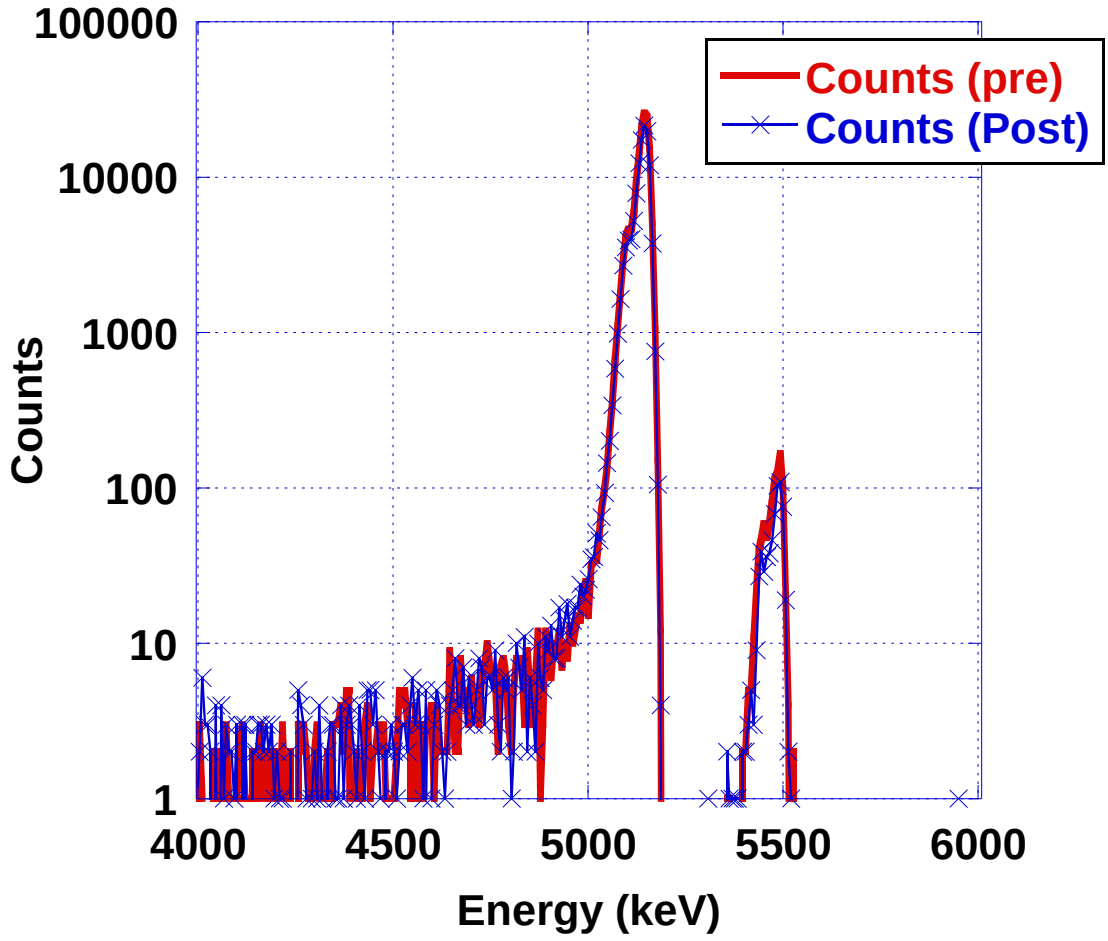

Figure 33. Spectral data collected for both the pre- and post-separation CeF_3 filters with approximately 2300 Bq total activity per filter. Total counts are presented on a log scale so that the contribution from the ^{238}Pu and ^{241}Am (higher energy peak) in the Pu solution can be readily seen. The background count rate was 0.0083 counts per second and the full width at half maximum (FWHM) of the $^{239+240}Pu$ and $^{238}Pu+^{241}Am$ peaks were 30.8 keV and 27.5 keV, respectively.

The filters were counted in two different alpha chambers for statistical purposes and the detector response was plotted as a function of count rate

versus activity (Figure 34). The detector response was not very linear with respect to activity, but the estimated average efficiency values that were determined using Equation 30 were 9.2 ± 1.1% (detector 1) and 9.3 ± 1.6% (detector 2).

The detector response is plotted as a function of CeF_3 filter activity for both the pre- and post- separation samples (Figure 34). An efficiency fitting function, which is based on the detection efficiency determined from Equation 30 is also plotted. At activity concentrations < 250 Bq, the detector response is linear. The pre-separation samples (blue squares) begin to diverge from the fitting function between 1200 and 2500 Bq. The cause of the apparent increase in detector efficiency for the pre-separation CeF_3 filters is unknown at this time and more samples within this activity range should be prepared to determine if this observation is consistent across the higher activity range. It is unlikely that the increase is due to an increase in CeF_3 co-precipitation efficiency with an increase in Pu concentration.

In these experiments, the precipitate wash was collected in 50 mL tubes and an aliquot was counted by LSC immediately after precipitation. Additionally, the remaining wash solutions were placed in a drying oven at 60°C and evaporated to dryness. The residue was reconstituted with 1% HNO_3 (1 mL) and an aliquot was taken for LSC counting. None of these samples had count rates distinguishable from background (~0.63 cps). The post- separation samples (red circles) with activity concentrations > 1200 Bq demonstrated the opposite effect.

Table 26. Alpha spectrometry isotopic analysis prior to and after ^{241}Am separation.

Radionuclide (X)	Pre-Separation		Post-Separation		
	^{239}Pu+^{240}Pu	^{238}Pu+^{241}Am	^{239}Pu+^{240}Pu	^{238}Pu	^{241}Am
Region of Interest (MeV)	4.96 to 5.21	5.31 to 5.57	4.96 to 5.21	5.31 to 5.57	
Expected Activity Ratio (X:Total α Activity)	0.996	0.0041	0.996	0.0035	0.00055
Observed Mean Activity Ratio (X: Total CPS)	0.991 - 0.994 ± 0.001	0.0065 – 0.0066 ± 0.0001	0.990 - 0.995 ± 0.001	0.0053 - 0.0056 ±0.0005	0.0012 Δ (pre-post)
[1]Detection Efficiency	9.2 ± 1.1 %	14.8 ± 2.4 %	9.3 ± 1.6 %	14.6 ± 2.4 %	
Full Width at Half-Maximum (FWHM)	29-31 keV	23-28 keV	30-31 keV	19-33 keV	

[1] Detector efficiency calculation was based on the isotopic data provided in Table 1. The discrepancy in efficiency values for the two ROIs is explained in Section 6.3.7.

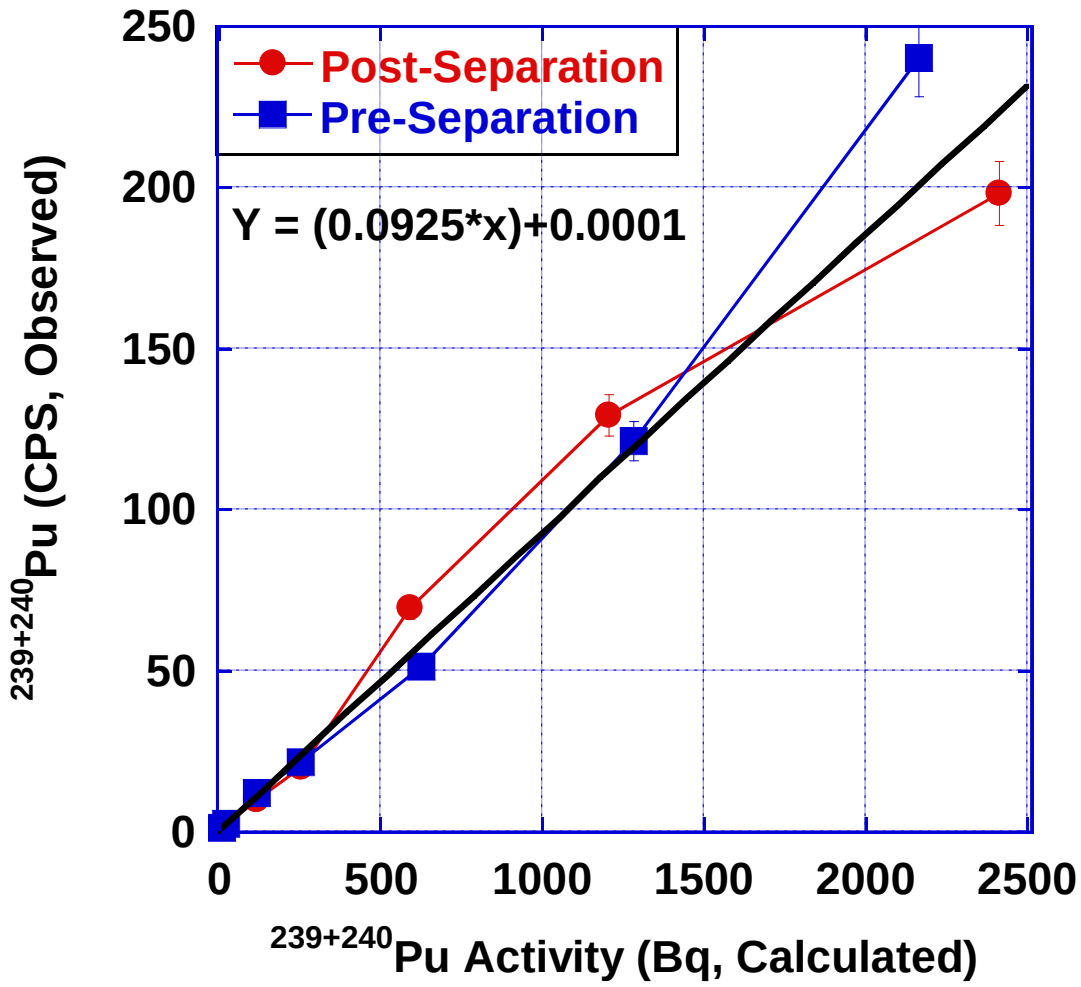

Figure 34. Alpha detector response for the CeF_3 prepared from the original Pu stock solution (pre-separation) and the purified Pu stock solution (post-separation). The solid black line represents the expected detector response determined from the efficiency calculations.

The diminution in detector response could be contributed to hydrolysis affects in the purified Pu stock solution (prepared in 0.01 M HNO_3). Activity determination of the purified samples was completed immediately after chemical separations. The purified stocks solution sat for 12 hours while LSC counting was performed and the aqueous solutions for ICP-MS and CeF_3 co-precipitation were

prepared after the activity concentration was verified (approximately 14 hours after chemical separation). It is well known that Pu can undergo hydrolysis in [HNO_3] < 0.5 M (66). Hydrolysis and subsequent polymerization of Pu in solution can significantly decrease the net concentration of Pu in solution. This affect should be observed in all filters prepared with the purified Pu stock solution. Once the purified solution was prepared for CeF_3 precipitation, the excess fluoride should quickly reverse the affects of hydrolysis. The supernate for each CeF_3 filter prepared with the purified stock solution was checked for residual activity as described above and none was detected above background. Sample vials were not checked for activity once the sample solutions were precipitated. Further work is needed to explain the analogous behavior of the higher activity filters with respect to detector response.

The ^{238}Pu+^{241}Am to total alpha activity ratios for the pre- and post-separation CeF_3 filters are provided in Table 26. The observed ratios were significantly higher than the expected values. As previously mentioned, the ^{241}Am content of the original Pu standard was not provided by the manufacturer; therefore, the higher ratio for the filters prepared from the original stock solution could be attributed to an Am excess. The observed ^{238}Pu to total Pu activity ratio was 1.5 times greater than the expected value for the filters prepared from the purified Pu stock solution. The original Pu stock solution was chemically purified using TEVA extraction chromatography resin. According to the initial resin characterization studies, (34), Pu^{4+} in the 3M HNO_3 loading matrix solution should strongly sorb to the resin, while Am^{3+}, NpO_2^{+} $^{+}$ and UO_2^{2+} remain in solution and pass

unhindered through the column.If it is assumed that most of the Am was removed from solution prior to CeF_3 co-precipitation and that the Pu isotopic activity percent values in Table 21 are correct, then the detector efficiency for the higher energy ROI (5.31 to 5.7 MeV) was 14.8 ± 2.4% (detector 1) and 14.6 ± 2.4% (detector 2).

Efficiency calibrations as a function of energy are usually not required for alpha spectrometry. The initial detector material encountered by the incident alpha particles is the detector dead layer. This layer is typically thin and is expected to have no impact on detector efficiency as a function of energy. The energy associated with the incident alpha particle is deposited within the active area of the Si detector, which is flush with the dead layer. This is because of the linear stopping power of the alpha particle within the silicon matrix of the detector. Stopping power is defined as the amount of energy lost per unit length of a given material (35). The stopping power of a wide range of alpha energies in silicon is provided in Figure 35 (124). For the 5.15 MeV and 5.5 MeV alpha particles in Si, the stopping power is 605.0 and 580.2 MeV cm^2/g, respectively. This translates to an alpha particle range of approximately 25.3 – 27.8 µm.

The active thickness of the silicon detector is approximately 140 µm, therefore all of the alpha energy is deposited in the detector. If it is assumed that the detector efficiency for both ROIs was equivalent, then the increased ^{238}Pu to the total Pu alpha activity observed in these samples was probably due to excess ^{238}Pu in solution beyond what is claimed in the data sheet accompanying the original Pu stock solution, and incomplete removal of ^{241}Am from the stock

solution at the reference time. This is supported by both gamma analysis and mass analysis (Sections 6.4.2 and 6.4.3).

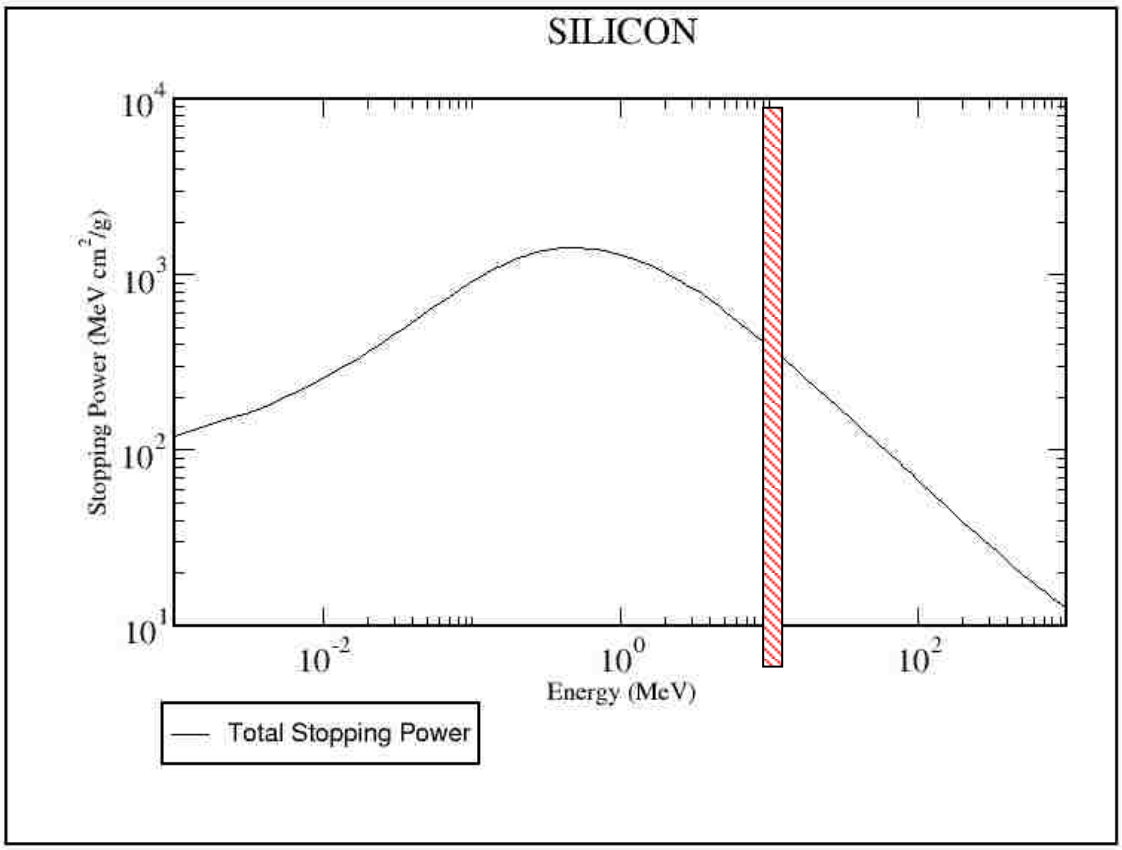

Figure 35. Stopping power for alpha particles in silicon generated by the National Institute of Standards and Technology ASTAR database (67). That portion of the curve due to 5-6 MeV alpha particles is set off by the shaded region.

6.4.2 Gamma Analysis

Isotopic analysis was also conducted with gamma spectrometry. An example of the spectral output for the pre- and post-separation CeF_3 filters is provided (Figure 36) and the results are summarized (Table 27). Figure 36 provides the

gamma spectra for the highest activity filters (approximately 2300 Bq/filter) prepared from both the original stock solution (pre-separation) and the purified stock solution (post-separation).

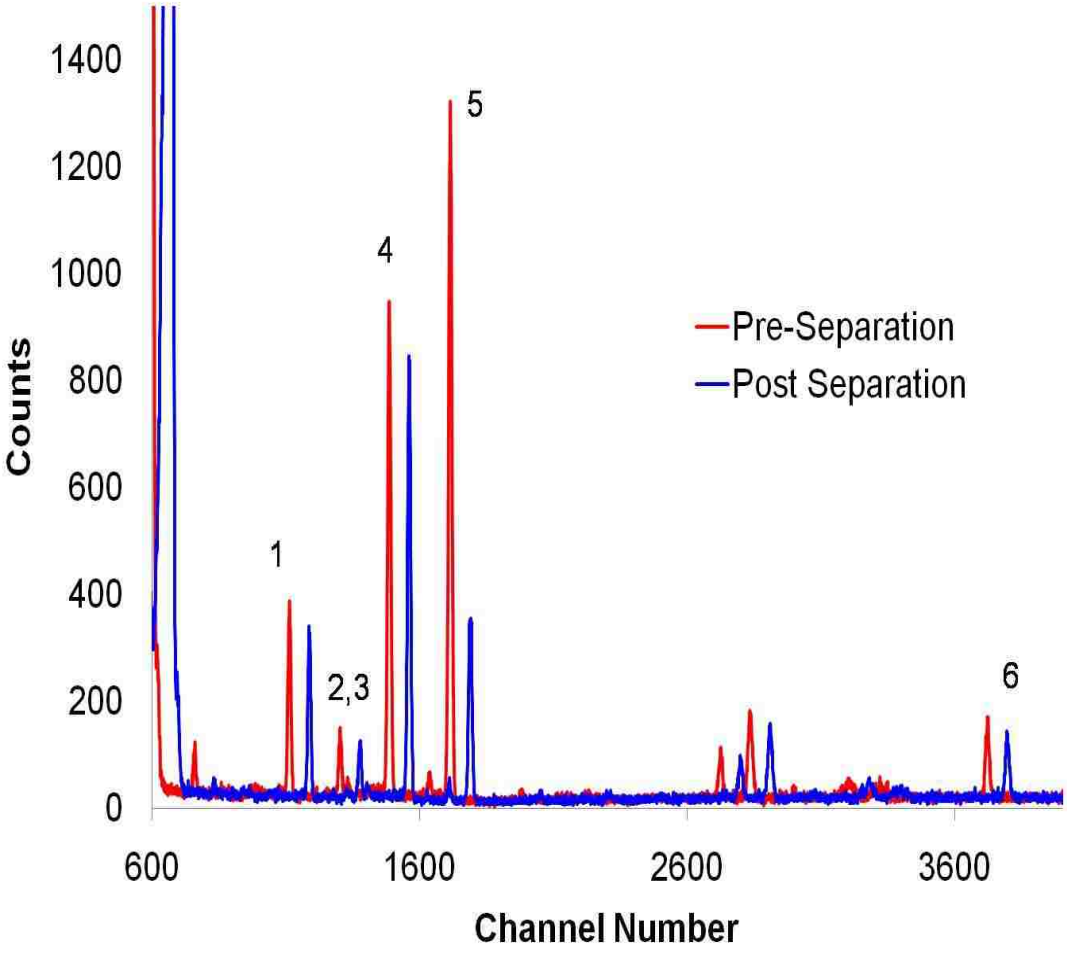

Figure 36. Gamma spectral data collected for both the pre- and post- separation CeF_3 filters with approximately 2300 Bq total activity per filter. Peak labels indicate photon energy where (1) 38.7 keV, ^{239}Pu; (2) 43.8 keV, ^{238}Pu; (3) 45.1 keV, ^{240}Pu; (4) 51.6 keV, ^{239}Pu; (5)59.5 keV, ^{241}Am; (6) 129 keV, ^{239}Pu. A 75 channel offset (x-axis shift) was applied to the post-separation spectrum for better peak comparison.

Table 27. Gamma spectrometry isotopic analysis prior to and after ^{241}Am separation.

Pre-Separation				
Isotopic Ratio ID	^{238}Pu:^{239}Pu	^{239}Pu:^{239}Pu	^{240}Pu:^{239}Pu	^{241}Am:^{239}Pu
Mean Activity Ratio	0.0078 ±0.0010	1.003 ± 0.003	0.067 ± 0.021	0.0011 ± 0.00001
[1]Expected Ratio	0.0038	1.00	0.077	0.0006
Post-Separation				
Isotopic Ratio ID	^{238}Pu:^{239}Pu	^{239}Pu:^{239}Pu	^{240}Pu:^{239}Pu	^{241}Am:^{239}Pu
Mean Activity Ratio	0.0073 ±0.0020	1.003 ± 0.001	0.077 ± 0.013	0.0003 ± 0.0001
[1]Expected Ratio	0.0038	1.00	0.077	0.00

[1] Expected ratios are based on the information provided in Table 21.

Count times were equivalent and the post-separation spectra were shifted by 75 channels for better peak comparison. It should be noted that activity was not normalized for filter comparison. The post-separation filter was expected to have

10% more ^{239}Pu activity relative to the pre-separation filter based on the LSC analysis and information from Table 21. The gamma spectra support the assumption that the net activity in the post-separation solution was lower than expected, which affected the alpha detector efficiency response (Figure 34). The ^{240}Pu:^{239}Pu observed activity ratios for both the pre- and post- separated filter sets were in agreement with the expected ratio. The ^{238}Pu and ^{241}Am observed ratios were twice as high as the expected ratios; this result supports the results of the alpha measurements. From the pre- and post-separation filter sets, it was determined that the Am separation efficiency of the utilized procedure was 72 ± 2%. It is suspected that the loading solution volume (5 mL) was not sufficient to remove all of the Am from the TEVA resin; residual Am was collected with Pu when it was eluted from the column.

6.4.3 Mass Analysis – Aqueous Solution

Mass analysis was performed on both the pre- and post- separation solutions to determine the LOD for each of the m/z ratios listed in Table 23. The approximate LOD for each m/z ratio was calculated as 3 times the standard deviation of the method blank intensity and the equivalent mass values are presented (Table 28).

The calibration results for some of the m/z ratios of interest are provided (Figure 37 through Figure 40). The original mass of each isotope (x-axis) was determined from information provided (Table 22) and from LSC data. It should be noted that the data for m/z ratios 238 and 242 were inconclusive. The background signal intensity for the 238 m/z ratio was high and it was suspected

that the HNO_3 used for initial sample preparation had a relatively high ^{238}U concentration. The signal intensity in counts per second is compared to the mass concentration of the ^{239}Pu in solution for both stock solutions (Figure 37).

Table 28. Aqueous ICP-MS detection limits for the Pu isotopic m/z ratios.

m/z Ratio	[1]Limit of Detection (ng per g solution)
238	[2]Not determined
239	0.37 - 0.45
240	0.040 - 0.041
241	0.0032 - 0.0040
242	>0.000744

[1] LOD values are calculated as (3 x $MB_{m/z}$), where MB is the signal intensity of the m/z ratio in the method blank.

[2] The background signal in the 238 m/z peak was too high. It was suspected that the nitric acid used for sample preparation had a relatively high concentration of ^{238}U.

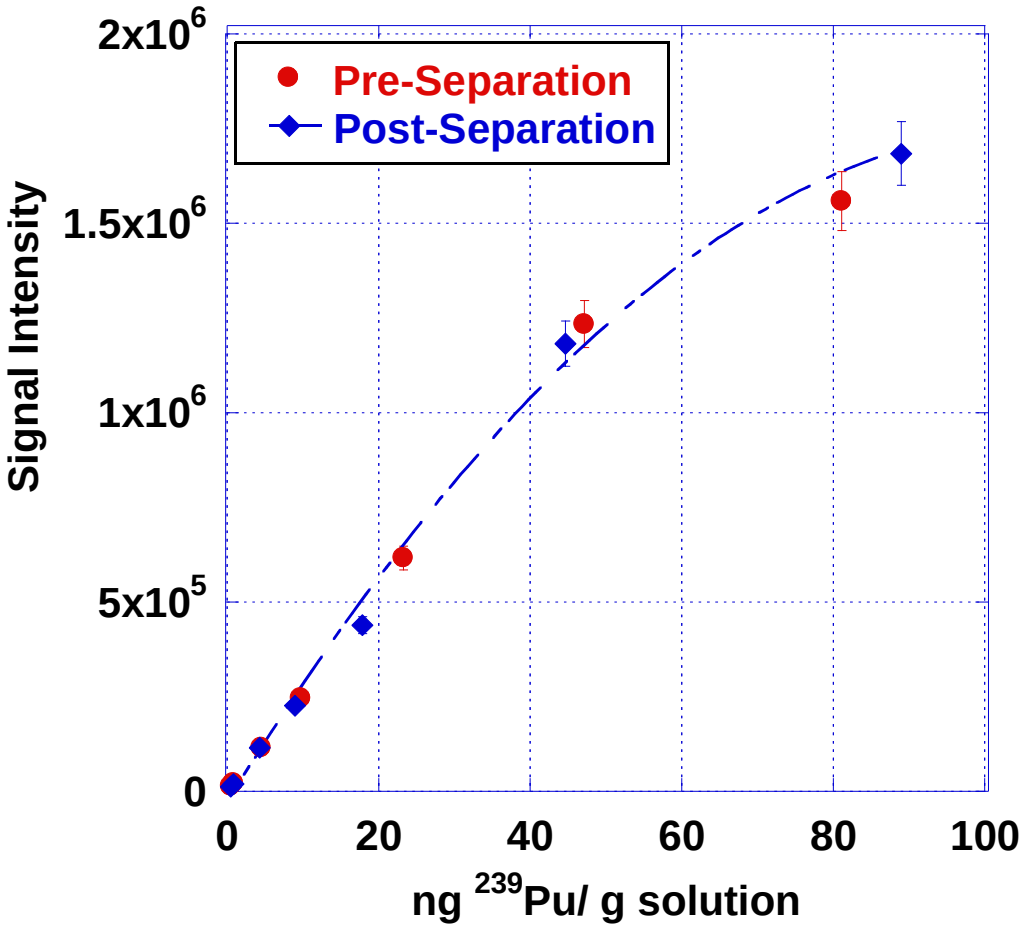

Figure 37. ICP-MS analysis of the ^{239}Pu signal intensity vs. mass for the aqueous standard solution prior to and after chemical separation. The curvature of the trend line at high concentration is due to detector saturation.

The curvature of the trend line associated with instrument sensitivity at mass concentrations above 50 ng ^{239}Pu per g solution indicates that the point of detector saturation has been reached. For analysis of the minor Pu isotopes, higher ^{239}Pu mass concentrations are required for adequate mass analysis. As mentioned earlier, the ^{242}Pu mass concentration in the most concentrated sample

is not sufficiently above the LOD for accurate determination of the 242 m/z ratio (Table 28).

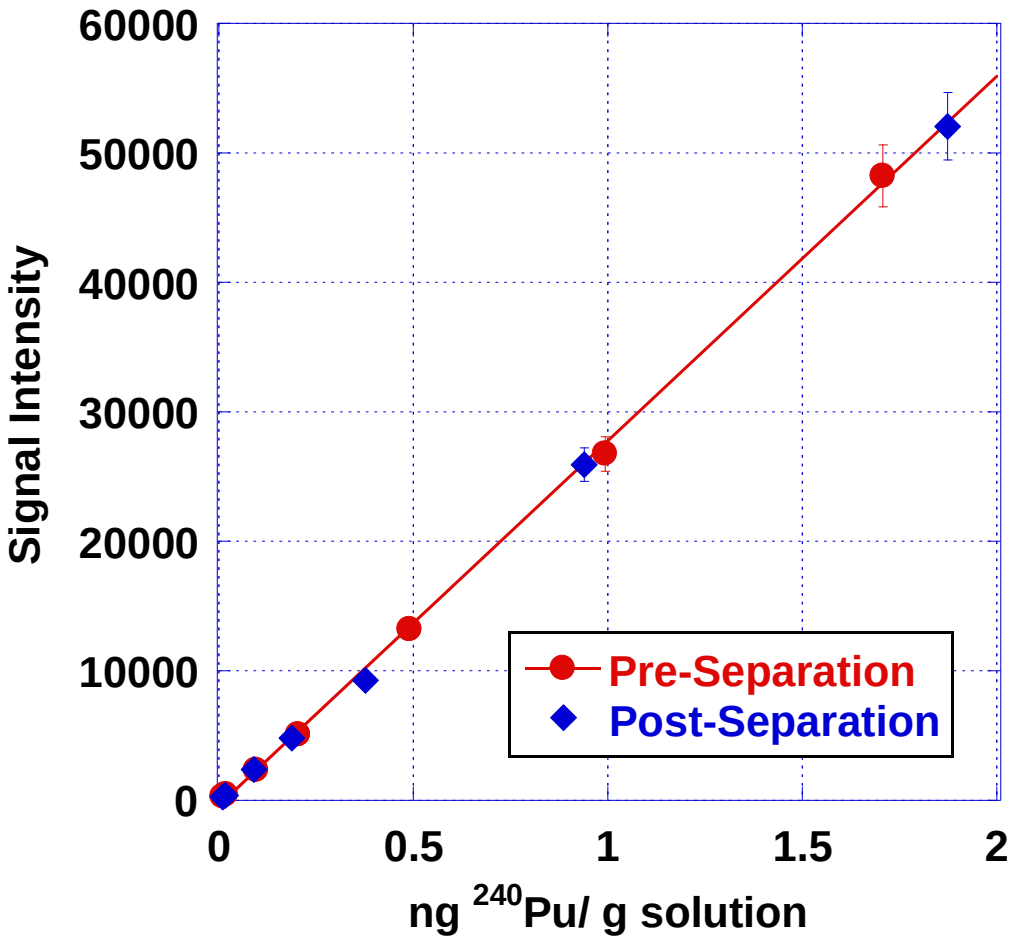

Figure 38. ICP-MS analysis of the ^{240}Pu signal intensity vs. mass for the aqueous standard solution prior to and after chemical separation.

The highest mass value for the ^{242}Pu in solution was close to the LOD, therefore the data (Figure 40) was not considered reliable for isotopic ratio determination. The observed mass ratio for ^{240}Pu:^{239}Pu was 0.021 ± 0.001 (both pre- and post- separation) and matched the expected mass ratio of 0.021.

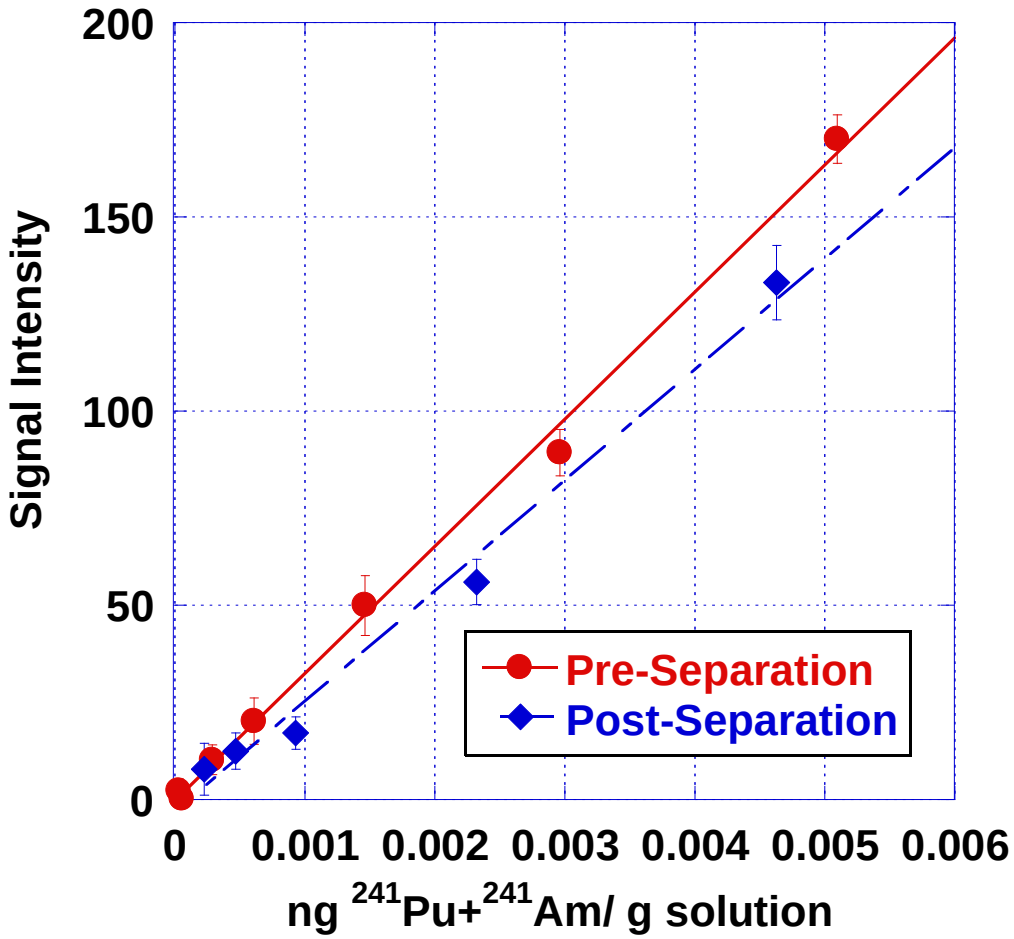

Figure 39. ICP-MS analysis of the ^{241}Pu + ^{241}Am signal intensity vs. mass for the aqueous standard solution prior to and after chemical separation.

The ^{241}Pu(^{241}Am):^{239}Pu isotopic ratio was 8.7 x10^{-5} ± 1.0 x 10^{-5} and 5.8 x 10^{-5} ± 1.0 x 10^{-5} for the pre- and post-separation filters, respectively. These ratio values were higher than the expected values of 6.2 x10^{-5} and 5.2 x 10^{-5}, in support of the excesses of both analytes observed in the alpha and gamma spectrometry measurements. The increased 241 m/z ratio in the pre-separation solution supports the premise that the ^{241}Am concentration in the original stock solution was higher than expected. The estimated separation efficiency of Am

from Pu in our procedure was 66 ± 14% based on the mass analysis; this is consistent with the value of 72% arising in gamma spectrometry measurements.

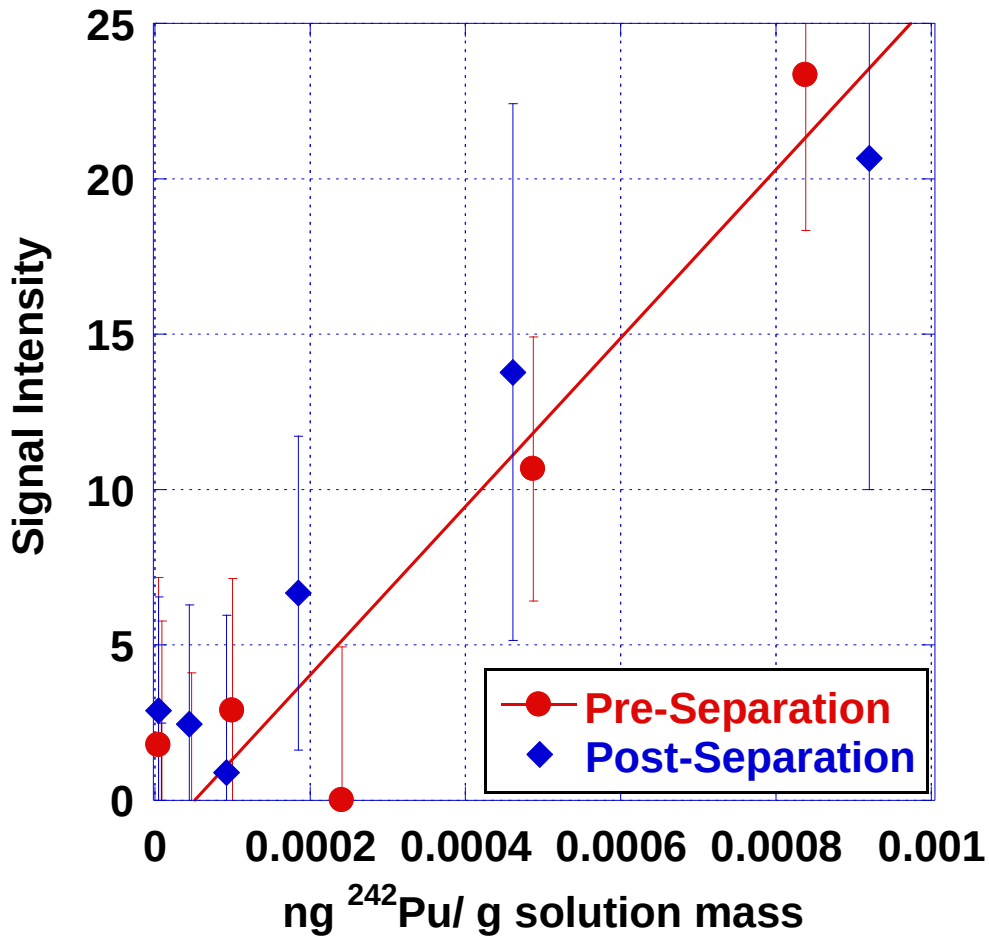

Figure 40. ICP-MS analysis of the ^{242}Pu ignal intensity vs. mass for the aqueous standard solution prior to and after chemical separation. The highest ^{242}Pu signals are near the limit of detection.

6.4.4 Mass Analysis – CeF_3 Filter

Mass analysis was also conducted on the CeF_3 filter surfaces using the LA-ICP-MS system. The filters were placed in the laser ablation system and line

scan analysis was performed for each of the filters. Precision and accuracy of sample introduction by laser ablation are affected by ablation and ionization efficiency, ion transmission efficiency from the ablation chamber to the plasma chamber, atomic mass number, and the relative isotopic abundance of the elements of interest (125). In this study, the amount of Ce added to each sample was approximately 50 µg which was at least 50 times higher than the mass of Pu used. If it is assumed that the Ce was homogenously distributed across the surface area of the filter, in a thin layer, then the amount of Ce ablated from the surface was approximately 1900 ng Ce or approximately 4% of the total ^{140}Ce mass per line scan. The ^{239}Pu and ^{240}Pu mass analyzed per line scan would be between 0.2 and 40 ng and 0.004 and 0.8 ng, respectively. The BEC (Equation 26) for ^{239}Pu was 0.09 ± 0.02 ng and for ^{240}Pu was 0.008 ± 0.002 ng per line scan. Based on the BEC for each m/z ratio and the assumptions above, only the filters with ^{239}Pu masses > 50 ng/filter (2 ng of ^{239}Pu per line scan) were suitable for measurement by LA-ICP-MS; below this value, the mass concentration of ^{240}Pu was <0.01 ng per line scan.

An example of the spectral output of the mass spectrometer during laser ablation is provided (Figure 41). The signal intensities for the 241 and 242 m/z ratios were not sufficient for measurement under the used operating parameters. There was considerable noise in the 238 m/z signal, which was also evident from aqueous sample analysis. It was assumed that the noise was the result of ^{238}U contamination either in the HNO_3 used for sample preparation or in the mass collector.

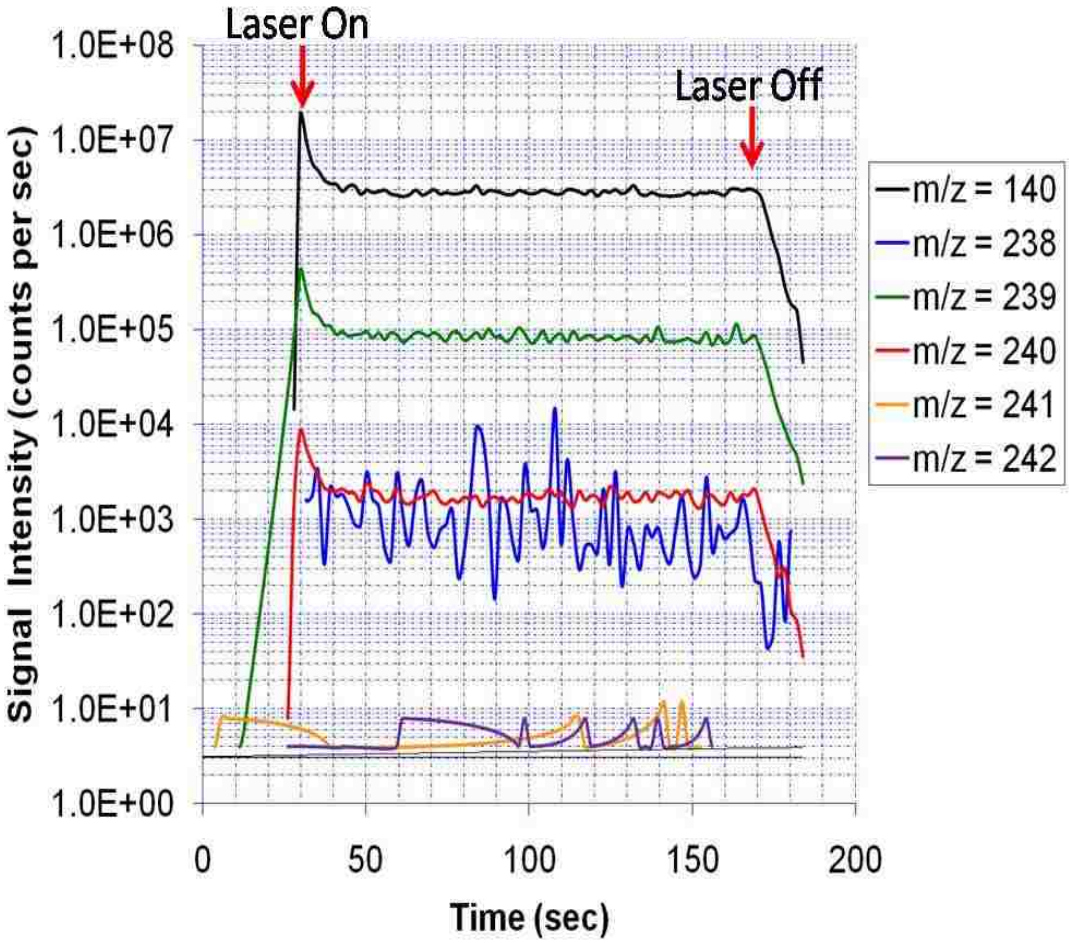

Figure 41. LA-ICP-MS signal intensity plotted as a function of scan time for the pre-separation CeF_3 filter containing 1000 ng of ^{239}Pu. Laser energy level = 100%, spot size = 50 µm, pulse rate = 20 Hz, scan rate = 10 µm/sec, single line scan setting.

The 238 m/z signal intensity for the CeF_3 method blank (prepared similarly to the CeF_3 samples with co-precipitated Pu, but without the addition of the Pu stock solution) was three times higher than the filter blank (no chemical treatment). This would suggest that the HNO_3 was the source of the elevated 238 m/z signal. A significant amount of ^{238}U in solution can lead to hydride formation

$^{238}U{\cdot}H^{+}$ which can influence the signal intensity in the 239 m/z channels. Uranium hydride formation was not evaluated in this work.

Accurate mass analysis with LA-ICP-MS is also dependent on the homogeneity of the solid sample. Prior to filtration, the Resolve filters were loaded onto a vacuum filtration unit that can precipitate 12 samples simultaneously. The filters were held in place by silicon o-rings (20 mm inner diameter, 25 mm outer diameter); therefore, the active area of the filter was slightly reduced, thus creating a visible ring or edge. The filters were first treated with ethanol to open the filter pore spacing, tested with DI water, and then the sample solution was poured into the top reservoir and allowed to pass through the filter. The original sample vial was rinsed with DI water, which was added to the filtrate. After the filtrate passed through the reservoir, the filters were treated with ethanol to drive off any remaining solution. The addition of these solutions could potentially cause the precipitate to migrate along the surface of the filter if the precipitate did not strongly adhere. This would result in depleted regions along the filter surface where little to no CeF_3 would be present. In the mass analysis studies conducted for this work, several line scans were collected across the CeF_3 filters. There was little discontinuity observed in the signal intensity for the 140 (Ce), 239 (Pu) and 240 (Pu) m/z ratios in the central region of the filter (Figure 42). Additional lines scans were collected along the filter edge for signal comparison and an example of an “edge effect” is provided (Figure 43).

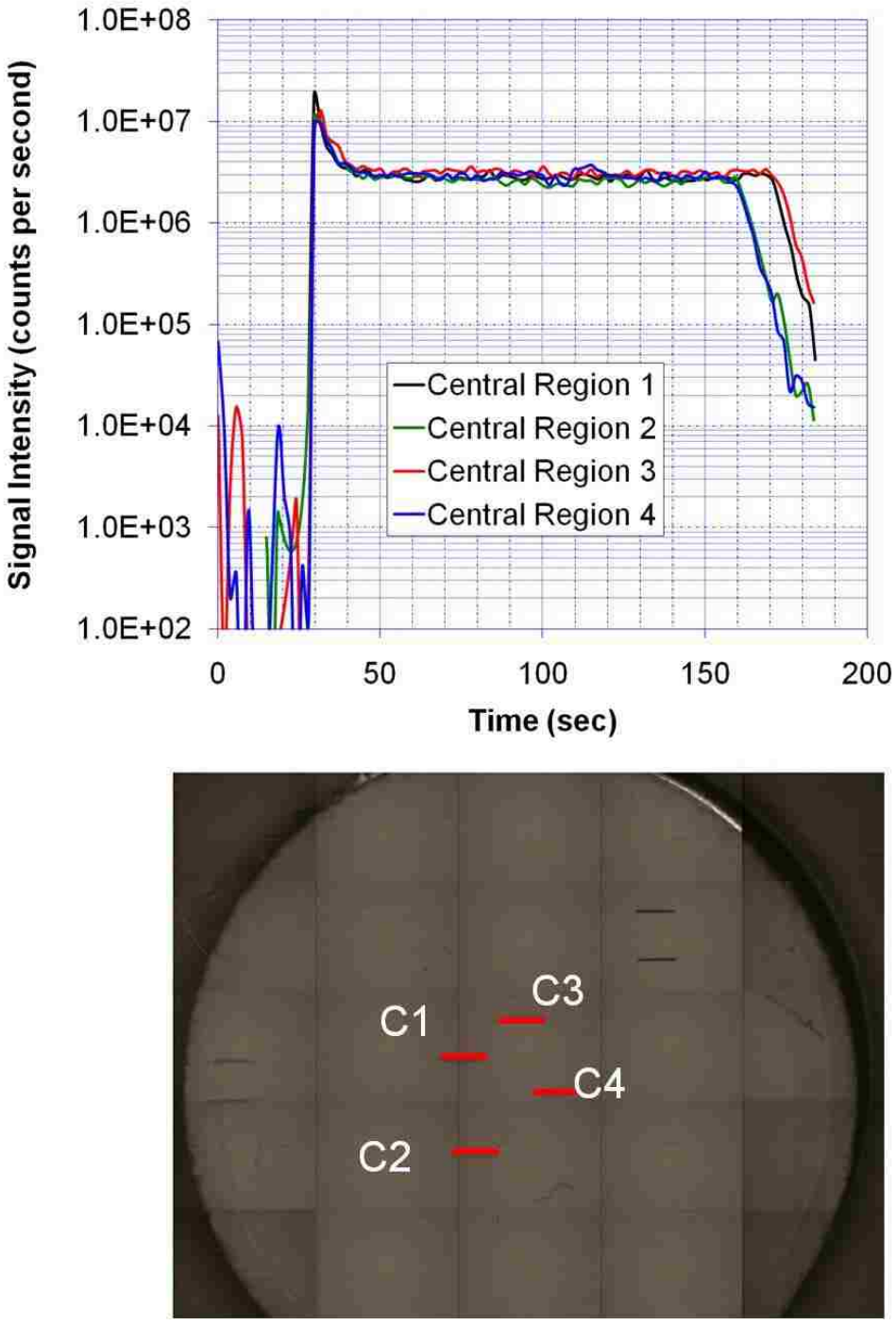

Figure 42. Cerium (m/z=140) signal intensity as a function of time during laser ablation for various line scans taken in the central region of one of the CeF_3 filters (Pu mass = 1000 ng). Laser energy level = 100%, spot size = 50 µm, pulse rate = 20 Hz, scan rate = 10 µm/sec, single line scan setting. Red solid lines highlight line scans whose results are depicted in the upper part of the figure.

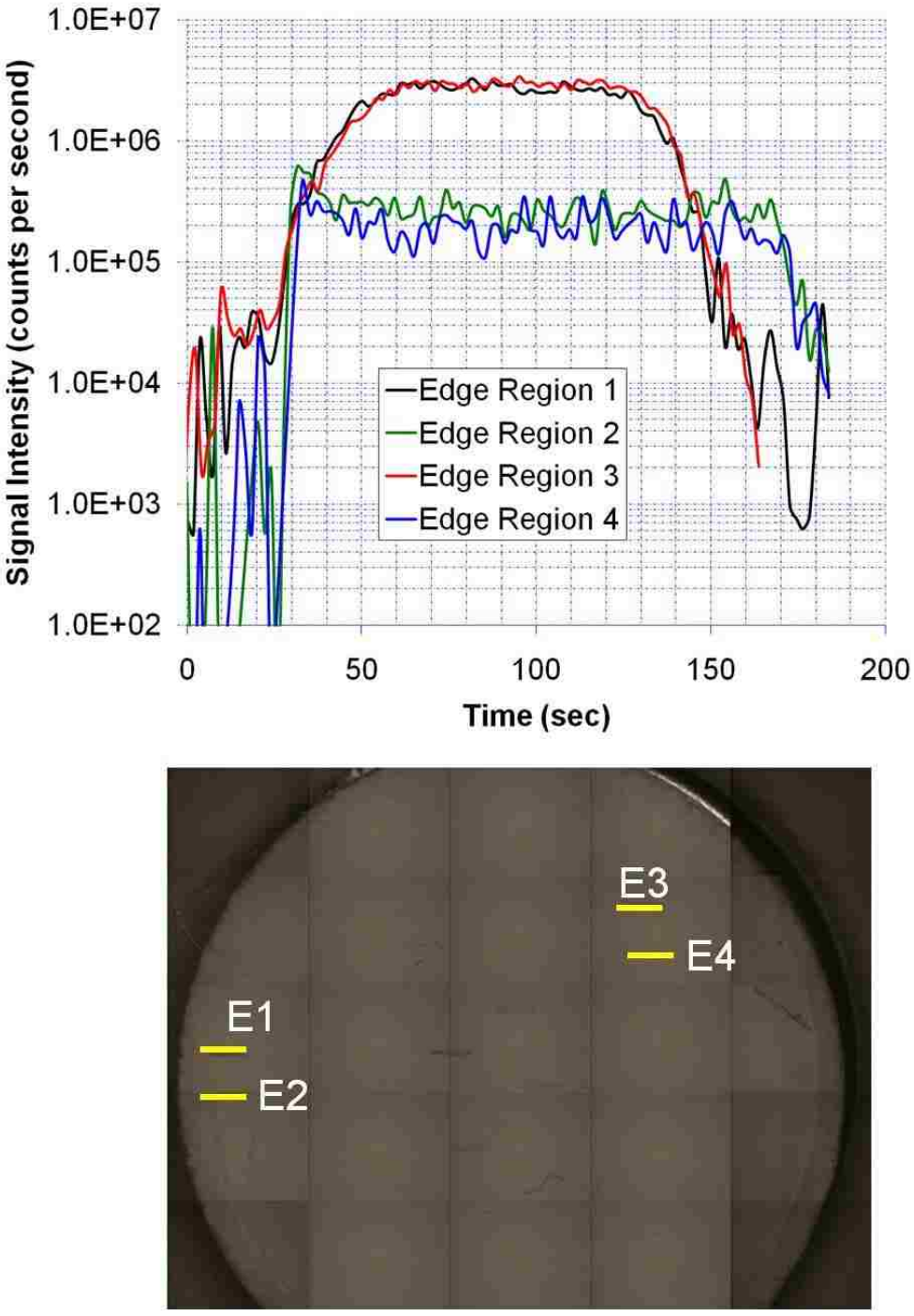

Figure 43. Cerium (m/z=140) signal intensity as a function of time for various line scans taken along the edge regions of a CeF_3 filter (Pu mass = 1000 ng). This is the same image that is the basis for Figure 42. Laser energy level = 100%, spot size = 50 µm, pulse rate = 20 Hz, scan rate = 10 µm/sec, single line scan setting. Yellow solid lines highlight line scans whose results are depicted in the upper part of the figure.

The edge regions labeled E1 and E2 in Figure 43 are close to the area sealed by the o-ring. The 140 m/z signal intensity drops off by an order of magnitude compared to the other regions and the central regions (Figure 42). It should be noted that the scan times for each line scan were manually selected by drawing a line on the filter image in the CETAC program and some scan times were slightly longer than others. In general, the signal intensity fluctuated at the beginning of the scan (prior to laser ignition) and toward the end of the scan (laser termination).

The Ce signal intensity resulting from line scan analysis was consistent across the central region of the filter for all samples. While the mass ratios for Pu cannot be directly compared to the Ce signal due to differences in mass discrimination and detection sensitivity, the real time signal ratio can be used to determine the homogeneity of the Pu within the precipitate (Figure 44). The signal ratios for both m/z=239 and m/z=240 relative to m/z=140 are consistent across all line scans for a given Pu mass concentration. The observed mass ratios are twice the expected mass ratios (Figure 45) and the slope of the linear regression for the 239:140 and 240:140 diverge as the Pu mass concentration increases. ICP-MS analysis of the aqueous Pu solutions determined that detector response was non-linear at higher ^{239}Pu mass concentrations (Figure 37). The Ce mass concentration in each filter was significantly higher than the ^{239}Pu mass concentrations used for aqueous analysis, therefore, it is likely that the Ce signal also saturated the detector. The Ce signal and degree of saturation was expected to be consistent across all filters. In combination with higher ^{239}Pu mass

concentrations, the 239 to 140 mass ratio would be expected to decrease slightly due to signal suppression in both m/z regions. The signal associated with ^{240}Pu was within the linear response region of the detector (Figure 38) therefore, at higher 240 concentrations, the 240:140 ratio was expected to be constant.

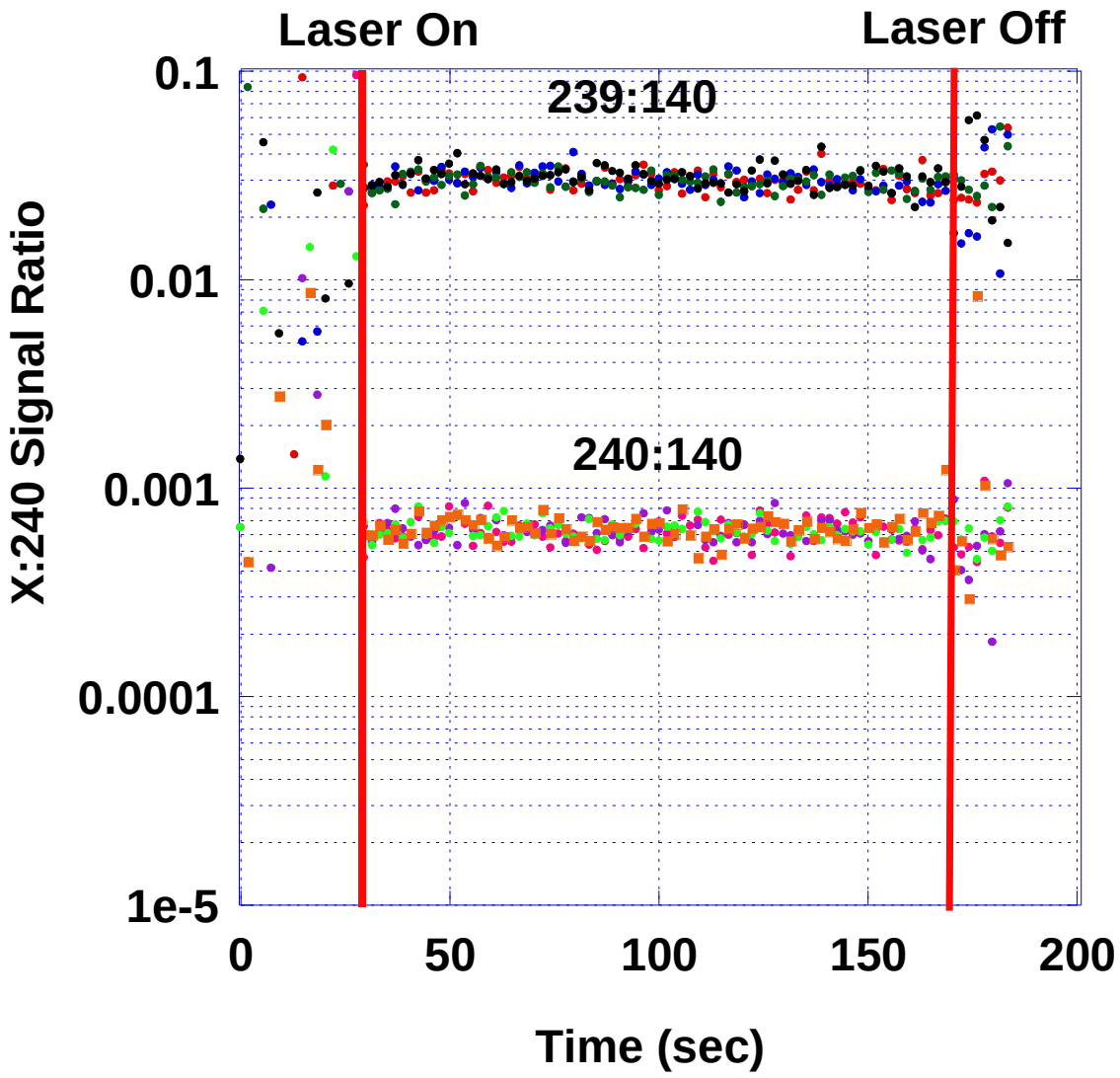

Figure 44. Mass signal ratio of 239 and 240 (Pu) to 140 (Ce) as a function of time for a filter containing approximately 1000 ng ^{239}Pu. All four line scans from Figure 42 are plotted on the graph for comparison.

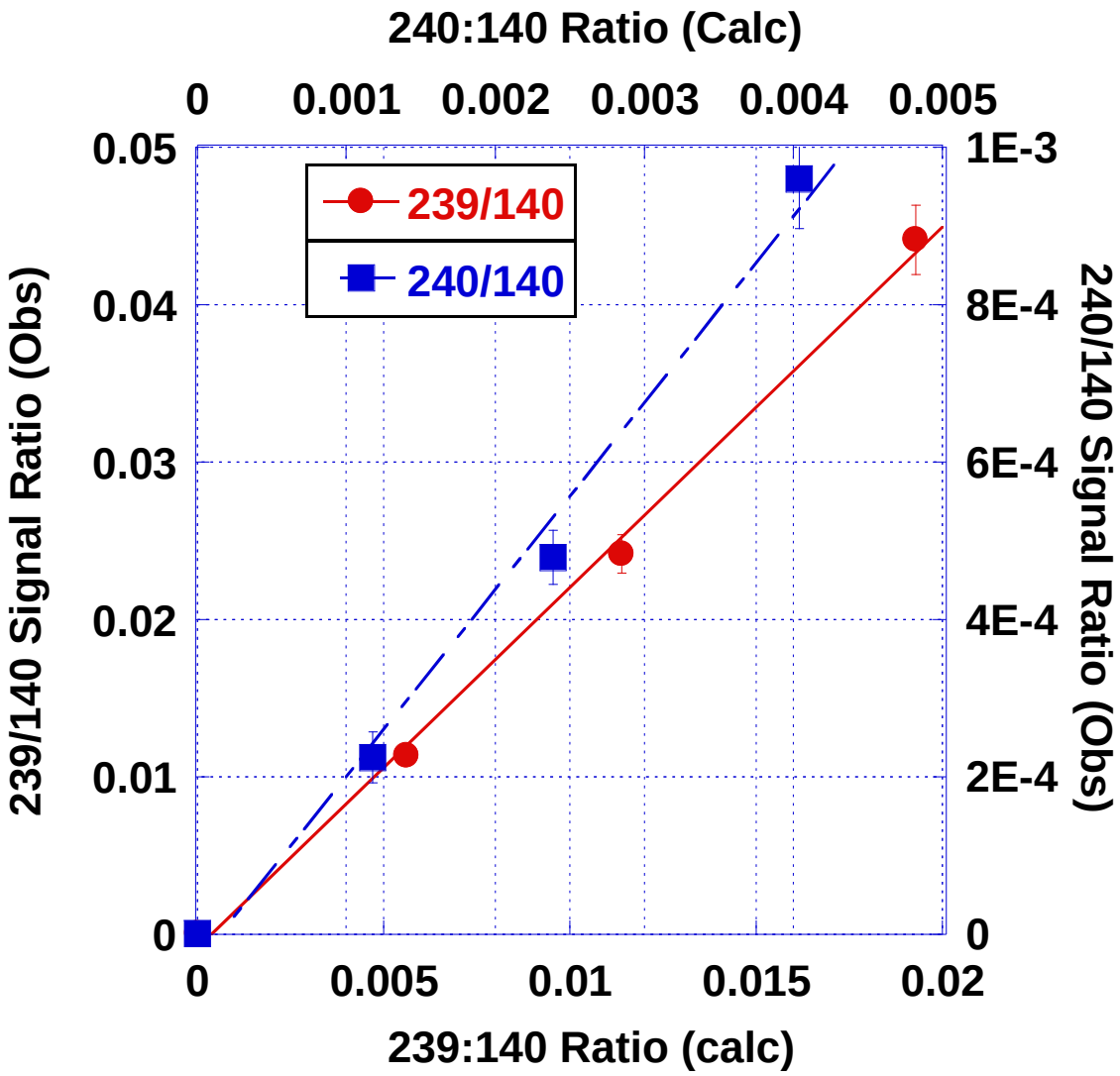

Figure 45. Mass ratios for m/z=239 (red circles) and m/z=240 (blue squares) with respect to m/z=140. The left y-axis and bottom x-axis correspond to the observed and calculated 239:140 ratios for ^{239}Pu masses ranging from 250 to 1000 ng. The right y axis and top x-axis correspond to the 240:140 ratios. Calculated values were determined from LSC activity analysis for Pu and gravimetric addition of Ce to the solution prior to precipitation. For both ratios, the observed Pu/Ce is about twice what is expected from the calculation.

The ^{240}Pu:^{239}Pu ratio determined from the LA-ICP-MS analysis using Equation 24 was 0.021 ± 0.001 for both filter sets, which was equivalent to the

results of aqueous mass analysis, radiation counting, and expected values. Other isotopic ratios were indeterminate under the current experimental conditions.

6.5 Concluding Remarks

Three methods were chosen for Pu isotopic ratio analysis of samples prepared by CeF_3 co-precipitation. The observed ^{238}Pu activity concentration was higher than expected using both radiometric analysis techniques and unresolved by mass analysis under the current experimental conditions. It is possible that the isotopic information provided with the Pu standard was incorrect for ^{238}Pu and it should be mentioned again that the Pu source used for this work was a NIST-traceable ^{239}Pu source and was not labeled as an isotopic Pu standard. Isotopic ratios for 240:239, 238:239, 241(Am):239 were determined for the filter samples using the combined analysis methods; when measured in duplicate by different means, the results were in good agreement with one another except for 238:239 by mass analysis, which indicates a U contamination in the reagents. It is suggested that in future work, these experiments be repeated with Pu isotopic standards and ultra-pure reagents to see if the 238, 241 and 242 mass signals can be resolved. Additionally, the preliminary data from LA-ICP-MS analysis has shown proof-of-concept for potential mass analysis from CeF_3 precipitated samples. The homogeneity of the CeF_3 precipitate across the central region of the filter makes it a prime candidate for laser ablation analysis. The major presence of Ce in the precipitate does not appear to affect Pu isotopic analysis, but more studies will be required to confirm this for the minor Pu isotopes.

CHAPTER 7

CONCLUDING REMARKS AND REFLECTIONS ON FUTURE RESEARCH

Some of the physical and chemical parameters associated with extraction chromatography (EC) separation procedures were investigated to facilitate the development of an automated chemistry platform. Physical characterization studies determined that the flow rate at a given vacuum setting was reproducible but was affected by ionic strength and viscosity of the various load and elution matrices. However, chemical characterization studies determined that a precisely known flow rate was not required for high purity Pu and Am solutions using TEVA, TRU and DGA resins. Studies conducted with solutions containing single matrix ion contaminants at a metal ion ratio of 1(Pu or Am):10^6 determined that the separation efficiency for Pu and Am was enhanced at lower flow rates on TEVA and DGA resins, while Am separation efficiency remained insensitive to flow rate on TRU. It was also established that variation in sample evacuation rate, which resulted in the resin bed running dry between elution steps, had no effect on separation efficiency. Methods that incorporate EC resins for chemistry often recommend two separate flow rates for sample loading/elution and column rinse, with slower flow rates for the former. In this work, it was determined that a constant vacuum pressure setting was sufficient for Pu and Am separation.

From a platform automation perspective, the EC vacuum system is amenable to automation. Flow rate can be reliably controlled by a digital vacuum regulator, and precise monitoring of flow rate during chemistry is not necessary. Sample evacuation can be monitored by an optical sensor implanted in the lid of the

vacuum box system. For mixed actinide samples requiring stacked resin cartridges, the following box modifications are suggested:

- Each resin type is placed in a separate cartridge tray and stacked on the sample loading box
- Each cartridge position on the resin-specific tray is permanently numbered which would allow tracking of the sample chemistry without having to label each individual cartridge
- Each cartridge tray is removed from the sample loading box and placed on a separate box for chemistry
- Collection vials should be placed in interchangeable tray holders that can be removed and replaced easily (in the current setup, vials are removed individually)
- Multiple vacuum box systems can be controlled by a multi-vacuum digital regulator and single vacuum pump

A conceptual schematic of the chemistry automation platform is provided (Figure 46). Aqueous sample and reagent delivery can be accomplished with a robotic arm that is positioned above the platform. This initial design is not fully automated but can increase sample throughput without risk of cross contamination and is versatile in terms of EC method selection. The foot print of the chemistry system (number of boxes) can be minimized with use of interchangeable cartridge and collection vial trays so that other sample pre-treatment steps can be added to the platform. Continued research efforts should focus on other actinides of interest, in particular U, and fission products. It would

be useful to have an enhanced method that minimizes the number of steps required for sample dissolution and actinide separation and isolation from matrix interferences.

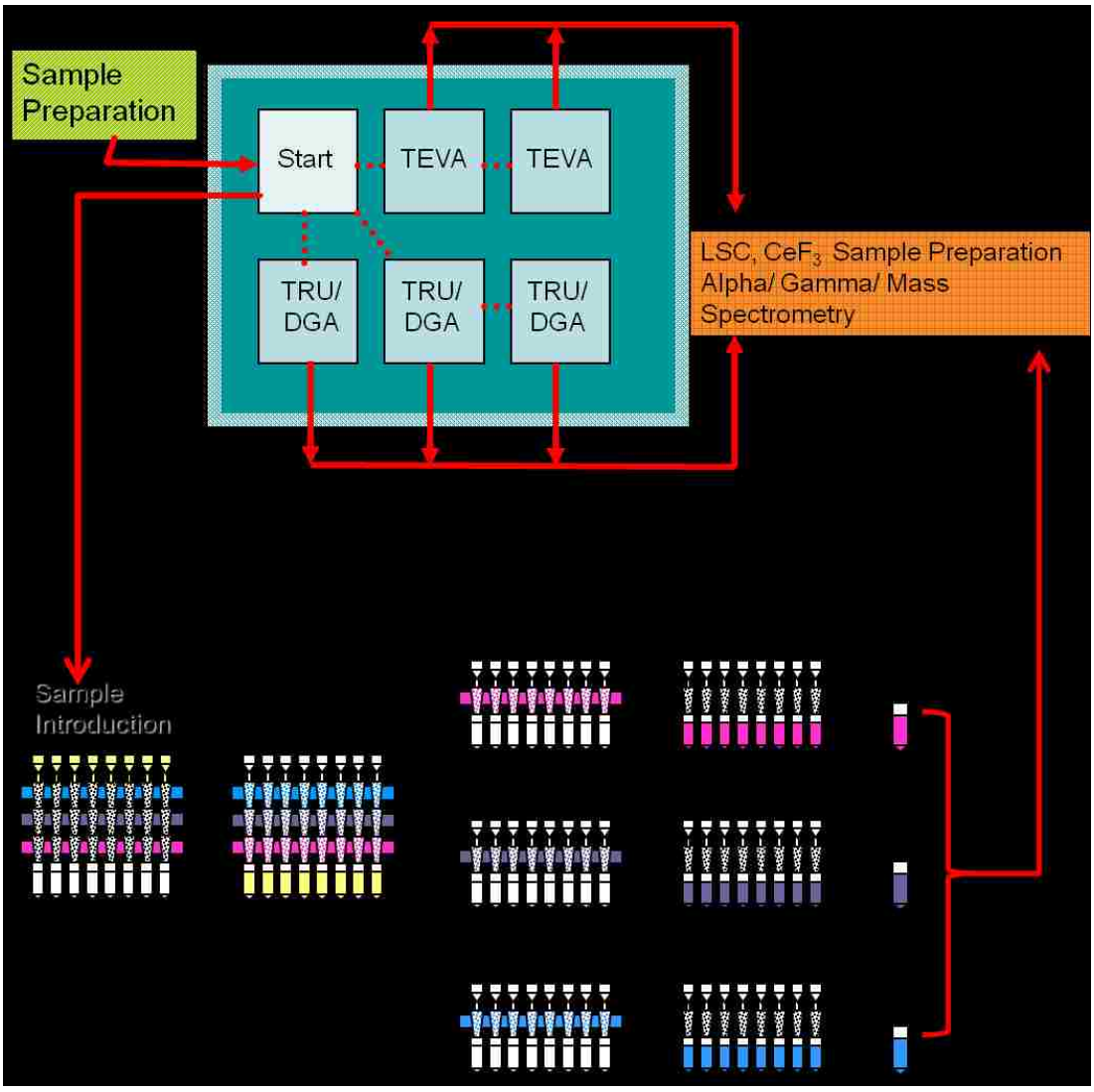

Figure 46. Conceptual schematic of a multiple vacuum system chemistry platform.

The EC methods evaluated were initially tested on laboratory simulated samples of Pu and Am. While this work was important for characterizing method efficiency, the simulated samples were not representative of real-world samples in that several matrix ions may be present in solution along with the Pu and Am and the concentrations of these ions may vary significantly across the samples selected for study. In this work, real-world samples containing both Pu and Am were obtained and chemistry was performed to determine the utility of EC vacuum system.

The samples consisted of weapons grade Pu (WGPu) hot particles (93) that were from an accident that occurred in 1960 involving a missile armed with a nuclear warhead. The missile caught fire and was completed destroyed. As a result, some of the missile debris was released into the environment where it persisted for several decades. The original weapon composition in terms of the relative Pu isotopic abundance was known (100,104) and this work compared the particle composition to the source term information. Hot particle dissolution studies along with non-destructive and minimally destructive techniques (6) confirmed that the source term was from WGPu and the Pu isotopic abundance agreed with the original weapon composition data. The utility of the EC system for rapid actinide analysis of real world samples was demonstrated with this work. Total sample analysis time from particle dissolution to sample preparation for analysis was accomplished in less than 4 hours and analysis time was limited by the detection method chosen and the availability of analytical instrumentation.

If an EC platform (Figure 46) was developed for this type of work, the sample throughput could be increased significantly.

Additional analyses will be required to determine the U isotopic content of the dissolved hot particles. Gamma spectrometry analysis of the intact hot particles determined that ^{235}U concentrations were variable in each hot particle relative to Pu, indicating that enriched U was also present in the original source term. From a forensic analysis perspective, the non-radioactive components of the particle matrix are also of interest. Several key elements including Fe, Al, Pb, Ti and U were present in the dissolved particle matrix. Many of these elements are present in the surrounding soil matrix and therefore, it is important to determine the environmental contribution factor. Dissolution studies should be conducted with soils in close proximity to the isolated hot particle to determine the background levels of the elements of interest. From analysis obtained by minimally destructive techniques, Ga was observed in several of the hot particles (6) but the concentration varied throughout the hot particle population. The presence of Ga from the elemental analysis studies performed on a small subset of hot particles in this work were inconclusive and therefore further study will be required. Gallium is used as a stabilizer for the δ-phase Pu and is expected to be present at 1-3 wt% in WGPu (126). It would be useful to compare the Ga distribution throughout the particle population to determine how the release scenario and environmental influences affect the minor constituents of the weapon material.

A current accepted method for Ga analysis from Pu metal samples is to isolate Ga from the Pu matrix by anion exchange chromatography, where yielding is determined by isotope dilution with ^{69}Ga. It would be useful to determine if an additional EC resin could be added to the separation procedure for Ga isolation and subsequent analysis. Gallium chemistry has not been characterized with EC resins discussed in this work. The LN resin (Eichrom Technologies, Inc.) contains the extractant bis-(2-ethylhexyl) phosphoric acid (HDEHP). From a literature review, HDEHP has been successfully used to isolate Ga and other activation products of interest including Co, Cu, Zn, As and Se using liquid-liquid extraction separation techniques (127). The utility of LN resin for nuclear forensic analysis should be explored in future work.

Preferential Am leaching from the particle matrix was supported by the hot particle dissolution data, but cannot be confirmed under the confines of this current work. Actinide analysis of the segmented soil cores using chemical dissolution could further support this observation by determining the ^{241}Am to ^{239}Pu activity ratio in the soil surrounding the hot particle.

The acid digestion method used for hot particle dissolution (HNO_3/HF/H_2O_2) should be further characterized in terms of complete dissolution. Work conducted with simulated inert matrix fuels containing various concentrations of Zr, Mg, Er, and Pu as oxides showed that 50 to 80 wt % of the Pu was dissolved with this method after 5 consecutive wet ashing steps (128). It would be useful to quantify the dissolution kinetics of the hot particles to optimize the acid digestion procedure.

In Chapter 6, mass and radiometric analysis methods were used to determine Pu isotopic composition. It would be useful to continue this work with standards produced with varied Pu isotopic compositions to determine the limitations of the analysis procedure. Additionally, isotope dilution methods are commonly used to determine method efficiency. It may be of interest to compare the relative isotopic ratios determined by alpha, gamma and mass spectrometry determined in the presence and absence of Pu tracer. The CeF_3 filter samples should also be characterized more fully in terms of Ce concentration and its affect on isotopic analysis. Once the method is fully characterized, the Pu fractions collected during chemistry on the dissolved hot particles should be characterized for complete mass analysis. This sample preparation method should also be optimized for U isotopic analysis.

In conclusion, this work has established the suitability of EC methods for the development of an automated chemistry platform. Future work should focus on characterizing U and other mixed actinide systems of interest for method automation. Both laboratory simulated samples and standards, and real-world samples (i.e. hot particles from various nuclear or radiological incidents) should be used for EC method optimization. Laboratory simulated samples and standards help establish the physical and chemical boundary conditions of the method and particles establish the utility and versatility of the method for a variety of sample matrices. Additionally, non-actinide elemental analysis should also be optimized for forensic analysis and eventually incorporated into the automated chemistry platform. The main focus of this work was to optimize the

aqueous chemistry component of the radioanalytical process. Continued research efforts should focus on optimizing sample dissolution for automation and how each component of the radioanalytical method (i.e. sample dissolution, separation chemistry and sample preparation for analysis) can be interconnected for automation.

This work was funded in part by the University of Nevada Radiochemistry Education and Research Center and the Department of Energy under the contract number UNLVRF-DOE-DE-FG02-05ER64123. The author would like to acknowledge the contributions of the Radiation Safety Director and Laboratory Manger at the Harry Reid Center for Environmental Studies, Tom O'Dou and Trevor Low for their due diligence in safety and laboratory management.

BIBLIOGRAPHY

1. Moody, K. J.; Hutcheon, I. D.; Grant, P. M. Nuclear Forensic Analysis; CRC Press, Taylor and Francis Group: Boca Raton, FL, USA, 2005.
2. Zheltonozhskya, V.; Mück, K.; Bondarkova, M. Classification of Hot Particles from the Chernobyl Accident and Nuclear Weapons Detonations by Non-destructive Methods. Journal of Environmental Radioactivity 2001, 57 (No. 2), 151-166.
3. Salbu, B. Hot Particles — A Challenge within Radioecology. Journal of Environmental Radioactivity 2001, 53, 267-268.
4. Musolino, S. V.; Harper, F. T. Emergency Response Guidance for the First 48 Hours After the Outdoor Detonation of An Explosive Radiological Dispersal Device. Health Physics 2006, 377-385.
5. American Physical Society and the American Association for the Advancement of Science. Nuclear Forensics - Role, State of the Art, and Program Needs; AAAS Center for Science Technology and Security Policy, 2008.
6. Gostic, R. C. Non-Destructive Characterization of Hot Particles from the BOMARC Accident Site; University of Nevada Las Vegas, 2009.
7. Eriksson, M.; Osán, J.; Jernström, J.; Wegrzynek, D.; Simon, R.; Chinea-Cano, E.; Markowicz, A.; Bamford, S.; Tamborini, G.; Török, S.; Falkenberg, G.; Alsecz, A.; Dahlgaard, H.; Wobrauschek, P.; Streli, C.; Zoeger, N.; Betti, M. Source Term Identification of Environmental Radioactive Pu/U Particles by their Characterization with Non-destructive Spectrochemical Analytical Techniques. 2005, 60 (No. 4), 455-469.
8. Jernstrom, J.; Eriksson, M.; Simon, R.; Tamborini, G.; Bildstein, O.; Marquez, R. C.; Kehl, S. R.; Hamilton, T. F.; Ranebo, Y.; Betti, M. Characterization and Source Term Assessments of Radioactive Particles from Marshall Islands Using Non-destructive Analytical Techniques. Spectrochimica Acta Part B: Atomic Spectroscopy 2006, 61 (No. 8), 971-979.

9. Mayer, K.; Wallenius, M.; Fanghänel, T. Nuclear Forensic Science - From Cradle to Maturity. Journal of Alloy and Compounds 2007, 444-445, 50-56.
10. Maxwell III, S. L. Rapid Column Extraction Method for Actinides and $^{89/90}$Sr in Water Samples. Journal of Radioanalytical and Nuclear Chemistry 2006, 267 (No.3), 537-543.
11. Maxwell, S. L. I. Rapid Method for Determination of Plutonium, Americium and Curium in large soil samples. Journal of Radioanalytical and Nuclear Chemistry 2008, 275 (No. 2), 395-402.
12. Maxwell, S. L. I. Rapid Separation Method for Emergency Water and Urine Samples. Journal of Radioanalytical and Nuclear Chemistry 2009, 279 (No. 3), 901-907.
13. Miura, T.; Oikawa, S.; Kishimoto, T.; Banba, S.; Morimoto, T. Rapid Separation of Plutonium in Environmental Samples Using an Anion Exchange Resin Disk. Journal of Radioanalytical and Nuclear Chemistry 2001, 250 (No. 3).
14. Varga, Z.; Surányi, G.; Vajda, N.; Stefánka, Z. Rapid Sequential Determination of Americium and Plutonium in Sediment and Soil Samples by ICP-SFMS and Alpha Spectrometry. Radiochimica Acta 2007, 95, 81-87.
15. Horwitz, E. P.; McAlister, D. R. Extraction Chromatography Versus Solvent Extraction: How Similar are They? Separation Science and Technology 2006, 41, 2163-2182.
16. Dimova, N.; Burnett, W. C.; Horwitz, E. P.; Lane-Smith, D. Automated Measurement of ^{224}Ra and ^{226}Ra in Water. Applied Radiation and Isotopes 2007, 65, 428-434.
17. Egorov, O. B.; O'Hara, M. J.; Grate, J. W. Automated Radiochemical Analysis of Total ^{99}Tc in Aged Nuclear Waste Processing Streams. Journal of Radioanalytical and Nuclear Chemistry 2005, 263 (No. 3), 629-633.

18. Egorov, O. B.; O'Hara, M. J.; Grate, J. W. Microwave-Assisted Sample Treatment in a Fully Automated Flow-Based Instrument: Oxidation of Reduced Technetium Species in the Analysis of Total ^{99}Tc in Caustic Aged Nuclear Waste Samples. Analytical Chemistry 2004, 76 (No. 14), 3869-3877.
19. Horwitz, E. P.; McAlister, D. R.; Bond, A. H.; Barrans, R. E.; Williamson, J. M. A Process for the Separation of ^{177}Lu from Neutron Irradiated ^{176}Yb Targets. Applied Radiation and Isotopes 2005, 63, 23-36.
20. O'Hara, M. J.; Burge, S. R.; Grate, J. W. Automated Radioanalytical System for the Determination of ^{90}Sr in Environmental Water Samples by ^{90}Y Cherenkov Radiation Counting. 2008, 81 (No. 3), 1228-1237.
21. Hang, W.; Zhu, L.; Zhong, W.; Mahan, C. Separation of Actinides at Ultra-trace Level from Urine Matrix Using Extraction Chromatography-Inductively Coupled Plasma Mass Spectrometry. Journal of Analytical Atomic Spectroscopy 2004, 19, 966-972.
22. Bond, A. H.; Horwitz, E. P.; Hines, J. J.; Young, J. E. A Compact Automated Radionuclide Separation System for Nuclear Medical Applications. Czechoslovak Journal of Physics 2003, 53 (Supplement 1), A717-A723.
23. Nevissi, A. E.; Strebin, R. S. Automated Radiochemical Procedure for Plutonium and Americium Measurement. Journal of Radioanalytical and Nuclear Chemistry 1995, 197 (No. 2), 211-218.
24. Horwitz, E. P. Extraction Chromatography of Actinides and Selected Fission Products: Principles and Achievement of Selectivity, 2008. Eichrom. http://www.eichrom.com/products/extraction.cfm (accessed May 14, 2009).
25. Maxwell, S. L. I. Rapid Actinide Separation Methods. Radioactivity and Radiochemistry 1997, 8 (No. 4), 36-44.
26. Tagami, K.; Uchida, U. Rapid Uranium Pre-concentration and Separation Method from Fresh Water Samples for Total U and ^{235}U/^{238}U Isotope Ratio

Measurements by ICP-MS. Analytica Chimica Acta 2007, 592 (No. 1), 101-105.

27. Taylor, V. F.; Evans, R. D.; Cornett, R. J. Determination of ^{90}Sr in Contaminated Environmental Samples by Tuneable Bandpass Dynamic Reaction Cell ICP–MS. Analytical and Bioanalytical Chemistry 2007, 387 (No. 1), 343-350.
28. Ayranov, M.; Krähenbühl, U.; Sahli, H.; Röllin, S.; Burger, M. Radiochemical Separation of Actinides from Environmental Samples for Determination with DF-ICP-MS and Alpha Spectrometry. Radiochimica Acta 2005, 93 (No. 5), 249-257.
29. Eichrom Technologies, Inc. Cerium Fluoride Microprecipitation for Alpha Spectrometry Source Preparation of Actinides. Eichrom Methods Compendium, SPA01, Rev 1.1.
30. Horwitz, E. P.; Chiarizia, R.; Dietz, M. L.; Diamond, H.; Nelson, D. Separation and Pre-concentration of Actinides from Acidic Media by Extraction Chromatography. Analytica Chemica Acta 1993, 537-543.
31. Horwitz, E. P.; McAlister, D. R.; Bond, A. H.; Barrans, R. E. Novel Extraction of Chromatographic Resins Based on Tetraalkyldiglycolamides: Characterization and Potential Applications. Solvent Extraction and Ion Exchange 2005, 23 (No. 3), 319-344.
32. Mark L. Dietz, E. P. H. a. A. H. B. Extraction Chromatography: Progress and Opportunities. Symposium Proceedings: Progress in Metal Ion Separation and Pre-concentration, 1997.
33. Braun, T.; Ghersini, G.; Katykhin, G. S. Extraction Chromatography; Elsevier, 1975; Vol. No. 2.
34. Horwitz, E. P.; Dietz, M. L.; Chiarizia, R.; Diamond, H.; Maxell, I. S. L.; Nelson, M. R. Separation and Pre-concentration of Actinides by Extraction Chromatography Using a Supported Liquid Anion Exchanger: Application to the Characterization of High-Level Nuclear Waste Solutions. Analytica Chimica Acta 1995, 310, 63-78.

35. Krane, K. S. Introductory Nuclear Physics; John Wiley and Sons, Inc., 1998.
36. Sill, C. W.; Williams, R. L. Preparation of Actinides for Alpha Spectrometry without Electrodeposition. Analytical Chemistry 1981, 53, 412-415.
37. Sill, C. W. Precipitation of Actinides as Fluorides or Hydroxides for High-Resolution Alpha Spectrometry. Nuclear and Chemical Waste Management 1987, 7, 201-215.
38. Molycorp, Inc. Cerium: A Guide to its Role in Chemical Technology; Molycorp, Inc.: Mountain Pass, CA, 1992.
39. Knoll, G. F. Radiation Detection and Measurement, 3rd Edition; John Wiley and Sons: New York, NY, 2000.
40. L'Annunziata, M. F. Handbook of Radioactivity Analysis; Academic Press: San Diego, 2003.
41. Floeckher, J. High Throughput Screening of Samples Containing Alpha and Beta Radionuclides: An Overview of Methods. Packard Instrument Company, 1992. Alpha Beta Application Note.
42. Thomson, J. Quench and Quench Curves. Karlsruhe, Germany, 2001; pp 65-73.
43. Robinson, J. W.; Frame, G. M.; Skelly-Frame, E. M. Undergraduate Instrumental Analysis; CRC, 2004.
44. Skoog, D. A.; Holler, F. J.; Crouch, S. R. Principles of Instrumental Analysis; Brooks Cole, 2006.
45. Tanner, S. D.; Baranov, V. I. Theory, Design, and Operation of a Dynamic Reaction Cell for ICP-MS. Atomic Spectroscopy 1999, 20 (No. 2), 45-52.
46. Stricklin, D. L.; Tjärnhage, Å.; Nygren, U. Application of Low Energy Gamma-Spectrometry in Rapid Actinide Analysis for Emergency Preparedness. Journal of Radioanalytical and Nuclear Chemistry 2002, 251 (No. 1), 69–74.
47. Peterson, D. S.; Plionis, A. A.; Gonzales, E. R. Optimization of Extraction Chromatography Separations of Trace Levels of Actinides with ICP-MS Detection. Journal of Separation Science 2007, 30, 1575-1582.

48. Varga, Z.; Surányi, G.; Vajda, N.; Stefánka, Z. Improved Sample Preparation Method for Environmental Plutonium Analysis by ICP-SFMS and Alpha Spectrometry. 2007, 274 (No. 1), 87–94.
49. Tavčar, P.; Jakopič, R.; Benedik, L. Sequential Determination of ^{241}Am, ^{237}Np, Pu Radioisotopes and ^{90}Sr in Soil and Sediment Samples. Acta Chimica Slovenica 2005, 52, 60-66.
50. Spry, N.; Parry, S.; Jerome, S. The Development of a Sequential Method for the Determination of Actinides and ^{90}Sr in Power Station Effluent Using Extraction Chromatography. Applied Radiation and Isotopes 2000, 163-171.
51. Horwitz, E. P.; Delphin, W. H.; Bloomquist, C. A. A.; Vandegrift, G. F. Radiochemical and Isotope Separations by High-Efficiency Liquid-Liquid Chromatography. Journal of Chromatography 1976, 125, 203-218.
52. Jiménez-Ramos, M. C.; García-Tenorio, R.; Vioque, I.; Manjón, G.; García-León, M. Presence of Plutonium Contamination in Soils from Palomares (Spain). Environmental Pollution 2006, 142 (No. 3), 487-492.
53. Boulyga, S. F.; Becker, J. S. Determination of Uranium Isotopic Composition and ^{236}U Content of Soil Samples and Hot Particles Using Inductively Coupled Plasma Mass Spectrometry. Fresenius' Journal of Analytical Chemistry 2001, 370 (No. 5), 612-617.
54. Sandalls, F. J.; Segal, M. G.; Victorova, N. Hot Particles from Chernobyl: A Review. Journal of Environmental Activity 1993, 18 (No. 1), 5-22.
55. Salbu, B.; Krekling, T. Characterization of Radioactive Particles in the Environment. Analyst 1998, 123, 843-850.
56. Salbu, B.; Lind, O. C.; Skipperud, L. Radionuclide Speciation and its Relevance in Environmental Impact Assessments. Journal of Environmental Radioactivity 2004, 74 (No. 1-3), 233-242.
57. Horwitz, E. P.; Bloomquist, C. A. A. Preparation, Performance , and Factors Affecting Band Spreading of High-Efficiency Extraction Chromatographic Columns for Actinide Separations. Journal of Inorganic and Nuclear Chemistry 1972, 34 (No.12), 3851-3871.

58. Burnett, W. C.; Corbett, D. R.; Schultz, M.; Horwitz, E. P.; Chiarizia, R.; Dietz, M.; Thakkar, A.; Fern, M. Pre-concentration of Actinide Elements from Soils and Large Volume Water Samples Using Extraction Chromatography. Journal of Radioanalytical and Nuclear Chemistry 1997, 226 (No. 1 and 2), 121-127.
59. Youngman, M. A.; Dax, S. L. Solid-Phase Mannich Condensation of Amines, Aldehydes, and Alkynes: Investigation of Diverse Aldehyde Inputs. Journal of Combinatorial Chemistry 2001, 3 (No. 5), 469-472.
60. Vaccaro, H. A.; Zhao, Z.; Clader, J.; Song, L.; Terracina, G.; Zhang, L.; Pissarnitski, D. Solution-Phase Parallel Synthesis of Carbamates as γ-Secretase Inhibitors. Journal of Combinatorial Chemsitry 2008, 10 (No. 1), 56-62.
61. J-Kem Scientific, Inc. Digital Vacuum Regulator User's Manual Model 200.
62. Hill, S. J. Inductively coupled plasma spectrometry and its applications; CRC Press, 1999.
63. McIsaac, L. D.; Baker, J. D. The Extraction of Zirconium from Nitric Acid by Di-hexyl N, N-Diethylcarbamoylphosphonate. Solvent Extraction and Ion Exchange 1983, 1 (No. 1), 27-41.
64. Alcock, K.; Bedford, F. C.; Hardwick, W. H.; McKay, H. A. C. Tri-N-Butyl Phosphate as an Extracting Solvent for Inorganic Nitrates: Zirconium nitrate. Journal of Inorganic and Nuclear Chemistry 1957, 4 (No. 2), 100-105.
65. Mathur, J. N.; Murali, M. S.; Natarajan, P. R.; Badheka, L. P.; Banerji, A. Extraction of Actinides and Fission Products by Octyl(phenyl)-N,N-Diisobutylcarbamoylmethyl-Phosphine Oxide from Nitric Acid Media. Talanta 1992, 39 (No. 5), 493-496.
66. Zhang, A.; Wei, Y.; Kumagai, M. Properties and Mechanism of Molybdenum and Zirconium Adsorption by a Macroporous Silica-Based Extraction Resin in the MAREC Process. Solvent Extraction and Ion Exchange, 2003, 21 (No. 4), 591-611.

67. Fujii, T.; Yamana, H.; Watanabe, M.; Moriyama, H. Extraction Study for TRUEX Process Using Short-Lived Radionuclides Prodcued by Neutorn Irradiation of Uranium. Solvent Extraction and Ion Exchange 2002, 20 (No.2), 151-175.

68. Brewer, K. N.; Herbst, R. S.; Todd, T. A.; Christian, J. D. Zirconium Extraction into Octyl(phenyl)-N,N-Diisobutylcarbamoylmethylphosphine Oxide and Tributyl Phosphate. Solvent Extraction and Ion Exchange 1998, 16 (No. 4), 1047-1066.

69. Horwitz, E. P.; Kalina, D. C.; Diamond, H.; Vandegrift, G. F.; Schulz, W. W. The TRUEX Process- A Process for the Extraction of the Transuranic Elements from Nitric Acid Wastes Utilizing Modified PUREX Solvent. Solvent Extraction and Ion Exchange 1985, 3 (No. 1), 75-109.

70. Horwitz, E. P.; Kalina, D. G.; Kaplan, L.; Mason, G. W.; Diamond, H. Selected Alkyl(phenyl)-N,N-Dialkylcarbamoylmethylphosphine Oxides as Extractants for Am(III) from Nitric Acid. Separation Science and Technology 1982, 17 (No. 10), 1261-1279.

71. Van Hecke, K.; Modolo, G. Separation of Actinides from Low Level Liquid Wastes (LLLW) by Extraction Chromatography Using Novel DMDOHEMA and TODGA Impregnated Resins. Journal of Radioanalytical and Nuclear Chemistry 2004, 261 (No. 2), 269-275.

72. Yaita, T.; Herlinger, A. W.; Thiyagarajan, P.; Jensen, M. P. Influence of Extractant Aggregation on the Extraction of Trivalent f-Element Cations by a Tetraalkyldiglycolamide. Solvent Extraction and Ion Exchange 2004, 22 (No. 4), 553-571.

73. Zhu, Z.; Sasaki, Y.; Suzuki, H.; Suzuki, S.; Kimura, T. Cumulative Study on Solvent Extraction of Elements by N,N,N',N'-Tetraoctyl-3-oxapentanediamide (TODGA) from Nitric Acid into N-Dodecane. Analytica Chimica Acta 2004, 527, 163-168.

74. Sasaki, Y.; Sugo, Y.; Suzuki, S.; Tachimori, S. The Novel Extractants, Diglycolamides, for the Extraction of Lanthanides and Actinides in HNO_3-

n-Dodecane System. Solvent Extraction and Ion Exchange 2001, 19 (No. 1), 91-103.

75. Sasaki, Y.; Choppin, G. Extraction and Mutual Separation of Actinide(III), (IV), (V) and (VI) Ions by N,N′-Dimethyl-N,N′-Dihexyl-3-Oxapentanediamide and Thenoyltrifluoroacetone. Journal of Radioanalytical and Nuclear Chemistry 2000, 246 (No. 2), 267-273.
76. Elcock, D.; Klemix, G. A.; Taboas, A. L. Establishing Remediation Levels in Response to a Radiological Dispersal Event (or “Dirty Bomb”). Environmental Science and Technology 2004, 38, 2505-2513.
77. Inn, K. G. W.; Outola, I.; Nour, S.; Kurosaki, H.; Albin, L.; Berne, A. Radioanalytical Emergency Response Exercise. Journal of Radioanalytical and Nuclear Chemistry 2006, 269 (No. 2), 351-360.
78. Eichrom Technologies, Inc. Americium, Neptunium, Plutonium, Thorium, Curium, Uranium and Strontium in Water (with Vacuum Box System). Eichrom Analytical Procedures. ACW17-VBS, Rev 1.0.
79. Clark, D. L.; Hecker, S. S.; Jarvinen, G. D.; Neu, M. P. The Chemistry of the Actinide and Transactinide Elements, 3rd ed.; Springer: Netherlands, 2006; Vol. 2, pp 813-1264.
80. Haschke, J. M. Disproportionation of Pu (IV): A Reassessment of Kinetic and Equilibrium Properties. Journal of Nuclear Materials 2007, 362, 60-74.
81. Coleman, G. H. The Radiochemistry of Plutonium; National Academy of Sciences and National Research Council (U.S.), 1965.
82. Margolis, S. A.; Park, E. Stability of Ascorbic Acid in Solutions Stored in Autosampler Vials. Clinical Chemistry 2001, 47, 1463-1464.
83. Golubitskii, G. B.; Budko, E. V.; Basova, E. M.; Kostarnoi, A. V.; Ivanov, V. M. Stability of ascorbic acid in aqueous and aqueous-organic solutions for quantitative determination. Journal of Analytical Chemistry 2007, 62 (No. 8), 742-747.
84. Siczek, A. A.; Steindler, M. J. Atomic Energy Review 1978, 16 (575-618).
85. Chiarizia, R.; Jensen, M. P.; Rickert, P. G.; Kolarik, Z.; Borkowski, M.; Thiyagarajan, P. Extraction of Zirconium Nitrate by TBP in N-Octane:

Influence of Cation Type on Third Phase Formation According to the “Sticky Spheres” Model. Langmuir 2004, 20, 10798-10808.

86. Salbu, B.; Krekling, T.; Oughton, D. H.; Østby, G.; Kashparov, V. A.; Brand, T. L.; Day, J. P. Hot Particles in Accidental Releases from Chernobyl and Windscale Nuclear Installations. Analyst 1994, 119 (No. 1), 125-130.
87. Sandalls, F. J.; Segal, M. G.; Victorova, N. Hot particles from Chernobyl: A review. Journal of Environmental Radioactivity 1993, 18 (No. 1), 5-22.
88. López, J. G.; Jiménez-Ramos, M. C.; García-León, M.; García-Tenorio, R. Characterization of Hot Particles Remaining in Soils from Palomares (Spain) Using a Nuclear Microprobe. 2007, 260 (No. 1), 343-348.
89. Ikäheimonen, T. K.; Ilus, E.; Klemola, S.; Dahlgaard, H.; Ryan, T.; Eriksson, M. Plutonium and Americium in the Sediments off the Thule Air Base, Greenland. Journal of Radioanalytical and Nuclear Chemistry 2002, 252 (No. 2), 339-344.
90. Wolf, S. F.; Bates, J. K.; Buck, E. C.; Dietz, N. L.; Fortner, J. A.; Brown, N. R. Physical and Chemical Characterization of Actinides in Soil from Johnston Atoll. Environmental Science and Technology 1997, 31 (No. 2), 467 - 471.
91. Hu, Q. H.; Weng, J. Q.; Wang, J. S. Sources of Anthropogenic Radionuclides in the Environment: A Review. Journal of Environmental Radioactivity 2008 (corrected proof), 1-12.
92. Rademacher, S. E.; Hubbell, J. L. BOMARC Missile Shelters and Bunkers Scoping Survey Workplan; United States Air Force AFIOH, 2007.
93. Defense Threat Reduction Agency (DTRA). Corrective Measures Study/Feasibility Study for the Disposition of Metal/Concrete Debris Radioactive Coral (above 13.5 pCi/g) Located in the Radiological Control Area of Johnston Atoll; DTRA, 2002.
94. Jernström, J.; Eriksson, M.; Osán**,** J.; Tamborini, G.; Török, S.; Simon, R.; Falkenberg**,** G.; Alsecz, A.; Betti, M. Non-destructive Characterization of Low Radioactive Particles from Irish Sea Sediment by Micro X-ray

Synchrotron Radiation Techniques: Micro X-ray Fluorescence (μ-XRF) and Micro X-ray Absorption Near Edge Structure (μ-XANES) Spectroscopy. Journal of Analytical Atomic Spectrometry 2004, 19, 1428-1433.

95. Salbu, B. Radioactive Particles Released from Different Nuclear Sources: With Focus on Nuclear Weapons Tests. In Nuclear Risks in Central Asia; Springer Netherlands, 2008; pp 7-17.

96. Tandon, L.; Hastings, E.; Banar, J.; Beddingfield, D.; Decker, D.; Dyke, J.; Farr, D.; FitzPatrick, J.; Gallimore, D.; Garner, S.; Gritzo, R.; Hahn, T.; Havrilla, G.; Johnson, B.; Kuhn, K.; LaMont, S.; Langner, D.; Lewis, C.; Majidi, V.; Martinez, P.; McCabe, R.; Mecklenburg, S.; Mercer, D.; Meyers, S.; Montoya, V.; Patterson, B.; Pereyra, R. A.; Porterfield, D.; Poths, J.; Rademacher, D.; Ruggiero, C.; Schwartz, D.; Scott, M.; Spencer, K.; Steiner, R.; Villarreal, R.; Volz, H.; Walker, L.; Wong, A.; Worley, C. Nuclear, Chemical and Physical Characterization of Nuclear Materials. Journal of Radioanalytical and Nuclear Chemistry 2008, 267 (No. 2), 467-473.

97. USAF. US Air Force Nuclear Weapons Accident/Incident Report Airmunitions Letter No. 136-11-56C; United States Air Force, 1960.

98. McCulla, W. H.; Rea, K. H.; Plannerer, H. N.; Farley, P. D. . B. W. R.; Wenzel, W. J. BOMARC Missile Accident Site Mitigation Review; Los Alamos National Laboratory, 1996.

99. Wallenius, M.; Lutzenkirchen, K.; Mayer, K.; Ray, I.; Aldave de las Heras, L.; Betti, M.; Cromboom, O.; Hild, M.; Lynch, B.; Nicholl, A.; Ottmar, H.; Rasmussen, G.; Schubert, A.; Tamborini, G.; Thiele, H.; Wagner, W.; Walker, C.; Zuleger, E. Nuclear Forensic Investigations with a Focus on Plutonium. Journal of Alloys and Compounds 2007, 444-445, 57-62.

100. Rademacher, S. E.; Hubbell, J. L. BOMARC Missile Shelters and Bunkers Scoping Survey Report (Volume 1); USAF, 2008.

101. Rademacher, S. E. The Influence of Heterogeneity in Gamma Spectroscopy Analysis of Contaminated with Weapons Grade Plutonium

at the BOMARC Missile Accident Site, McGuire AFB NJ; Air Force Institute for Environment, Safety and Occupation Health Risk Analysis, Brooks AFB, TX, 2001.

102. Hastings, T.; McKenzie-Carter, M.; Ryan, D.; Smith, J. Environmental Impact Statement for BOMARC Missile Site, McGuire AFB, New Jersey; Headquarters Military Airlift Command and Environmental Technology Group, 1992.
103. Demuth, S. Pre-conceptual Design for Separation of Plutonium and Gallium by Ion Exchange; Los Alamos National Laboratory, 1997.
104. Lee, M. H.; Clark, S. B. Activities of Pu and Am Isotopes and Isotopic Ratios in a Soil Contaminated by Weapons-Grade Plutonium. Environmental Science and Technology 2005, 39 (No. 15), 5512-5516.
105. Alamelu, C.; Aggarwal, S. K. Determination of $^{241}Pu/^{239}Pu$ Atom Ratio in Pressurized Heavy Water Reactor (PHWR)-Pu Samples Using Liquid Scintillation Counting. Journal of Alloys and Compounds 2007, 444-445, 652-655.
106. A New Approach to Quench Correction When Measuring ^{241}Pu in the Presence of Pu-alpha by Supported-Disc Liquid Scintillation Spectrometry. Applied Radiation and Isotopes 1996, 47 (No. 9-10), 875-878.
107. Hrnecek, E.; Aldave de las Heras, L.; Betti, M. Application of Microprecipitation on Membrane Filters for Alpha Spectrometry, Liquid Scintillation Counting and Mass Spectrometric Determination of Plutonium Isotopes. Radiochimica Acta 2002, 90, 721-725.
108. Paatero, J.; Jaakola, T.; Reponen, A. Determination of the ^{241}Pu Deposition in Finland After the Chernobyl Accident. Radiochimica Acta 1994, 64, 139-144.
109. Payne, R. F.; Clark, S. B.; Elliston, J. T. Radioanalytical Approach to Determine ^{238}Pu, $^{239+240}Pu$, ^{241}Pu and ^{241}Am in Soils. Journal of Radioanalytical and Nuclear Chemistry 2008, 277 (No. 1), 269-274.

110. PNNL. History of the Plutonium Production Facilities at the Hanford Site Historic District, 1943-1990; U.S. Department of Energy: Richland, WA, 2002, Pacific Northwest National Laboratory.
111. Boulyga, S. F.; Desideri, D.; Assunta Meli, M.; Testa, C.; Becker, S. Plutonium and Americium Determination in Mosses by Laser Ablation ICP-MS Combined with Isotope Dilution Technique. International Journal of Mass Spectrometry 2003, 226, 329-339.
112. Aggarwal, S. K.; Shah, P. M.; Saxena, M. K. Preparation and Characterization of ^{234}U for Mass Spectrometry and Alpha Spectrometry. Journal of Radioanalytical and Nuclear Chemistry 1998, 230 (No. 1-2), 307-309.
113. Ayranov, M.; Krähenbühl, U.; Sahli, H.; Röllin, S.; Burger, M. Radiochemical Separation of Actinides from Environmental Samples for Determination with DF-ICP-MS and Alpha Spectrometry. Radiochimica Acta 2005, 93, 249-257.
114. Ramebäck, H.; Skĺlberg, M. Separation of Neptunium, Plutonium, Americium and Curium from Uranium with Di-(2-ethylhexyl)-Phosphoric Acid (HDEHP) for Radiometric and ICP-MS Analysis. Journal of Radioanalytical and Nuclear Chemistry 1998, 235 (No. 1-2), 229-234.
115. Cizdziel, J.; Farmer, D.; Hodge, V.; Lindley, K.; Stezenback, K. $^{234}U/^{238}U$ Isotope Ratios in Groundwater from Southern Nevada: A Comparison of Alpha Counting and Magnetic Sector ICP-MS. Science of The Total Environment 2005, 350 (No. 1-3), 248-260.
116. Wallenius, M.; Morgenstern, A.; Apostolidis, C.; Mayer, K. Determination of the Age of Highly Enriched Uranium. Analytical and Bioanalytical Chemistry 2002, 374 (No. 3), 379-384.
117. Nygren, U.; Ramebäck, H.; Nilsson, C. Age Determination of Plutonium Using Inductively Coupled Plasma Mass Spectrometry. Journal of Radioanalytical and Nuclear Chemistry 2007, 272 (No. 1), 45-51.
118. Varga, Z.; Suranyi, G.; Vajda, N.; Stefanka, Z. Rapid Sequential Determination of Americium and Plutonium in Sediment and Soil Samples

by ICP-SFMS and Alpha Spectrometry. Radiochimica Acta 2007, 95, 81-87.

119. Michel, H.; Ketter, M. E.; Barci-Funel, G. ICP-MS Analysis of Plutonium Activities and $^{240}Pu/^{239}Pu$ Ratio in Alpha Spectrometry Planchet Deposits. Journal of Radioanalytical and Nuclear Chemistry 2007, 273 (No. 2), 485-490.

120. Becker, J. S. Inductively Coupled Plasma Mass Spectrometry (ICP-MS) and Laser Ablation ICP-MS for Isotope Analysis of Long-Lived Radionuclides. International Journal of Mass Spectrometry 2005, 242 (No. 2-3) 183-195.

121. Becker, J. S.; Sela, H.; Dobrowolska, J.; Zoriy, M.; Becker, J. S. Recent Applications on Isotope Ratio Measurements by ICP-MS and LA-ICP-MS on Biological Samples and Single Particles. International Journal of Mass Spectrometry 2008, 270, 1-7.

122. Cizdziel, J. V.; Ketter, M. E.; Farmer, D.; Faller, S. H.; Hodge, V. F. $^{239,240,241}Pu$ Fingerprinting of Plutonium in Western US Soils Using ICPMS: Solution and Laser Ablation Measurements. Analytical and Bioanalytical Chemistry 2008, 390 (No. 2), 521-530.

123. Thomas, R. Practical Guide to ICP-MS; Marcel Dekker, Inc.: New York, NY, 2004.

124. Berger, M. J.; Coursey, J. S.; Zucker, M. A.; Chang, J. ESTAR, PSTAR, and ASTAR: Computer Programs for Calculating Stopping-Power and Range Tables for Electrons, Protons, and Helium Ions. http://physics.nist.gov/Star (accessed Septemeber 09, 2009).

125. D'Oriano, C.; Da Pelo, S.; Poda, F.; Cioni, R. Laser-Ablation Inductively Coupled Plasma Mass Spectrometry (LA-ICP-MS): Setting Operating Conditions and Instrumental Performance. Periodico di Mineralogia 2008, 77 (No. 3), 65-74.

126. Conradson, S. D. Where is the Gallium? Searching the Plutonium Lattice with XAFS. Los Alamos Science 2000, 26, 356-363.

127. Nayak, D.; Lahiri, S. Sequential Separation of ^{61}Cu, ^{62,63}Zn, ^{66,67,68}Ga, ^{71,72}As, and ^{73}Se Produced by Heavy Ion Activation on Cobalt Target. Journal of Nuclear and Radiochemical Sciences 2003, 4 (No. 1), 1-3.
128. Holliday, K. S. Zirconia-Magnesia Inert Matrix Fuel and Waste Form: Synthesis, Characterization and Chemical Performance in an Advanced Fuel Cycle; University of Nevada Las Vegas, 2009.

VITA

Graduate College
University of Nevada, Las Vegas

Julie Marisa Gostic

Degrees:

Bachelor of Arts, Physics, 2000
Bachelor of Arts, Biology, 2000
College of Charleston

Master's of Science, Radiological Sciences and Protection, 2004
University of Massachusetts, Lowell

Dissertation Title: Evaluation of Extraction Chromatography Resins for Rapid Actinide Analysis

Special Honors and Awards:

Glenn T. Seaborg Institute, Lawrence Livermore National Laboratory, Nuclear Forensics Summer Internship, 2008

Dissertation Examination Committee:

Chairperson, Kenneth R. Czerwinski, Ph.D.
Committee Member, Kenton J. Moody, Ph. D.
Committee Member, Gary Cerefice, Ph. D.
Graduate Faculty Representative, Ralf Sudowe, Ph. D.